UNIVERSITÉ D'ANGERS **2008**

Etude de lasers à contre-réaction distribuée (DFB) en configuration de réflexion

Thèse de Doctorat

Spécialité : Physique

Ecole Doctorale d'Angers

Présentée et soutenue publiquement

Le 11 Avril 2008 à Angers

par : Fei CHEN

Devant le jury ci-dessous :

Rapporteurs: Alain FORT, Directeur de Recherche CNRS, IPCMS Strasbourg, France
Hongwu LI, Professeur, IREENA Nantes, Université de Nantes, France
Examinateurs: Licinio ROCHA, Ingénieur CEA, Saclay, France
Jean-Michel NUNZI, Professeur, Université d'Angers, France
Denis GINDRE, Maître de conférences, Université d'Angers, France

Directeur de thèse : **Jean-Michel NUNZI**
Co-encadrant : Denis GINDRE

Laboratoire POMA , FRE CNRS 2988
Université d'Angers, Bâtiment Db
2 Boulevard Lavoisier, 49045 Angers

ED 363

This thesis is dedicated to

my parents . . . Hui Fang HOU and Wen Hou CHEN

Résumé

Les lasers à rétroaction répartie (DFB) permettent de générer des impulsions à spectre très étroit, et sont des sources lasers compactes et accordables en fréquence pour des applications en optique intégrée. Au cours de cette thèse, un laser DFB dynamique a été obtenu pour la première fois dans une configuration de pompage en réflexion. Un DFB accordable à bande photonique interdite, créé par la superposition de deux faisceaux de pompe, a été réalisé dans un matériau laser dopé par des colorants, indiquant l'existence d'une modulation photoinduite de l'indice de réfraction.

La modulation de la polarisation, réalisée par l'ajustement de l'état de polarisation des deux faisceaux de pompe, est une technique très efficace afin d'obtenir le feedback pour l'oscillation du laser DFB dans la configuration du pompage en réflexion. Une structure photonique DFB accordable et chirale a été observée avec certains choix de polarisation des faisceaux de pompe, ce qui peut être identifié comme un laser DFB dynamique, chiral, à bande photonique interdite dépendante de la polarisation. Une émission laser à polarisation circulaire a été ainsi obtenue.

Abstract

Distributed feedback (DFB) lasers allow the generation of pulses with narrow linewidth, and are compact tunable laser sources for applications in integrated optics. In this thesis, for the first time, dynamic DFB lasing action was achieved in a *reflection* pumping configuration instead of the traditional transmission pumping one. A tunable one-dimensional (1-D) DFB photonic crystal (PC) created by transient interference pattern of two crossing pump beams was obtained in dye doped laser media, which indicated the existence of an index modulation.

The polarization modulation, realized by readily manipulating the state of polarization of the pumping beams, was demonstrated effective in providing feedback for DFB lasing oscillation in the reflection pumping configuration. A tunable *chiral* photonic DFB structure was observed in certain polarization pumping schemes, which can be identified as a *dynamic* polarization-dependent chiral PC. Tunable circularly-polarized laser output was obtained.

Acknowledgements

This is the bit where I thank people for their help, support and care, for allowing me to spend lots of money, to enjoy the magic in science, and to play with expensive toys. Not to mention deny all knowledge if I happened to break it.

Right. First and most, I would like to express my heartfelt gratitude to my advisor Prof. Jean-Michel Nunzi. He is the man responsible for providing me continuous, constructive and inspiring guidance, patience and constant encouragement throughout the course of my research works. Jean-Michel was very generous in providing me with a maintenance grant from his own grant money for which I am especially grateful. Without this opportunity I wouldn’t have been able to change the world as we know it. The insightful ideas and attitude to science that I required from him will benefit my whole life.

I would like to convey my personal thanks to Prof. Denis Gindre for his big favors time to time in helping me dealing with the problems caused by the language during my stay in Angers. His effort in arranging my jury and revising this thesis is much appreciated and well-remembered.

Next up are everyone on my thesis jury. My sincere thanks go to Professors Alain Fort and Hongwu LI for sparing their invaluable time in

reviewing the manuscript and making comments. I would like to thank Dr. Licinio Rocha and Prof. Denis Gindre in addition to my advisor for agreeing to serve on my thesis jury.

I have been enjoying so much the atmosphere of the diverse cultures in POMA due to its widely gathering of graduate students, post-docs from all over of the world. Thanks are due to Prof. Andre Monteil, the director of POMA, for accepting me to work as a part of it.

Closer to home I must thank my colleagues Christophe and Alain for their assistance with the laser system maintenance and their timely meeting my needs of the optics all the time. I am indebted to Dr. Sylvie Dabos-Seignon for supplying the organic solvents and chemicals in my experiments.

I would like to thank Prof. Alexandra Djurisic for allowing my short stay in her well-equipped laboratory in Hong Kong to learn the synthesis of ZnO nanorods. My thanks to all the group members in her lab for their help and memorable time spent there.

I would like to thank all the POMers, I have had wonderful time to stay with: Adrien Vesperini, who has introduced his related work in my research topic without any reservation; Hassina Derbal, who has given me much help in my personal affairs when I was a fresher here; Sorharb Ahmadi-my funny officemate, a talkative guy, who always shared his living skills in France with

me, and his pretty daughter, who made so much fun; Wallace Chan, his collection of Chinese novels helped me killing time when I felt dull; and my other groupmates Katherine Pacheco and Ajay Pandey. Thanks also go to my great colleagues and friends: Serge and Zacaria, for being nice and concerned to me all the time. I'd also like to thank the members of POMA: Nicolas, Christian and Marie-Therese for their kindness.

Finally, and most importantly, I am deeply grateful to my parents who have been supporting me emotionally, intellectually and financially for all my life, and my boyfriend for his affection I always have. Although they are quite far away from me, their love, support and encouragements make me survive, make me feel safe always.

Table of contents

List of figures

Chapter I

Introduction

The LASER, which stands for Light Amplification by Stimulated Emission of Radiation, has been applied over virtually all areas of modern life, e. g. science, technology, medicine and telecommunication. At present, a variety of laser sources is available, e. g. gas lasers, dye lasers, and semiconductor lasers etc., covering a wide spectral range.

The key features of a laser are a material that amplifies light (known as the gain medium) and a resonator that applies feedback [1]. As light passes through the gain medium, it stimulates the emission of more light, thereby gaining intensity. The resonator reflects the light backward and forward through the gain medium to build up a very intense light field. The additional light stimulated has the same wavelength, direction, and phase as the light passing through the gain medium, which leads to the distinctive coherence properties of laser light, e.g. being collimated in a narrow beam and monochromatic. There are usually two main ways of supplying energy to a laser: optical pumping (exciting the gain medium with a powerful light source), this would normally be either another laser or a flash lamp discharge and electrical pumping (exciting the gain medium electrically by passing a current through it). Currently, injection electrical pumping is the approach used in inorganic semiconductor diode lasers.

The most common laser configuration is to have a gain medium in a resonator consisting of two (or more) mirrors. Light passes repeatedly through the gain medium as it bounces backward and forward between mirrors. One of the mirrors (the output coupler) reflects most of the light, but transmits a small portion, giving the output beam of the laser. Fig. 1.1 shows several

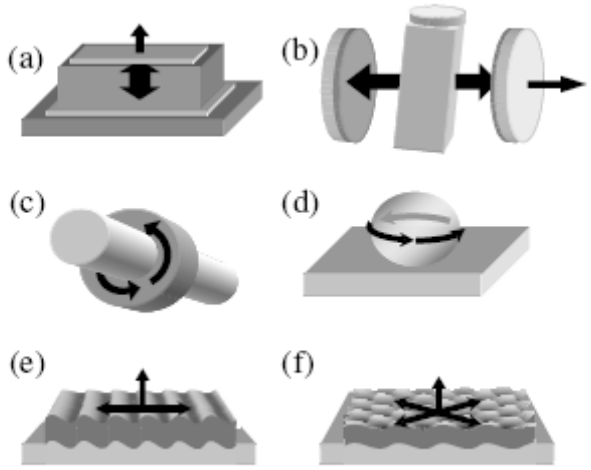

Fig. 1.1 Schematic of several resonant structures used for lasers showing propagation directions of the resonant laser field. a) Planar microcavity; b) Fabry-Perot dye laser cavity; c) Microring cavity, coated around an optical fiber; d) Spherical microcavity (Micro-drop); e) One-dimensional distributed feedback (DFB) resonator ; f) 2D DFB/photonic crystal resonator [1].

representative microcavity structures used for lasing oscillation. They can be easily made by low-cost fabrication processes, such as dip-coating, spin-coating, evaporation coating, etc. , with many kinds of laser materials (dye doped sol-gel materials, dye doped polymers, photopolymers, semiconductor polymers, etc.). Tessler *et al.* made the first conjugated polymer laser based on a microcavity shown in Fig. 1.1 (a) [2]. The lasing output was observed perpendicularly from the substrate plane, this feature is very useful for many

applications. Microring cavity (Fig. 1.1 (c)) can be employed to realize low-threshold lasers [3-4]. In micro-ring resonators, light is totally internally reflected around the perimeter of the ring in so-called “whispering gallery” modes. Resonances occur at wavelengths where the circumference is equal to an integer multiple of the wavelength. The easiest way to make whispering gallery mode lasers is to dip-coat a film onto a glass fiber [3, 5-6] or to melt small pieces of film onto substrate in such a way that they bead up into nearly spherical microdrops (Fig. 1.1 (d)) [7]. Micro-disk lasers can also be made by photolithography and etching [8]. Lasers of this type typically show narrow-linewidth lasing modes with spacing that varies inversely with the ring diameter. However, although they have low thresholds, micro-ring lasers are less convenient for most applications because they do not deliver a beam of light.

An alternative way to reflect light in a laser medium is to incorporate a periodic modulation of gain and/or refractive index to get a distributed feedback (DFB) structure (Fig. 1.1 (e)) [9-10]. This approach can easily be combined with the techniques for depositing the emission layer and can be readily used for large-area geometries. The feedback relies on the diffraction of light by a periodic modulation of either the refractive index and/or the gain coefficient. Different (soft) lithographic methods, such as, embossing, injection molding and electron beam lithography can be utilized for the fabrication of periodical DFB perturbations [11-15]. Alternatively, the DFB structure can also be temporarily generated by an interference pattern [16-20].

Two-dimensional (2-D) DFB structure (Fig. 1.1 (f)) forming a 2-D photonic crystal (PC) has also been an effective approach to realize 2-D DFB PC lasers. The Bragg reflections caused by the grating diminish the group velocity of light along some directions of crystallographic symmetry to zero, and the resulting feedback gives rise to laser oscillation. Meier *et al.* reported the operation of 2-D DFB PC laser from dye doped polymer deposited on lithographically patterned Si/SiO_2 structures [21]. M. Notomi *et al.* observed lasing oscillation from the four lowest bandgaps of 2D organic PC lasers fabricated by *e*-beam lithography [22]. Jakubiak *et al.* obtained dynamic lasing from all-organic 2D PCs [23]. A circular grating surface emitting distributed Bragg reflector was also used to provide complete 2D feedback to lasing oscillation [24].

In 1971, the first tunable DFB dye laser was demonstrated by C. V. Shank *et al.* [16]. The oscillation mechanism results in a compact laser structure and realizes narrow linewidth lasing emission. Since then, many research interests have been concentrated on DFB lasers. J. E. Bjorkholm *et al.* observed high-order DFB oscillations [25] and obtained DFB laser actions in thin-film optical waveguides [26]; R. L. Fork *et al.* demonstrated a solid state DFB laser in an optical-memory material [27]; Z. Bor carried out many works on picosecond pulse generation in DFB dye lasers [28-29]. Moreover, the DFB mechanism enormously promoted the development of semiconductor lasers [30]. Currently, the DFB semiconductor laser can completely fulfill the quality requirements of the light source in optical fiber communication networks: stable single frequency output; modulation capability of gigabit/s; stable

operating lifetime, and manufacturability. The DFB semiconductor laser has become a key standard component for modern optical communication systems.

The first DFB theory based on coupled-wave model was presented by H. Kogelnik *et al.* in 1972 [10]. Then a related coupled-mode theory was developed by Yariv [31] for guide-wave optics in 1973. Kneubűhl gives us a review book on the theories of DFB lasers [32]. An introduction of coupled-wave theory of DFB lasers is given in Chapter II of this thesis.

The progress of development of DFB lasers is generally promoted by the improvements of both laser materials and resonators. In the early development of the DFB lasers, most of works were concentrated on the laser dye-doped solutions and inorganic semiconductors, while the improvement of DFB cavities was mainly dependent on the semiconductor techniques. In the last decade, DFB lasers based on new materials and cavity structures have undergone a remarkable process.

Since Heeger's group discovered the metallic properties of doped polyacetylene in 1977 [33]. Many DFB lasers were realized based on conjugated polymers. G. Kanzelbinder *et al.* reported optically written DFB MEH-PPV waveguide lasers [34]; G. A. Turnbull *et al.* observed DFB lasing in MEH-PPV films [35]; McGehee *et al.* made low-threshold DFB lasers by spin-casting of BuEH-PPV onto gratings in silica [36] and so on. Whilst, the researchers have addressed their next aim towards electrically pumping conjugated polymer lasers. Many kinds of DFB lasers were also fabricated based on dye doped solid-state materials. Inorganic glasses and polymers were both adopted as solid hosts for organic dyes. Lo's group demonstrated various

DFB lasers based on dye doped sol-gel glasses. The lasing emission wavelength covered from the near violet at 367 nm [37] to the near infrared at 932 nm [38]. The host materials used included silica [37, 39-40], titania-silica [41], zirconia [18, 20, and 42] and their alternative combinations [19]. J.-M. Nunzi's group and A. Penzkofer's group studied DFB laser action in dye doped polymers and photopolymers [43-44]. DFB lasing has also been demonstrated in other materials. The representative materials include such as inorganic crystals [45-47]; liquid crystals [48-49]; holographic polymer dispersed liquid crystals (H-PDLC) [50-53] and dye doped cholesteric liquid crystals (CLCs) [54-59]. These materials have created new paths for the development of the DFB lasers.

In the previous works, the traditional dynamic DFB lasers pumped by two interference beams were operated in a transmission grating configuration. The two pumping beams, which generate the DFB grating reach the sample from the same side, the vector of the so-called transmission grating is parallel to the sample surface, e.g. the cell surface for a solution sample or the substrate for a thin film sample. In this thesis, we will present our works on DFB dye laser in a reflection pumping configuration. That is to say, the two interference beams reach the sample from opposite sides; the vector of the reflection DFB grating is perpendicular to the sample surface. To the best of our knowledge, this is the first work of dynamic DFB laser action in the reflection pumping geometry.

In this thesis, firstly, an introduction is given in Chapter Ⅰ. The coupled-wave theory of DFB lasers is introduced in Chapter Ⅱ. Secondly, the laser media employed in our DFB laser experiments and the experimental setup are illustrated in Chapter Ⅲ. Thirdly, first-order DFB lasing effect in R6G doped ethanol, DCM doped methanol and R6G doped PMMA are presented in Chapter Ⅳ. Several important properties, such as wavelength tuning, threshold, and slope, etc., are given. Then we study the polarization properties of the reflection DFB lasers. DFB lasing action is obtained by polarization modulation in different polarization pumping schemes, and the state of polarization of DFB laser output is also investigated in detail. The results are reported in Chapter Ⅴ. Finally, in Chapter Ⅵ, we calculate the gain coefficients of the two orthogonal components of DFB lasing output from the various polarization pumping schemes based on reflection geometry. A summary is given in Chapter Ⅶ.

References

[1] I. D. W. Samuel and G. A. Turnbull, "Organic Semiconductor Lasers", *Chem. Rev.* **107**, p1272, 2007

[2] N. Tessler, G. J. Denton, R. H. Friend, "Lasing from conjugated-polymer microcavities", *Nature*, **382**, p695 1996

[3] S. V. Frolov, Z. V. Vardeny, K. Yoshino, A. Zakhidov, R. H. Baughman, "Simulated emission in high-gain organic media", *Phys. Rev. B* **59**, pR5284, 1999

[4] M. Kuwata-Gonokami, R. H. Jordan, A. Dodabalapur, H. E. Katz, M. L. Schilling, R. E. Slusher, S. Ozawa, "Polymer microdisk and microring lasers", *Opt. Lett.* **20**, p2093, 1995

[5] S. V. Frolov, M. Shkunov, Z. V. Vardeny, K. Yoshino, "Ring microlasers from conducting lasers", *Phys. Rev. B* **56**, pR4363, 1997

[6] Y. Kawabe, C. Spiegelberg, A. Schulzgen, M. F. Nabor, B. Kippelen, E. A. Mash, P. M. Allemand, M. Kuwata-Gonokami, K. Takeda, N. Peyghambarian, "Whispering-gallery-mode microring laser using a conjugated polymer", *Appl. Phys. Lett.* **72**, p141, 1998

[7] M. Berggren, A. Dodabalapur, Z. Bao, R. E. Slusher, "Solid-state droplet laser made from an organic blend with a conjugated polymer emitter", *Adv. Mater.* **9**, p968, 1997

[8] S. V. Frolov, A. Fujii, D. Chinn, M. Hirohata, R. Hidayat, M. Taraguchi, T. Masuda, K. Yoshino, Z. V. Vardeny, "Microlaser and

Micro-LEDs from Disubstituted Polyacetylene", *Adv. Mater.* **10**, p869, 1998

[9] H. Kogelnik, C. V. Shank, "Stimulated emission in a periodic structure", *Appl. Phys. Lett.* **18**, p152, 1971

[10] H. Kogelnik, C. V. Shank, "Coupled-wave theory of distributed feedback lasers", *J. Appl. Phys.* **453**, p2327, 1972

[11] M. D. McGehee, M. A. Diaz-Garcia, F. Hide, R. Gupta, E. K. Miller, D. Moses *et al.* ,"Semiconductor polymer distributed feedback lasers", *Appl. Phys. Lett.* **72**, p1536, 1998

[12] C. Kallinger, M. Hilmer, A. Haugeneder, M. Perner, W. Spirkl, U. Lemmer *et al.* "A flexible conjugated polymer laser", *Adv. Mater.* **10,** p920, 1998

[13] J. A. Rogers, M. Meier, A. Dodabalapur, "Using printing and modling techniques to produce distributed feedback and Bragg reflector resonators for plastic lasers", *Appl. Phys. Lett.* **73**, p1766, 1998

[14] J. A. Rogers, M. Meier, A. Dodabalapur, E. J. Laskowski, M. A. Cappuzzo, "Distributed feedback ridge waveguide lasers fabricated by nanoscale printing and molding on nonplanar substrate", *Appl. Phys. Lett.* **74**, p3257, 1999

[15] S. Riechel, U. Lemmer, J. Feldmann, T. Benstern, W. Kowalsky, A. Gombert *et al.* "Laser modes in organic solid state distributed feedback lasers", *Appl. Phys. B* **71**, p897, 2000

[16] C. V. Shank, J. E. Bjorkholm, H. Kogelnik, "Tunable distributed-feedback dye laser", *Appl. Phys. Lett.* **18**, p395, 1971

[17] K. P. Kretsch, W. J. Blau, V. Dumarcher, L. Rocha, C. Fiorini, J. M. Nunzi *et al*., "Distributed feedback laser action from polymeric waveguides doped with oligo-phenylenevinylene model compounds", *Appl. Phys. Lett.* **76**, p2149, 2000

[18] D. Lo, L. Shi, J. Wang, G.-X. Zhang, X.-L. Zhu, "Zirconia and Zirconia-organically modified silicate distributed feedback waveguide lasers tunable in the visible", *Appl. Phys. Lett.* **81**, p2707, 2002

[19] C. Ye, L. Shi, J. Wang, D. Lo, X.-L. Zhu, "Simultaneously generation of multiple pairs of transverse electric and transverse magnetic output modes from titania and zirconia organically modified silicate distributed feedback waveguide lasers", *Appl. Phys. Lett.* **83**, p4101, 2003

[20] F. Chen, J. Wang, C. Ye, D. Lo, X.-L. Zhu, "Distributed feedback sol-gel zirconia channel waveguide lasers", *Appl. Phys. Lett.* **85**, p4284, 2004

[21] M. Meier, A. Mekis, A. Dodabalapur, A. Timko, R. E. Slusher, J. D. Joannopoulos, O. Nalamasu, "Laser action from two-dimensional distributed feedback in photonic crystals", *Appl. Phys. Lett.* **74**, p7, 1999

[22] M. Notomi, H. Suzuki, T. Tamamura, "Directional lasing oscillation of two-dimensional organic photonic crystal lasers at several photonic band gaps", *Appl. Phys. Lett.* **78**, p1325, 2001

[23] R. Jakubiak, V. P. Tondiglia, L. V. Natarajan, R. L. Sutherland, P. Lloyd, T. J. Bunning and R. A. Vaia, "Dynamic Lasing from All-Organic Two-Dimensional Photonic Crystals", *Adv. Mater.* **17**, p2807, 2005

[24] G. A. Turnbull, A. Carleton, A. Tahraouhi, T. F. Krauss, I. D. W. Samuel, G. F. Barlow and K. A. Shore, "Effect of gain localization in circular-grating distributed feedback lasers", *Appl. Phys. Lett.* **87**, p201101, 2005

[25] J. E. Bjorkholm and C. V. Shank, "Higher-Order Distributed Feedback Oscillators", *Appl. Phys. Lett.* **20**, p306, 1972

[26] J. E. Bjorkholm and C. V. Shank, "Distributed-Feedback Lasers in Thin-Film Optical Waveguides", *IEEE J. Quantum Electronics* **8**, p833, 1972

[27] R. L. Fork, K. R. German and E. A. Chandross, "Photodimer Distributed Feedback Laser", *Appl. Phys. Lett.* **20**, p139, 1972

[28] Z. Bor, "A novel pumping arrangement for tunable single picosecond pulse generation with a N_2 laser pumped distributed feedback dye laser", *Opt. Commun.* **29**, p103, 1979

[29] Z. Bor, "10 Å continuous pressure tuning of single-frequency distributed feedback laser", *Opt. Commun.* **29**, p329, 1979

[30] J. Carroll, J. Whiteaway and D. Plumb, *Distributed feedback semiconductor lasers*, London: Institute of Electrical Engineers, 1998

[31] A. Yariv, "Coupled-mode Theory for Guided-Wave Optics", *IEEE J. Quantum Electronics* **9**, p919, 1973

[32] F. K. Kneubűhl, *Theories on distributed feedback lasers*, USA: Harwood Academic Publishers, 1993

[33] C. K. Chiang, C. R. Fincher, Y. W. Park, A. J. Heeger, H. Shirakawa, E. J. Louis, S. C. Gau, A. G. MacDiarmid, "Electrical Conductivity in doped Polyacetylene", *Phys. Rew. Lett.* **39**, p1098, 1977

[34] G. Kanzelbinder, E. Toussaere, J. Zyss, A. Pogantsch, E. W. J. List, H. Tillmann, and H.-H. Hörhold, "Optically written solid-state lasers with broadly tunable mode emission based on improved poly(2,5-dialkoxy-phenylene-vinylene)", *Appl. Phys. Lett.* **80**, p716, 2002

[35] G. A. Turnbull, T. F. Krauss, W. L. Barnes, I. D. W. Samuel, "Tunable distributed feedback lasing in MEH-PPV films", *Synth. Met.* **121**, p1757, 2001

[36] M. D. McGehee, M. A. Diaz-Garcia, F. Hide, R. Gupta, E. K. Miller, D. Moses, A. J. Heeger, "Semiconducting polymer distributed feedback lasers", *Appl. Phys. Lett.* **72,** p1536, 1998

[37] X. L. Zhu and D. Lo, "Distributed feedback sol-gel dye laser tunable in the near ultraviolet", *Appl. Phys. Lett.* **77**, p2647, 2000

[38] F. Chen, J. Wang, C. Ye, W. H. Ni, J. Chan, Y. Yang, and D. Lo, "Near infrared distributed feedback lasers based on LDS dye doped

zirconia-organically modified silicate channel waveguides", *Opt. Express*, **13**, p1643, 2005

[39] X. L. Zhu, S. K. Lam, and D. Lo, "Distributed-feedback dye-doped solgel silica lasers", *Appl. Opt.* **39**, p3104, 2000

[40] X. L. Zhu, D. Lo, "Temperature tuning of output wavelength for solid-state dye lasers", *J. Opt. A-Pure Appl. Opt.* **3**, p225, 2001

[41] X. L. Zhu and D. Lo, "Sol-gel glass distributed feedback waveguide laser", *Appl. Phys. Lett.* **80**, p917, 2002

[42] J. Wang, G. X. Zhang, L. Shi, D. Lo, and X.-L. Zhu, "Tunable multiwavelength distributed-feedback zirconia waveguide lasers", *Opt. Lett.* **28**, p90, 2003

[43] F. Sobel, D. Gindre, J.-M. Nunzi, C. Denis, V. Dumarcher, C. Fiorini Debuisschert, K. P. Kretsch, and L. Rocha, "Multimode distributed feedback laser emission in a dye-doped optically pumped polymer thin-film", *Opt. Mater.* **27**, p199, 2004

[44] W. Holzer, A. Penzkofer, A. Lux, H.-H. Hörhold, and E. B. Kley, "Photo-physical and lasing characterisation of neat films of a thianthrene-substituted distyrylbenzene dye (Thianthrene-DSB)", *Synth. Met.* **145**, p119, 2004

[45] J. F. Pinto and L. Esterowitz, "Distributed-feedback, tunable Ce^{3+}-doped colquiriite lasers", *Appl. Phys. Lett.* **71**, p205, 1997

[46] K. Kawamura, M. Hirano, T. Kurobori, D. Takamizu, T. Kamiya, and H. Hosono, "Femtosecond-laser-encoded distributed-feedback color

centre laser in lithium fluoride single crystals", *Appl. Phys. Lett.* **84**, p311, 2004

[47] D. V. Martyshkin, J. G. Parker, V. V. Fedorov and S. B. Mirov, "Tunable distributed feedback color centre laser using stabilized F_2^+** color centres in LiF Crystal", *Appl. Phys. Lett.* **84**, p3022, 2004

[48] T. Matsui, M. Ozaki, and K. Yoshino, "Electro-tunable laser action in a dye-doped nematic liquid crystal waveguide under holographic excitation", *Appl. Phys. Lett.* **83**, p422, 2003

[49] T. Matsui, M. Ozaki, and K. Yoshino, "Single-Mode Operation of Electrotunable Laser in a Dye-doped Nematic Liquid-Crystal Waveguide under Holographic Excitation", *Jpn. J. Appl. Phys.* **42**, pL1462, 2003

[50] R. Jakubiak, L. V. Natarajan, V. Tondiglia, G. S. He, P. N. Prasad, T. J. Bunning and R. A. Vaia, "Electrically switchable lasing from pyrromethene 597 embedded holographic-polymer dispersed liquid crystals", *Appl. Phys. Lett.* **85**, p6095, 2004

[51] V. Hsiao, C. Lu, G. S. He, M. Pan, A. N. Cartwright, P. N. Prasad, "High contrast switching of distributed-feedback lasing in dye-doped H-PDLC transmission grating structures", *Opt. Express* **13**, p3787, 2005

[52] D. E. Lucchetta, L. Criante, O. Francescangeli, F. Simoni, "Compact lasers based on HPDLC gratings", *Mol. Cryst. Liq. Cryst.* **441**, p97, 2005

[53] S. T. Wu and A. Y. G. Fuh, "Lasing in Photonic Crystals based on Dye-doped Holographic Polymer-Dispersed Liquid-Crystal Reflection Gratings", *Jpn. J. Appl. Phys.* **44**, p977, 2005

[54] V. I. Kopp, B. Fan, H. K. M. Vithana, A. Z. Genack, "Low threshold lasing at the edge of a photonic stop band in cholesteric liquid crystals", *Opt. Lett.* **23**, p1707, 1998

[55] V. I. Kopp, Z.-Q. Zhang, A. Z. Genack, "Lasing in chiral photonic structures", *Process in Quantum Electronics* **27**, p369, 2003

[56] G. Chilaya, A. Chanishvili, G. Petriashvili, R. Barberi, M. P. De Santo, M. A. Matrange, "Enhancing cholesteric liquid crystal laser stability by cell rotation", *Opt. Express* **14**, p9939, 2006

[57] Y. Zhou, Y. H. Huang, Z. B. Ge, L.-P. Chen, Q. Hong, T. X. Wu, S.-T. Wu, "Enhanced photonic band edge laser emission in a cholesteric liquid crystal resonator", *Phys. Rew.* **74**, p061705, 2006

[58] Y. Matsuhisa, Y. H. Huang, Y. Zhou, S.-T. Wu, Y. Takao, A. Fujii, M. Ozaki, "Cholesteric liquid crystal laser in a dielectric mirror cavity upon band-edge excitation", *Opt. Express* **15**, p616, 2007

[59] Y. Matsuhisa, Y. H. Huang, Y. Zhou, S.-T. Wu, R. Ozaki, Y. Takao, A. Fujii, M. Ozaki, "Low-threshold and high efficiency lasing upon band-edge excitation in a cholesteric liquid crystal", *Appl. Phys. Lett.* **90**, p091114, 2007

Chapter II

Theories of Distributed Feedback Dye Lasers in Reflection Pumping Configuration

2.1 Coupled-wave theory of distributed feedback lasers [1]

2.1.1 Coupled-wave model

Distributed feedback (DFB) laser action is made by the presence of periodic perturbations in the gain medium that provide feedback by backward Bragg scattering [2]. Instead of the conventional cavity mirrors, the feedback for lasing oscillation was provided via backward Bragg scattering in periodic structures. So the DFB structures are compact and provide a spectral selection of high degree. The periodic perturbations can be realized from the spatial modulation of the refractive index [2] or gain, or a combination of both [3]. In a waveguide structure, a periodic change of the guiding film thickness was also proven effective in producing DFB laser action [4].The periodic perturbations can be permanent or transient, with the transient effect often produced by crossing two beams from the output of the same laser to generate a concentration grating [3, 5]. The linear coupled-wave model based on the scalar wave equation developed by Kogelnik and Shank is described in this thesis.

Figure 2.1 shows a simplified illustration which demonstrates the oscillation mechanism of a DFB structure. There are two waves in the diagram represented by arrows, one of which travels to the left and the other to the right.

As each wave travels in the periodic structure, it receives light at each point along its path by Bragg scattering from the oppositely traveling wave. This creates a feedback mechanism which is distributed throughout the length of the periodic structure. So we name it as "distributed feedback". Since the periodic structure has gain, with sufficient feedback, there will be a condition for laser oscillation. Also, spectral selection occurs due to the wavelength sensitivity of the Bragg effect.

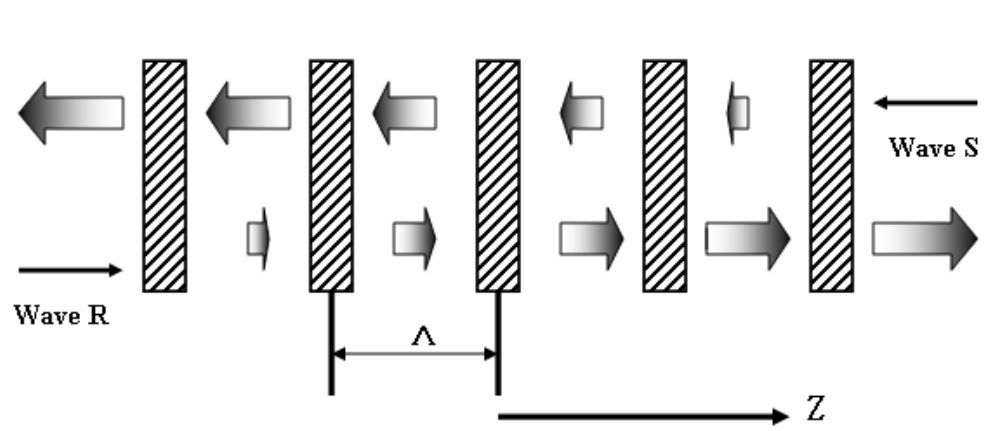

(a)

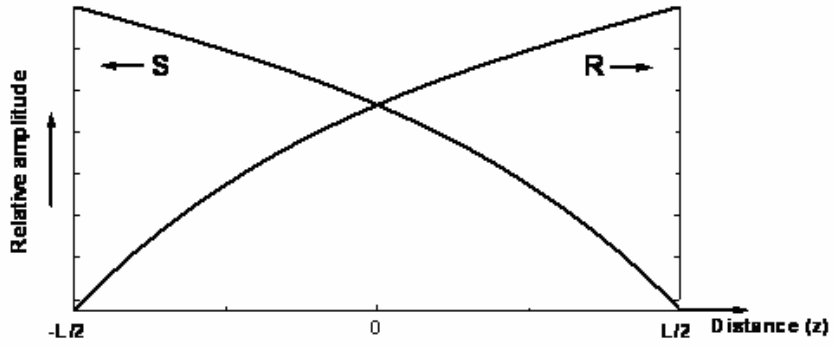

(b)

Fig. 2.1 (a) Illustration demonstrating laser oscillation in a periodic structure. (b) Plot of the amplitudes of left traveling wave S and right traveling wave R vs. distance.

Coupled-wave theory of DFB lasers is a linear theory. A linear analysis is made to describe the modes of a DFB structure, and to predict the resonant

frequencies, the corresponding threshold gain and the spectral selectivity. Nonlinear effect such as gain saturation is not considered. The model is based on the scalar wave equation for the electric field

$$\frac{\partial^2}{\partial z^2}E + k^2 E = 0, \tag{2.1}$$

where E is the complex amplitude of a field of angular frequency ω, which is assumed to be independent of the x and y coordinates. The constants of the laser medium are also independent of x and y, but vary periodically as a function of the z coordinate, which points in the direction of propagation (Fig.2.1).

We assume a spatial modulation of the refractive index $n(z)$ and of the gain constant $\alpha(z)$ of the form

$$\begin{aligned} n(z) &= n + n_1 \cos 2\beta_0 z, \\ \alpha(z) &= \alpha + \alpha_1 \cos 2\beta_0 z, \end{aligned} \tag{2.2}$$

where n and α are the average values of the parameters of the medium and n_1 and α_1 are the amplitudes of the spatial modulation. At the Bragg condition we have

$$\beta_0 = n\omega_0 / c = n\omega / c, \tag{2.3}$$

which implies a spatial periodicity π / β_0 equal to half the wavelength λ / n of the light in the medium. In addition, it is assumed that the DFB laser oscillates at or near the Bragg frequency ω_0 (i.e., $\omega \approx \omega_0$), that the gain is small over distance of the order of a wavelength λ_0, and that the perturbation of the refractive index and the gain are small, i.e.,

$$\begin{aligned} &\alpha \ll \beta_0 \equiv 2\pi n / \lambda_0, \\ &n_1 \ll n, \\ &\alpha_1 \ll \beta_0. \end{aligned} \tag{2.4}$$

These assumptions, discussed in greater detail in [6], allow us to write the k constant of the wave equation (2.1) in the form

$$k^2 = \beta^2 + 2j\alpha\beta + 4\kappa\beta\cos 2\beta_0 z, \tag{2.5}$$

where $\beta = n\omega / c$ and the coupling constant κ is defined by

$$\kappa = \pi n_1 / \lambda_0 + \tfrac{1}{2} j\alpha_1. \tag{2.6}$$

The coupling constant is a central parameter of this model. It measures the strength of the backward Bragg scattering and thus the amount of feedback (per unit length) provided by the structure.

In principle, a periodic perturbation of the medium generates an infinite set of diffraction orders. But in the vicinity of the Bragg frequency only two orders are in phase synchronism and of significant amplitude. All other orders are neglected in the coupled-wave model [6]. As indicated in Fig. 2.1 (b), the two significant waves in the DFB structure are two counter-propagating waves R and S. These waves grow because of the presence of gain and they feed energy into each other due to Bragg scattering. We describe these waves by complex amplitudes R (z) and S (z), and write the electric field as the sum

$$E(z) = R(z)\exp(-j\beta_0 z) + S(z)\exp(j\beta_0 z). \tag{2.7}$$

In view of Eq. (2.4) these amplitudes are varying slowly so that their second derivatives $\partial^2 R / \partial z^2$ and $\partial^2 S / \partial z^2$ can be neglected [6].

With all these assumption we insert Eq. (2.7) into the wave equation, compare terms with equal exponentials, and obtain a pair of coupled-wave equations of the form

$$\begin{aligned} -R' + (\alpha - j\delta)R &= j\kappa S, \\ S' + (\alpha - j\delta)S &= j\kappa R. \end{aligned} \tag{2.8}$$

The parameter δ is a normalized frequency parameter defined by

$$\delta \equiv (\beta^2 - \beta_0^2)/2\beta \approx \beta - \beta_0 = n(\omega - \omega_0)/c. \tag{2.9}$$

It is a measure for the departure of the oscillation frequency ω from the Bragg frequency ω_0. At the Bragg condition, we have $\delta = 0$.

The coupled-wave equations (2.8) describe wave propagation in the DFB structure in the presence of a gain and periodic perturbations of the medium. Since this model is that of a self-oscillating device, there are no incoming waves, and the internal waves start with zero amplitudes at the device boundaries, receiving their initial energy via scattering from the counter-running wave, we consider a structure of length L, extending from $z = -\frac{1}{2}L$ to $z = \frac{1}{2}L$. The boundary condition for the wave amplitudes are then

$$R(-\tfrac{1}{2}L) = S(\tfrac{1}{2}L) = 0. \tag{2.10}$$

The coupled-wave equations (2.8) together with the boundary conditions of (2.10) specify the electromagnetic field in this model of the DFB laser. The corresponding solution yields self-consistent steady-state field configurations or oscillation states, i.e., the "modes" of the periodic structure.

The general solution to the coupled-wave equations (2.8) is of the form

$$\begin{aligned} R &= r_1 e^{\gamma z} + r_2 e^{-\gamma z}, \\ S &= s_1 e^{\gamma z} + s_2 e^{-\gamma z}, \end{aligned} \tag{2.11}$$

with the complex propagation constant γ obeying the dispersion relation

$$\gamma^2 = \kappa^2 + (\alpha - j\delta)^2. \tag{2.12}$$

Because of the assumed symmetry of the device, symmetric $[E(-z) = E(z)]$ and anti-symmetric $[E(-z) = -E(z)]$ field solutions can be got, which implies the relationships

$$\begin{aligned} r_1 &= \pm s_2, \\ r_2 &= \pm s_1. \end{aligned} \tag{2.13}$$

The boundary condition (2.10) provides a further set of relations, namely,

$$r_1 / r_2 = s_2 / s_1 = -e^{\gamma L}. \tag{2.14}$$

Using the above results, the longitudinal field distribution of the modes of a DFB structure can be described in the compact form

$$\begin{aligned} R &= \sinh \gamma(z + \tfrac{1}{2}L), \\ S &= \pm \sinh \gamma(z - \tfrac{1}{2}L) \end{aligned} \tag{2.15}$$

where L is the length of the structure. A discrete set of eigenvalues γ corresponds to a set of modes and this set corresponds to a structure with given length and given coupling κ. To determine the eigenvalues, insert (2.15) into the coupled-wave equations (2.8), form the sum and the difference of the resulting equations, and obtain

$$\begin{aligned} \gamma + (\alpha - j\delta) &= \pm j\kappa e^{\gamma L}, \\ \gamma - (\alpha - j\delta) &= \mp j\kappa e^{-\gamma L}. \end{aligned} \tag{2.16}$$

Note that one obtains dispersion relation (2.12) by multiplying these two expressions. Addition of the two expressions yields a transcendental equation for the eigenvalue γ

$$\kappa = \pm j\gamma / \sinh \gamma L. \tag{2.17}$$

These eigenvalues are generally complex valued and each value of γ has a corresponding threshold gain constant α and a resonant frequency δ. They obey the relation

$$\alpha - j\delta = \pm j\kappa \cosh \gamma L = \gamma \coth \gamma L, \tag{2.18}$$

which is derived by subtraction of equations (2.16).

Hereto, the (threshold) modes of the DFB structure have been obtained from the above solutions of the coupled-wave equations. For a given length L and coupling κ, the eigenvalue γ of each mode can be calculated by solving equation (2.17), to obtain the characteristic field pattern, the characteristic threshold gain and the resonant frequency of each mode.

2.1.2 Approximate results

A. High-Gain Approximations

In the limit where $\alpha \gg \kappa$, an approximate expression for γ from Eq. (2.12), which is

$$\gamma \approx \alpha - j\delta. \tag{2.19}$$

Inserting this into the first of equations (2.16), we get

$$2(\alpha - j\delta) \approx j\kappa \exp(\alpha - j\delta)L. \tag{2.20}$$

The absolute value of Eq. (2.20) gives the threshold condition

$$4(\alpha^2 + \delta^2) \approx \kappa\kappa^* e^{2\alpha L}, \tag{2.21}$$

In the vicinity of the Bragg frequency $\delta = 0,$ which can be written as

$$4\alpha^2 e^{-2\alpha L} \approx (\pi n_1 / \lambda)^2 + \tfrac{1}{4}\alpha_1^2. \tag{2.22}$$

Equation (2.21) also gives us an idea about the spectral selectivity of the DFB structure. For example, for a frequency deviation from the Bragg frequency of

$$\delta = \alpha , \tag{2.23}$$

the power coupling $\kappa\kappa^*$ has to be doubled to keep the threshold gain the same. With Eq. (2.9), Eq. (2.23) can be written in the form

$$\Delta\lambda / \lambda \approx \alpha\lambda / 2\pi n = \alpha / \beta, \tag{2.24}$$

where $\Delta\lambda$ is the wavelength deviation from the Bragg condition. For devices with fixed gain $e^{2\alpha L}$, the spectral selectivity is inversely proportional to the device length L.

Comparing the phases in Eq. (2.20), we can get the resonant condition for $\delta \ll \alpha$, i.e., near the Bragg frequency ν_0,

$$\delta L = (q + \tfrac{1}{2})\pi + phase(\kappa), \tag{2.25}$$

where q is an integer. Rewrite this in terms of the resonant frequencies $\nu = \omega / 2\pi$ as

$$(\nu - \nu_0)(c / 2nL)^{-1} \approx q + \tfrac{1}{2} + (\tfrac{1}{\pi})phase(\kappa). \tag{2.26}$$

So the resonances are spaced approximately $c / 2nL$ apart, which is the same as in a usual two-mirror laser cavity of length L. For index coupling (κ real), there is no resonance at the Bragg frequency ν_0, while for gain coupling (κ imaginary) there is a resonance exactly at $\nu = \nu_0$.

B. Low-gain Approximations

For the limit of low gain $\alpha \ll \kappa$, we start by separating Eqs. (2.17) and (2.18) into their real and imaginary parts, near $\alpha = 0$, we can get the following results:

For index coupling the first resonances are near $\delta \approx \kappa$, i.e., just outside *the stop band* (in the next section). The threshold condition becomes

$$\alpha L \approx (\lambda / n_1 L)^2. \tag{2.27}$$

For gain coupling near $\alpha \approx 0$, there exists a resonance which is exactly at the Bragg frequency, i.e., $\delta = 0$. It is the same as high-gain limit. The threshold is of the form

$$\alpha_1 \approx \pi / L. \tag{2.28}$$

2.1.3 Stop band, Dispersion and Mode Spectra

It is well known [7] that periodic structures are dispersive and they have stop bands of frequencies in which propagation is forbidden. Applying questions of this kind to the coupled-wave model, the character of the dispersion curves has a profound influence on the resonance spectrum of the DFB structure.

In the last section, we have learned that there exist four waves in the structure, and they propagate as $\exp\left[\pm(j\beta_0 \pm \gamma)z\right]$. The complex propagation constant γ is determined by the dispersion relation Eq. (2.12).

A. Index coupling

Examine a gain-free structure, with $\alpha = 0$ and κ real (i.e., "index coupling"). In this case, Eq. (2.12) yields imaginary values for γ if $\delta^2 > \kappa^2$, and real γ values for $\delta^2 < \kappa^2$. The dispersion curves are sketched in Fig. 2.2

(a), where the propagation constants ($\beta_0 \pm \mathrm{Im}\,\gamma$) are plotted as a function of ω/c. There is a stop band centered at the Bragg frequency ω_0, in which real γ values indicate evanescent waves. The width of the band is 2κ. Outside the stop band the dispersive curve is a hyperbola which approaches asymptotically the line where the propagation constant equals ω/c, and the reflection of that line through the Bragg frequency.

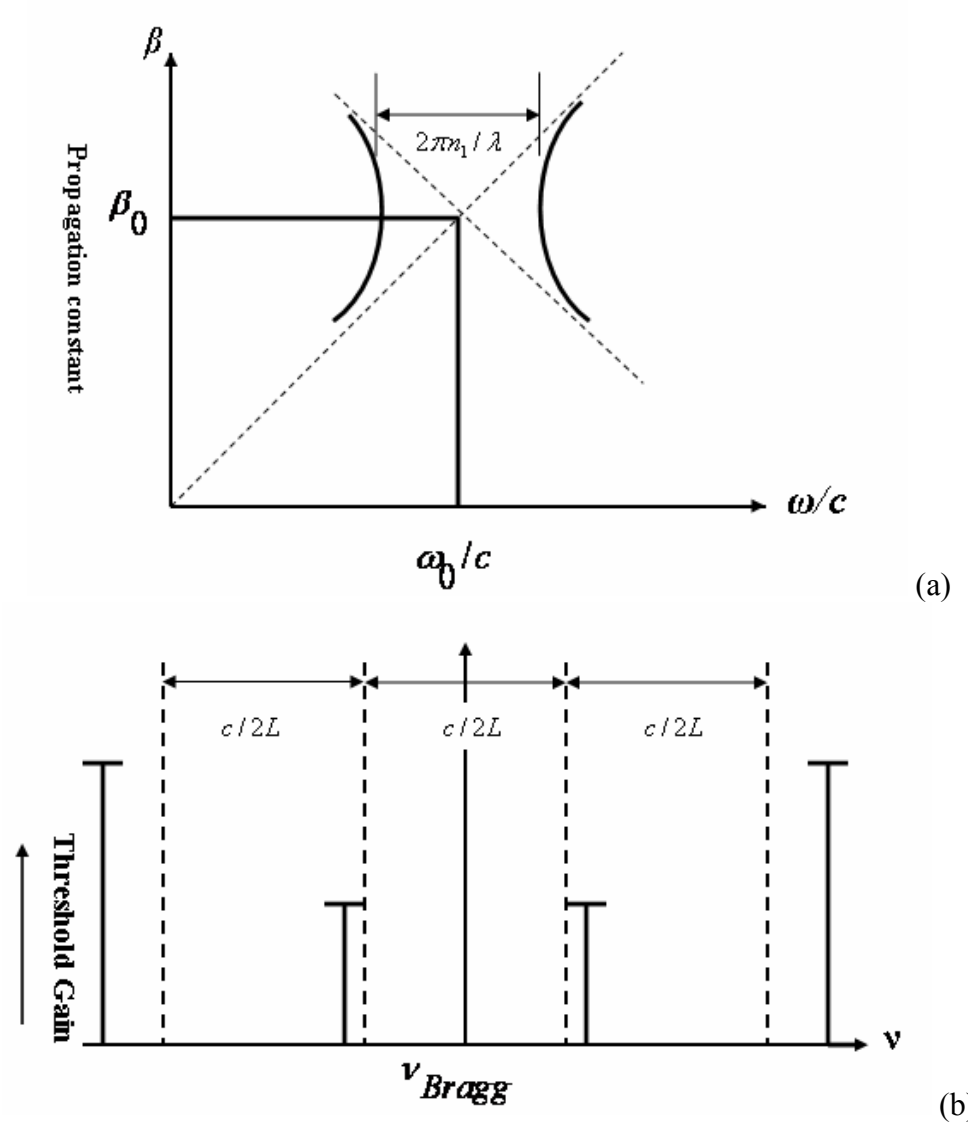

Fig. 2.2 (a) Dispersion diagram for index modulation with no loss or gain. (b) Diagram illustrating the mode spectrum and required threshold gains for an index periodicity.

Figure 2.2 (b) shows the resonant characteristic spectrum of the modes of the periodic structure for the case of index coupling. The dashed lines indicate the basic $c/2nL$ frequency spacing, which is equal to the longitudinal mode spacing of a two-mirror laser cavity of the same length L as the DFB structure. We see that the mode spectrum is symmetric with respect to the Bragg frequency ν_0, and there is *no resonance* at ν_0. The stop band is centered at ν_0, and it prevents all oscillations inside the band. As the band increases with increasing coupling κ, it eventually becomes comparable to $c/2nL$ and starts pushing the resonances away from ν_0. A small amount of pushing is shown in Fig. 2.2 (b). The threshold gain of the modes is also indicated, which increases with the frequency spacing from ν_0. This provides the spectral selectivity of the structure.

B. Gain coupling

Consider the dispersion of a structure with zero average gain ($\alpha = 0$) and "gain coupling" (κ imaginary), again, hyperbolic dispersion curves with the same asymptotes as in the case of index coupling are shown in Fig. 2.3 (a). But the curves are turned by 90^o. There is no stop band in frequency. We have, however, a forbidden band of propagation constants with the width of α_1, and again, centered at the Bragg condition.

The resonance spectra of the case of gain coupling ($n_1 = 0$) is indicated in Fig. 2.3 (b). There is a resonance exactly at the Bragg condition. As in the case of index coupling, the spectrum is symmetric with respect to the Bragg frequency ν_0, the threshold increase with the spacing from ν_0, and the modes oscillate near the $c/2nL$ resonances when the coupling is small. There are no

frequency stop bands for gain coupling, but the dispersion of the periodic structure produces shifts in the resonances when the coupling gets larger.

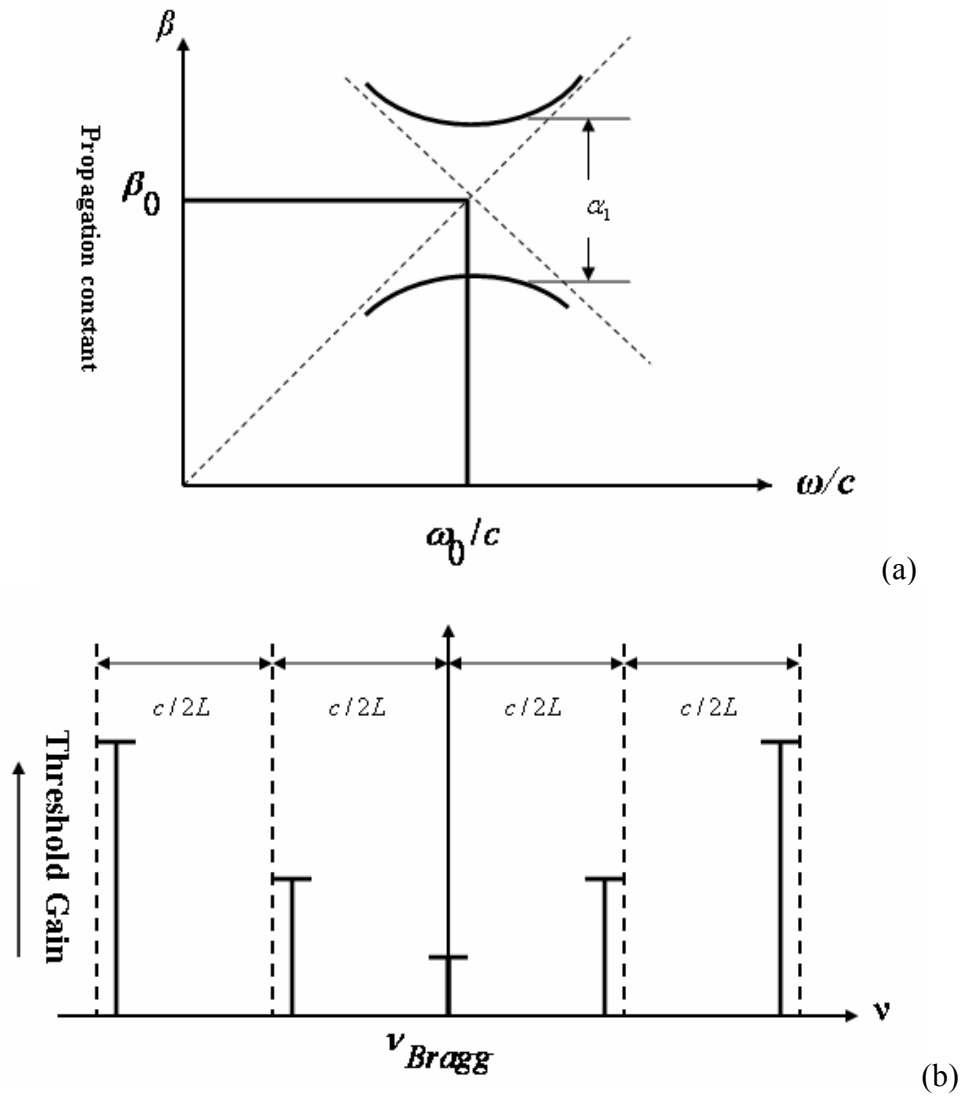

Fig. 2.3 (a) Dispersion diagram for gain modulation with no average loss or gain. (b) Diagram illustrating the mode spectrum and required threshold gains for a gain periodicity.

The above discussions only concern about the limiting cases of index coupling and gain coupling. In practice, mixed cases may occur. The mode spectra are no longer symmetric. The location of the corresponding $c/2nL$ resonances will shift by an amount dependent on the coupling mixture as given by Eq. (2.26).

2.2 Configurations of one dimensional (1-D) DFB lasers

2.2.1 Introduction

DFB lasers have been studied extensively in various configurations since the first observation of the laser oscillation in a periodic structure in rhodamine 6G (R6G) dissolved gelatin films by H. Kogelnik and C. V. Shank in 1970 [2], and followed by their realizations of tunable DFB lasers and higher-order DFB oscillators in R6G doped ethanol [3, 8].

There have been many techniques employed to induce a gain and/or an index modulation in laser media, with the objective to get a 1-D DFB structure for lasing oscillation: Room-temperature nanoimprint lithography (RT-NIL) [9, 10]; electron beam lithographically patterning and subsequent dry etching in thick SiO_2 layers [11, 12]; direct electron beam lithography on conjugated polymers[13]; spin coating and alternate stacking of high and low refractive-index polymers (1-D photonic crystal (PC)) [14]; UV embossing process in combination with producing the stamper [15, 16]; spatially modulating the pump intensity, and thereby the gain and/or index , by interfering two coherent beams at the proper angles in the active laser media [17-20]. Holographic photopolymerization for creating a reflection PC DFB structure in polymer-dispersed liquid crystal (H-PDLC) system was used to demonstrate DFB lasing action [21-24]. Cholesteric liquid crystals (CLCs), due to their inherent natural periodicity caused by their self-organized helical structure were widely adopted to realize DFB lasing [25-27]. Surface relief gratings (SRGs) on the surfaces of azobenzene-containing polymers (azo-polymers) films were also investigated to have effective feedback for lasing oscillation, which are induced by the self-

organization of the azo-polymers into regular structures on micrometer or nanometer scales when assisted by light [28-29].

The above-mentioned 1-D DFB structures for lasing oscillation were either permanent grating or dynamic (transient) gratings. With the scientific terms in the standard holography, they can be classified into two categories: transmission gratings and reflection gratings. Namely, generally speaking, the 1-D DFB lasers were operated in transmission grating geometry or reflection grating geometry.

The following figure shows several 1-D DFB laser configurations:

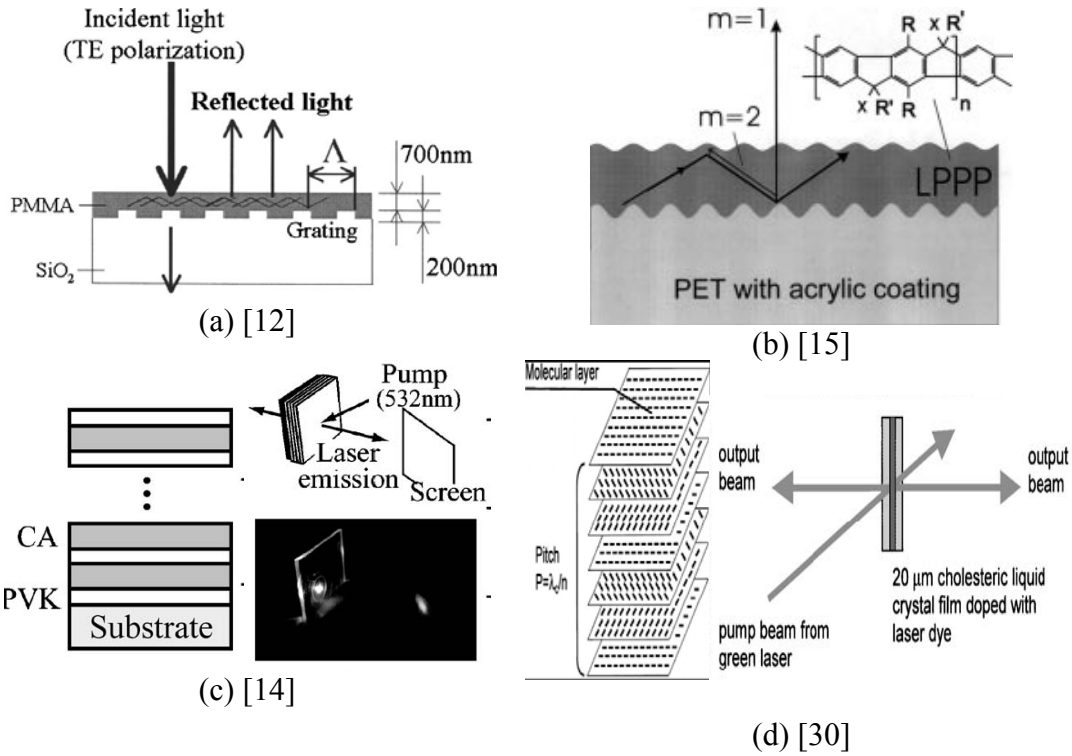

Fig. 2.4 Several configurations of 1-D distributed feedback lasers

In Fig. 2.4, (a) and (b) are 1-D DFB structures in transmission grating geometry; while (c) and (d) are in reflection grating geometry. The periodic

perturbations were formed by periodic spatial corrugations on the surfaces of the samples ((a) and (b)), or periodic dielectric layers ((c) and (d)). The same point is: they are all operated in a *permanent* DFB structure.

Thereafter, I will concentrate on the discussion of 1-D *dynamic* DFB structures induced by the interference of two coherent pumping beams at a variable intersection angle in a laser medium. During the past years, the 1-D DFB lasers were intensively demonstrated in a transient transmission grating geometry. Lo's group successfully realized tunable DFB lasers in different waveguides using two crossing pump beams [17-20, 31-35]. There were also kinds of DFB lasers obtained by adopting the Lloyd mirror device [36-38]. Fig. 2.5 shows these two kinds of devices.

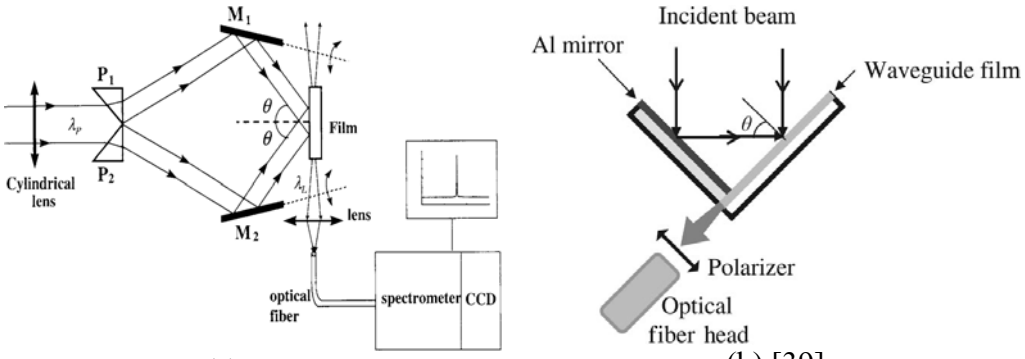

(a) [35] (b) [39]

Fig. 2.5 Several configurations of 1-D dynamic distributed feedback lasers. (a) Two crossing beams configuration; (b) Lloyd-mirror configuration.

For the transmission grating pumping geometry mentioned, the two interfering beams reach the sample from the same side, the vector of the so-called transmission grating is parallel to the sample surface (Fig. 2.7(a)), i.e., the cell surface for a solution sample or the substrate for a thin-film sample. In contrast, when the two interfering beams reach the sample from opposite sides,

the so-called reflection DFB grating would be generated, the grating vector is perpendicular to the sample surface (Fig. 2.7(b)). To the best of our knowledge, there have not been reports on *dynamic* DFB laser action in the reflection pumping geometry. In our recent work, we realized the configuration for DFB lasing output (in Fig. 2.6) [40].

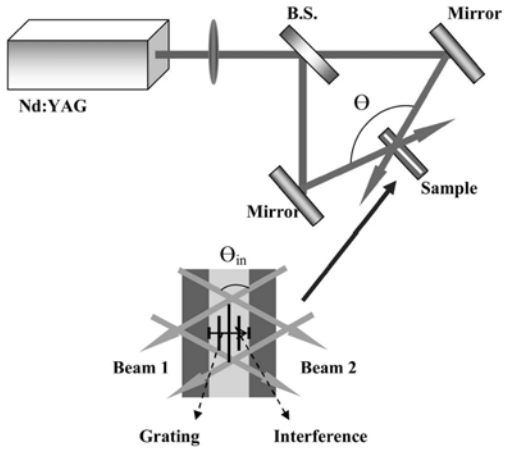

Fig. 2.6 Experimental setup used for DFB lasing based on the reflection grating geometry [40]

2.2.2 Dynamics of the transmission and reflection grating geometries

In 2.2.1, we have concluded the 1-D dynamic DFB lasers in transmission pumping and reflection pumping. Fig. 2.7 shows the simplified geometries for both cases. In the following, the tuning equations for the two kinds of DFB lasers will be deduced.

A. Transmission pumping geometry

In Fig. 2.7 (a), the period of the interference patterns of gain and/or index modulations induced in the active layers by the two coherent pumping beams can be expressed by

$$\Lambda = \lambda_p / 2\sin\theta \tag{2.29}$$

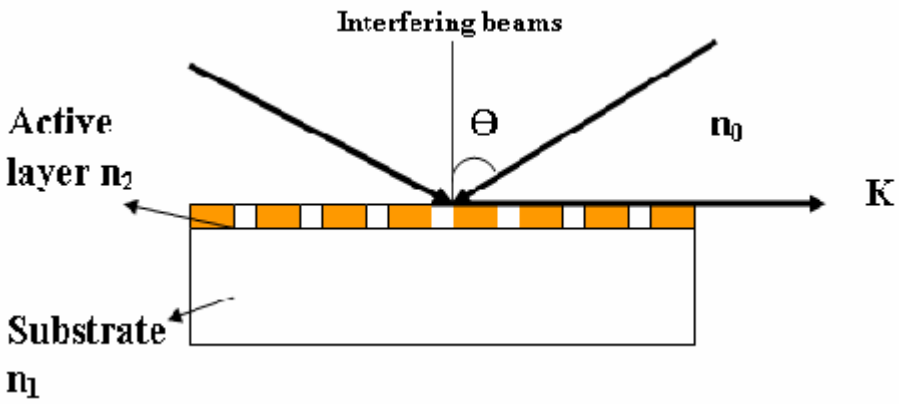

(a) Transmission grating pumping

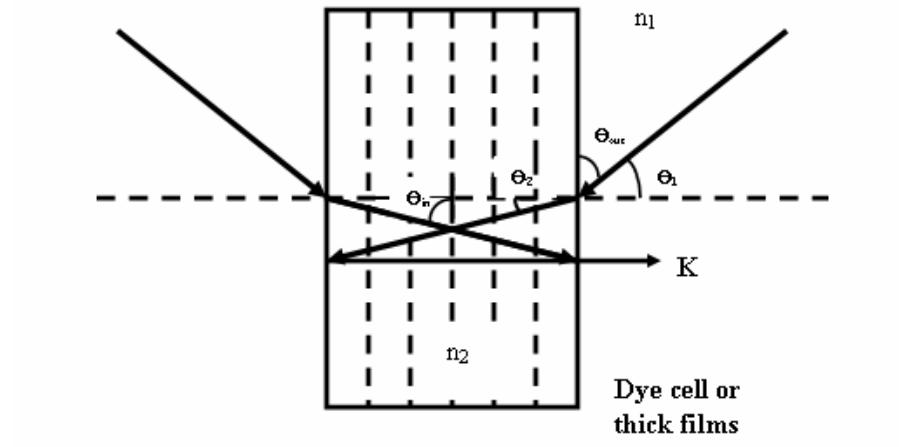

(b) Reflection grating pumping

Fig. 2.7 Two pumping geometries

where λ_p is the wavelength of the pump laser source, θ is the pump beam intersection angle at the laser gain medium. The variation of the period of the modulations can be achieved by continuous variation of the intersection angle. Distributed feedback occurs near the Bragg condition [1]:

$$2\vec{k}\bullet\vec{K} = \left|\vec{K}\right|^2 \tag{2.30}$$

where the wavevector of the guided mode is $\vec{k} = n_{eff}\vec{k}_0$ ($\vec{k}_0$ is the free-space vector) and $\vec{K}$ denotes a vector of the reciprocal lattice of the periodic modulation with $\left|\vec{K}\right| = M\bullet 2\pi\Lambda^{-1}$, M is the Bragg reflection order. n_{eff} is the effective index of the waveguiding modes at laser oscillations, as determined

by the guide parameters and the modes being considered. When the DFB tuning was operated in a bulk laser media, n_{eff} will only be dependent on the refractive index at the lasing wavelength [41, 42]. Combing Eq. (2.29) and Eq. (2.30), we can obtain the spectral selection equation in transmission pumping:

$$\lambda_L = \frac{n_{eff}\lambda_p}{M \sin\theta}. \tag{2.31}$$

This equation is the theoretical base of the wavelength tuning of DFB lasers. Tunable DFB laser emission has been demonstrated in active planar waveguides [17, 18, 35-37] and channel waveguides respectively [19, 20]. The DFB lasing action obeys the mode and propagation properties of the 1-D and 2-D waveguides, presented by the effective indices of the waveguides.

B. Reflection pumping geometry

For the reflection pumping geometry, the key point is: the periodic spatial pattern inside the gain medium is formed by the interference of the two pumping beams after their refraction at the interfaces between the sample and air. The grating planes are parallel to the sample surface, and the lasing is emitted normal to the substrate. In Fig. 2.7 (b), according to the Snell's Law: $n_1 \sin(90-\theta_{out}) = n_2 \sin\theta_2$, one can get $n_1 \cos\theta_{out} = n_2 \cos\theta_{in}$. The period of the interference pattern can be referred as:

$$\Lambda = \lambda_p / 2n_2 \sin\theta_{in}, \tag{2.32}$$

In combination with the Bragg condition Eq. (2.30), we can obtain the tuning equation in reflection pumping geometry as follows:

$$\lambda_L = \frac{\lambda_p}{M \sin\theta_{in}}. \tag{2.33}$$

Comparing Eq. (2.33) with Eq. (2.31), one can see an obvious difference of the tuning behaviors between the transmission pumping and reflection pumping. The DFB lasing wavelength is independent on the refractive indices of the laser media. We will verify this effect in our experiments in the following chapter.

2.3 One-dimensional photonic crystal

Photonic crystals (PCs) possessing a periodic dielectric structures with a periodicity in a range of optical wavelength attract considerable interest from both fundamental and technological viewpoints since their pioneering works by Yablonovitch [43] and John [44]. In PCs, the propagation of light is inhibited in a certain energy range of photons, which results in the appearance of a photonic bandgap (PBG) [43]. It is in an analogy with energy gap in semiconductors, which is produced by coherent scattering of the electronic wavefunction in the periodic potential of the crystal lattice.

Within the photonic bandgap, the wave is evanescent and decays exponentially; the density of states (DOS) within the gap vanishes in large structures. Since the rate of the spontaneous emission is proportional to the DOS, spontaneous emission is suppressed within the gap [43, 44]. A simplified PC is a 1-D system consisting of an alternating layers of material with dielectric constants of ε_a and ε_b (refractive indices, $n_a = \sqrt{\varepsilon_a}$ and $n_b = \sqrt{\varepsilon_b}$), the analytical result has been obtained for the optical properties of such multilayer

systems [45, 46]. A representative case of such a multilayer system is the quarter-wave stack, called a DFB reflector. In the laying direction, wavefunctions of the electric or magnetic fields are Bloch waves and stop bands exist. Fig. 2.8 shows the photonic band structure of a layered dielectric system.

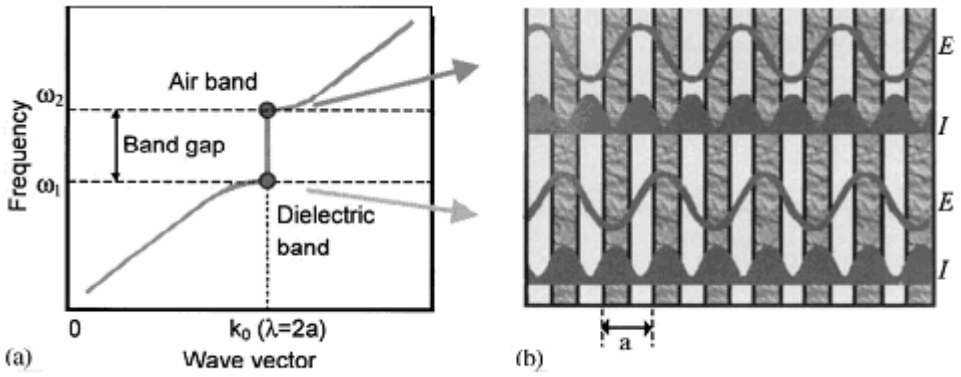

Fig. 2.8 (a) Photonic band structure of a layered dielectric system; (b) Dark and light layers correspond to high and low refractive indices, respectively. The electric field (E) and intensity (I) near the centre of the sample are shown [30].

Consider the index-coupling case in DFB lasers (in 2.1.3 A), when an index-modulation is induced in the laser media, then a periodical dielectric structure is generated, so it can be referred as a 1-D PC. In the case of small modulation of dielectric function ($\Delta n \approx 0.001$), the coupled-wave theory could be valid to explain the properties of DFB lasers. It will be verified in the experimental results in the following chapters.

Chiral liquid crystal (CLCs) containing optically active moieties show the spontaneous formation of supramolecular helical assemblages such as chiral nematic, blue, smectic phases as a result of their intrinsic helical twisting power [44]. Selection reflection of light is the unique optical property arising

from the supramolecular helical structures of CLCs. For instance, when the linearly polarized light propagates into right-handed chiral nematic liquid crystal (LC) layers in parallel with the helical axis, the right- and left-handed circularly polarized light are reflected and transmitted around the wavelength, respectively. The supramolecular helical assemblages regarding as 1-D polarization-dependent PBGs have made the potential use of the mirrorless laser action at the PBGs edges by the internal DFB effect. Low-threshold bandedge lasing was observed in the structure of CLCs [26]. During recently years, intensive interests have been drawn to realize DFB lasing effect in CLCs [47-52].

In our works, we successfully demonstrated tunable 1-D DFB lasers in reflection pumping geometry. A 1-D PC with tunable PBG was induced in DCM doped methanol; an index-coupling dominated the optical feedback. The width of the bandgap was proportional to the amplitude of the induced dielectric constant difference due to the Kerr-nonlinearity effect ($\varepsilon_{eff} = \varepsilon + \chi^{(3)} |E|^2$) caused by the interference of two coherent pumping beams. The detail results are included in Chapter IV. In Chapter V, we obtained chiral tunable DFB lasers in reflection pumping geometry. A tunable chiral PBG was generated by effectively controlling the polarization states of the two pumping beams. The spectra properties of DFB lasing output was in analogy with those in CLCs.

2.4 Summary

In this Chapter, the coupled-wave model of DFB lasers by Kogelnik and Shank was introduced. Based on the scalar wave equation, approximate results of the modes of DFB structures were deduced. Dispersion and Mode spectra were analyzed for two kinds of coupling existing in the DFB structures: gain coupling and index coupling, respectively. For the index coupling case, a weak index modulation due to a periodic dielectric layers was generated. A stop band centered at the Bragg frequency appeared in the mode spectra of the DFB structures.

Many kinds of 1-D DFB lasers of the state of art were illustrated. The dynamics of tunable DFB lasers by two interfering beams based on the traditional transmission grating geometry and our reflection grating geometry were compared in detail.

For better understanding the index modulation in the reflection DFB lasers, a simple introduction of 1-D PC was given.

References

[1] H. Kogelnik and C. V. Shank, “Coupled-wave theory of distributed feedback lasers”, *J. Appl. Phys.* **43**, p2327, 1972

[2] H. Kogelnik and C. V. Shank, “Stimulated emission in a periodic structure”, *Appl. Phys. Lett.* **18**, p152, 1971

[3] C. V. Shank, J. E. Bjorkholm and H. Kogelnik, “Tunable distributed-feedback dye laser”, *Appl. Phys. Lett.* **18**, p395, 1971

[4] D. P. Schinke, R. G. Smith, E. G. Spencer and M. F. Galvin, “Thin-film distributed feedback laser fabricated by ion milling”, *Appl. Phys. Lett.* **21**, p494, 1972

[5] J. E. Bjorkholm and C. V. Shank, “Distributed-Feedback Lasers in Thin-Film Optical Waveguides”, *IEEE J. Quantum Electron.* **8**, p833, 1972

[6] H. Kogelnik, “Coupled wave theory for thick hologram gratings”, *Bell System Tech. J.* **48**, p2909, 1969

[7] L. Brillouin, *Wave Propagation in Periodic Structures*, McGraw-Hill, New York, 1946

[8] J. E. Bjorkholm and C. V. Shank, “Higher-order distributed feedback oscillators”, *Appl. Phys. Lett.* **20**, p306, 1972

[9] P. Del Carro, A. Camposeo, R. Stabile, E. Mele, L. Persano, R. Cingolani, and D. Pisignano, “Near-infrared imprinted distributed feedback lasers”, *Appl. Phys. Lett.* **89**, p201105-1, 2006

[10] E. Mele, A. Camposeo, R. Stabile, P. Del Carro, “Polymeric distributed feedbacks by room-temperature nanoimprint lithography”, *Appl. Phys. Lett.* **89**, p131109, 2006

[11] C. Karnutsch, C. Gýrtner, V. Hang, U. Lemmer, T. Farrell, B. S. Nehls, U. Scherf, J. Wang, T. Weimann, G. Heliotis, C. Pflumm, J. C. deMello, and D. D. C. Bradley, “Low threshold blue conjugated polymer lasers with first- and second-order distributed feedback”, *Appl. Phys. Lett.* **89**, p201108, 2006

[12] T. Kobayashi, Y. Kanamori and K. Hane, “Surface laser emission from solid polymer dye in a guided mode resonant grating filter structure”, *Appl. Phys. Lett.* **87**, p151106, 2005

[13] R. Stabile, A. Camposeo, L. Persano, S. Tavazzi, R. Cingolani and D. Pisignano, “Organic-based distributed feedback lasers by direct electron-beam lithography on conjugated polymers” *Appl. Phys. Lett.* **91**, p101110, 2007

[14] T. Komikado, S. Yoshida and S. Umegaki, “Surface-emitting distributed-feedback dye laser of a polymeric multilayer fabricated by spin coating”, *Appl. Phys. Lett.* **89**, p061123, 2006

[15] C. Kallinger, M. Hilmer, A. Haugeneder, M. Perner, W. Spirkl, K. Müllen, A. Gombert, and V. Wittwer, “A flexible conjugated polymer laser”, *Adv. Mater*. **10**, p920, 1998

[16] S. Riechel, U. Lemmer, J. Feldmann, T. Benstem, W. kowalsky, U. Scherf, A. Gombert, V. Wittwer, “Laser modes in organic solid-state distributed feedback lasers”, *Appl. Phys. B* **71**, p897, 2000

[17] D. Lo, L. Shi, J. Wang, G.-X. Zhang and X.-L. Zhu, "Zirconia and zirconia-organically modified silicate distributed feedback waveguide lasers tunable in the visible", *Appl. Phys. Lett.* **81**, p2707, 2002

[18] J. Wang, G.-X. Zhang, L. Shi, D. Lo and X.-L. Zhu, "Tunable multiwavelength distributed feedback zirconia waveguide lasers", *Opt. Lett.* **28**, p90, 2003

[19] F. Chen, J. Wang, C. Ye, D. Lo and X.-L. Zhu, "Distributed feedback sol-gel zirconia channel waveguide lasers", *Appl. Phys. Lett.* **85**, p4284, 2004

[20] F. Chen, J. Wang, C. Ye, W. H. Ni, J. Chan, Y. Yang and D. Lo, "Near infrared distributed feedback lasers based on LDS dye-doped zirconia-organically modified silicate channel waveguides", *Opt. Express* **13**, p1643, 2005

[21] R. Jakubiak, T. J. Bunning, R. A. Vaia, L. V. Natarajan and V. P. Tondiglia, "Electrically Switchable, One-Dimensional Polymeric Resonators from Holographic Photopolymerization: A New Approach for Active Photonic Bandgap Materials", *Adv. Mater.* **15**, p241, 2003

[22] R. Jakubiak, L. V. Natarajan, V. Tondiglia, G. S. He, P. N. Prasad, T. J. Bunning and R. A. Vaia, "Electrically switchable lasing from pyrromethene 597 embedded holographic-polymer dispersed liquid crystals", *Appl. Phys. Lett.* **85**, p6095, 2004

[23] V. K. S. Hsiao, C. G. Lu, G. S. He, M. Pan, A. N. Cartwright, P. N. Prasad, R. Jakubiak, R. A. Vaia and T. J. Bunning, "High contrast

switching of distributed-feedback lasing in dye-doped H-PDLC transmission grating structures", *Opt. Express* **13**, p3787, 2005

[24] Y. J. Liu, X. W. Sun, P. Shum, H. P. Li, J. Mi, W. Ji and X. H. Zhang, "Low-threshold and narrow-linewidth lasing from dye-doped holographic polymer-dispersed liquid crystal transmission gratings", *Appl. Phys. Lett.* **88**, p061107, 2006

[25] A. Muñoz F., P. Palffy-Muhoray, and B. Taheri, "Ultraviolet lasing in cholesteric liquid crystals", *Opt. Lett.* **26**, p804, 2001

[26] V. I. Kopp, B. Fan, H. K. M. Vithana, A. Z. Genack, "Low-threshold lasing at the edge of a photonic stop band in cholesteric liquid crystals", *Opt. Lett.* **23**, p1707, 1998

[27] Y. H. Huang, L.-P. Chen, C. Doyle, Y. Zhou, and S.-T. Wu, "Spatially tunable laser emission in dye-doped cholesteric polymer films", *Appl. Phys. Lett.* **89**, p111106, 2006

[28] T. Ubukata, T. Isoshima, and M. Hara, "Wavelength-Programmable Organic Distributed-Feedback Laser Based on a Photoassisted Polymer-Migration System", *Adv. Mater.* **17**, p1630, 2005

[29] C. Ye, K. Y. Wong, Y. N. He and X. G. Wang, "Distributed feedback sol-gel zirconia waveguide lasers based on surface relief gratings", *Opt. Express* **15**, p936, 2007

[30] V. I. Kopp, Z.-Q. Zhang, A. Z. Genack, "Lasing in chiral photonic structures", *Progress in Quantum Electronics* **27**, p369, 2003

[31] L. Shi, G.-X. Zhang, J. Wang, and D. Lo, "Distributed feedback laser action in sol-gel glass symmetric waveguides", *J. Opt. A: Pure Appl. Opt.* **5**, pL1, 2003

[32] C. Ye, L. Shi, J. Wang, D. Lo, X.-L. Zhu, "Simultaneous generation of multiple pairs of transverse electric and transverse magnetic output modes from titania zirconia-organically modified silicate distributed feedback waveguide lasers", *Appl. Phys. Lett.* **83**, p4101, 2006

[33] D. Lo, C. Ye, J. Wang, "Distributed feedback laser action by polarization modulation", *Appl. Phys. B* **76**, p649, 2003

[34] C. Ye, J. Wang, D. Lo, "Two-photon-pumped distributed feedback zirconia waveguide lasers", *Appl. Phys. B* **78**, p539, 2004

[35] V. Dumarcher, L. Rocha, C. Denis, C. Fiorini, J.-M. Nunzi, F. Sobel, B. Sahraoui, D. Gindre, "Polymer thin-film distributed feedback tunable lasers", *J. Opt. A: Pure Appl. Opt.* **2**, p279, 2000

[36] N. Tsutsumi and A. Fujihara, "Tunable distribute feedback lasing with narrowed emission using holographic dynamic gratings in a polymeric waveguide", *Appl. Phys. Lett.* **86**, p061101, 2005

[37] D. Gindre, A. Vesperini, J.-M. Nunzi, H. Leblond and K. D. Dorkenoo, "Refractive-index saturation-mediated multiple line emission in polymer thin-film distributed feedback lasers", *Opt. Lett.* **31**, p1657, 2006

[38] D. C. Oliveira, Y. Messaddeq, K. Dahmouche, S. J. L. Ribeiro, R. R. Gonçalves, A. Vesperini, D. Gindre, J.-M. Nunzi, "Distributed

feedback multipeak laser emission in Rhodamine 6G doped organic-inorganic hybrids", *J. Sol-Gel Sci. Techn.* **40**, p359, 2006

[39] N. Tsutsumi, A. Fujihara and D. Hayashi, "Tunable distributed feedback lasing with a threshold in the nanojoule range in an organic guest-host polymeric waveguide", *Appl. Opt.* **45**, p5748, 2006

[40] F. Chen, D. Gindre and J.-M. Nunzi, "First-order distributed feedback dye laser effect in reflection pumping geometry", *Opt. Lett.* **32**, p805, 2007

[41] X. L. Zhu and D. Lo, "Distributed-feedback sol-gel dye laser tunable in the near ultraviolet", *Appl. Phys. Lett.* **77**, p2647, 2000

[42] X. L. Zhu and D. Lo, "Sol-gel glass distributed feedback waveguide laser", *Appl. Phys. Lett.* **82**, p917, 2002

[43] E. Yablonovitch, "Inhibited Spontaneous emission in Solid-state Physics and Electronics", *Phys. Rev. Lett.* **58**, p2059, 1987

[44] S. John, "Strong Localization of Photons in Certain Disordered Dielectric Superlattices", *Phys. Rev. Lett.* **58**, p2487, 1987

[45] J. M. Bendickson, J. P. Dowling, M. Scalora, "Analytic expressions for the electromagnetic mode density in finite, one-dimensional, photonic band-gap structures", *Phys. Rev. E* **53**, p4107, 1987

[46] J. P. Dowling and C. M. Bowden, "Atomic emission rates in inhomogeneous media with applications to photonic band structures", *Phys. Rev. A* **46**, p612, 1992

[47] H. Finkelmann, S. T. Kim, A. Muñoz, P. Palffy-Muhoray, B. Taheri, "Tunable Mirrorless Lasing in Cholesteric Liquid Crystalline", *Adv. Mater.* **13**, p1069, 2001

[48] M. Ozaki, M. Kasano, D. Ganzke, W. Hasse, K. Yoshino, "Mirrorless Lasing in a Dye-Doped Ferroelectric Liquid Crystal", *Adv. Mater.* **14**, p306, 2002

[49] J. Schmidtke, W. Stille, H. Finkelmann, S. T. Kim, "Laser Emission in a Dye Doped Cholesteric polymer network", *Adv. Mater.* **14**, p746, 2002

[50] T. Matsui, R. Ozaki, K. Funamoto, M. Ozaki, K. Yoshino, "Flexible mirrorless laser based on a free-standing film of photopolymerized cholesteric liquid crystal", *Appl. Phys. Lett.* **81**, p3741, 2002

[51] M. Ozaki, M. Kasano, T. Kitasho, D. Ganzke, W. Haase, and K. Yoshino, "Electro-Tunable Liquid Laser", *Adv. Mater.* **15**, p974, 2003

[52] A. Chanishvili, G. Chilaya, G. Petriashvili, R. Barberi, R. Bartolino, G. Lipparrone, A. Mazzulla, L. Orid, "Lasing in Dye-Doped Cholesteric Liquid Crystals: Two New Tuning Strategies", *Adv. Mater.* **16**, p791, 2004

Chapter III

Materials and Experimental Configuration

3.1 Materials

Organic laser dyes doped organic solvents and polymers were adopted as laser media in our dynamic reflection DFB lasers. Rhodamine 6G (R6G) and 4-dicyanomethylene-2-methyl-6-(*p*-dimethylaminostyryl)-4*H*-pyran-(DCM) were doped into ethanol and methanol, with desired concentrations, respectively, forming liquid solution laser media for lasing experiments. R6G doped poly(methyl methacrylate) (PMMA) thick films were prepared on glass substrates by cast-coating method, serving as solid state gain medium.

3.1.1 Organic laser dyes

Organic dyes, according to commonly accepted terminology, are a class of coloured substances which are useful for their ability to impact colour to other substances. The definition can be broadened to include organic compounds which have a strong absorption band somewhere from the ultraviolet to the near infrared. Organic compounds with this property contain an extended system of conjugated bonds (altering single and double bonds). Compared to gases and most solid state lasing media, a dye can usually be used for a much wider range of wavelengths. The wide bandwidth makes them particularly suitable for tunable lasers. Moreover, the dye can be replaced by another type in order to generate different wavelengths with the same laser.

The energy levels of a typical organic dye are shown in Fig. 3.1. Each electric level is a band composed of a continuum of vibrational and rotational levels. The lowest energy absorption is due to absorption from the electronic

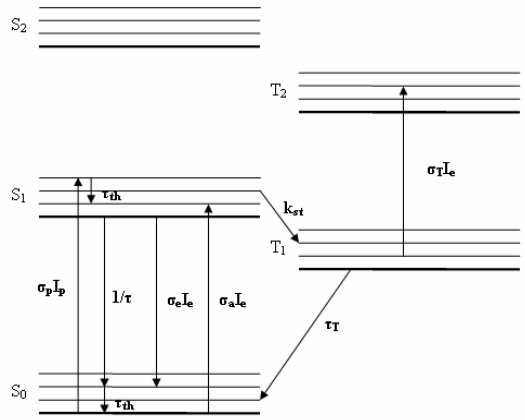

Fig. 3.1 Energy level diagram of a typical organic molecule.

singlet ground state S_0 to the first excited singlet S_1. This strong absorption, usually in the visible region of the spectrum, is responsible for the useful property of dyes. Not all dyes exhibit strong fluorescence, but the more useful laser dyes exhibit a near unity quantum efficiency. The nonradiative pathways can reduce the fluorescent emission. For example, the triplet-triplet absorption often overlaps the fluorescence band and can inhibit laser action. Simulated emission or laser action can occur over the fluorescent band. Of the thousands of organic dyes available, only a few classes of dyes meet the stringent criteria for becoming laser dyes. The various classes of dyes and the region of the spectrum they cover are illustrated in Fig. 3.2. The lasing emission wavelength achieved from DFB lasers has covered from the near ultraviolet at 367 nm (with 377E dye) [1] to the near infrared at 932 nm (with LDS 925 dye) [2].

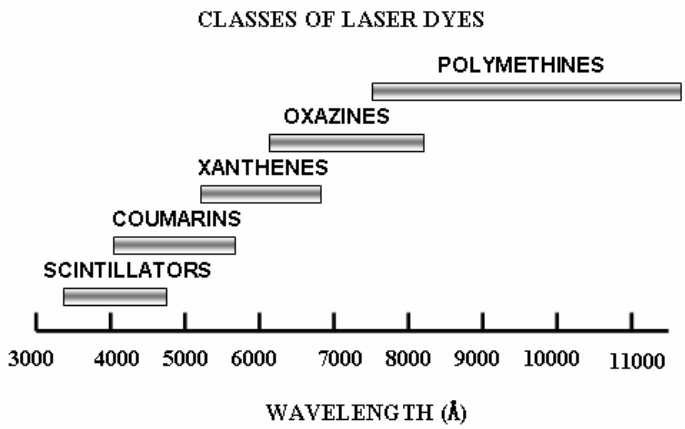

Fig. 3.2 Wavelength tunability ranges for various classes of organic dyes.

The tuning range of a laser dye is often limited on the short wavelength side by an overlapping absorption. The degree of this overlap is determined by the *Stokes shift* of the fluorescence. The Stokes shift means that the difference (usually in frequency units) between the spectral positions of the band maxima (or the band origin) of the absorption and luminescence arising from the same electronic transition.

In our experiments, we chose laser dyes R6G and DCM as light emitters in the laser media. They are the best known of all laser dyes. They have high fluorescence quantum yield, high photostability, low intersystem crossing rate, and low excited-state absorption. Fig. 3.3 shows the molecular structures of these two kinds of laser dyes.

Fig. 3.4 (a) and (b) are the graphs of the molar extinction coefficient and the fluorescence emission spectrum of R6G dissolved in ethanol, respectively[3]. R6G has a molar extinction coefficient of 116,000 $M^{-1}cm^{-1}$ at 529.75 nm [4]. The quantum yield is 0.95 [5]. The absorption cross section at 532 nm is 1.1×10^5 l $mole^{-1}$ cm^{-1}[5], which allows efficient pumping by the

frequency-doubled Nd:YAG laser. The fluorescence maximum is around 555 nm.

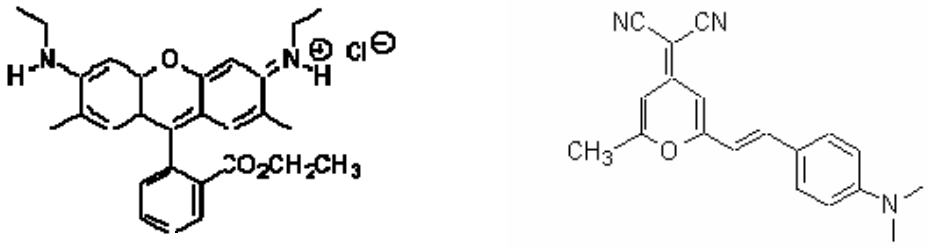

(a) R6G (b) DCM

Fig. 3.3 Molecular structures of laser dyes R6G (a) and DCM (b).

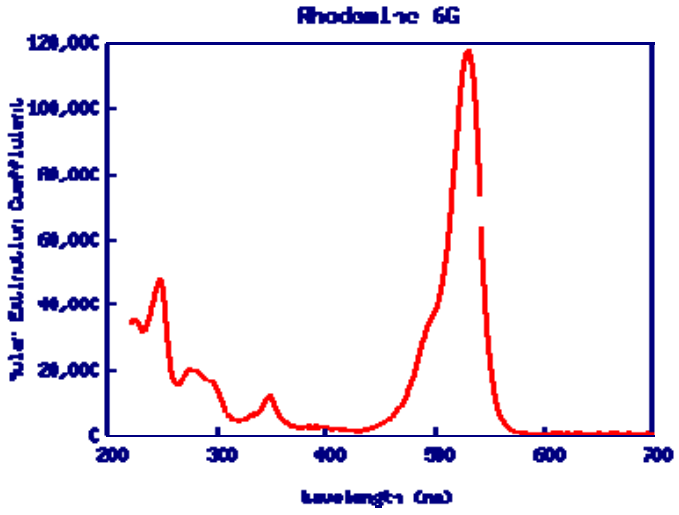

(a)

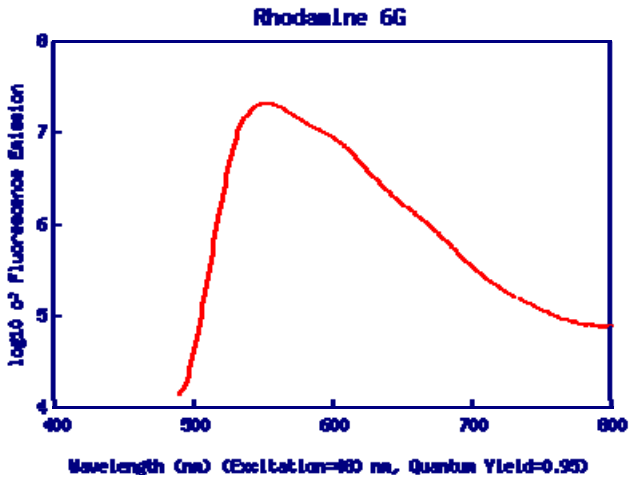

(b)

Fig. 3.4 (a) The molar extinction coefficient of R6G dissolved in ethanol; (b) The fluorescence spectrum of R6G dissolved in ethanol. (http://omlc.ogi.edu/spectra/PhotochemCAD/html/rhodamine6G.html)

Fig. 3.5 (a) and (b) are the graphs of the molar extinction coefficient and the fluorescence emission spectrum of DCM dissolved in methanol, respectively [3]. DCM has a molar extinction coefficient of 42,000 $M^{-1}cm^{-1}$ at 468.5 nm [6]. The quantum yield is 0.43 [5]. The absorption cross section at 532 nm is 1.68×10^4 l $mole^{-1}$ cm^{-1} [5]. The fluorescence maximum is around 627 nm.

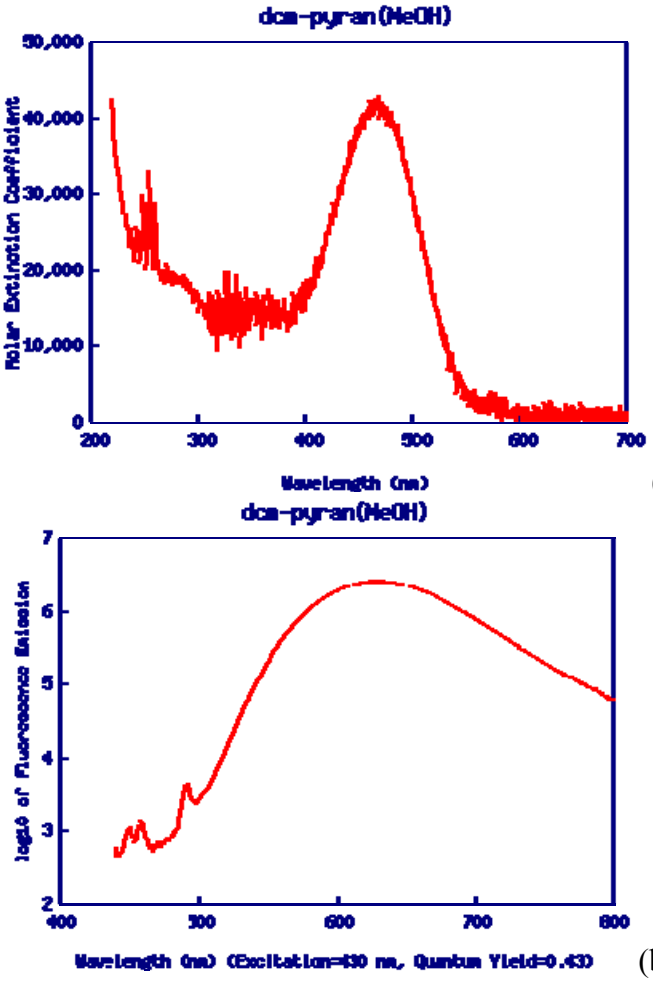

Fig. 3.5 (a) The molar extinction coefficient of DCM dissolved in methanol; (b) The fluorescence spectrum of DCM dissolved in methanol. (http://omlc.ogi.edu/spectra/PhotochemCAD/html/dcm-pyran(MeOH).html)

From the absorption spectra and fluorescence spectra of R6G and DCM, we see that there is a Stokes shift of 17 nm and 147 nm for R6G and DCM, respectively. The energy loss of the absorbed pump energy goes into the

collisional excitation of the molecules of the dyes and the suspending media. This energy heats up the laser media and can reversely affect laser operation, such as, by altering the refractive index of the laser media. In our experiments, one can see that a one-dimensional (1-D) photonic bandgap (PBG) structure induced in DCM doped methanol, which, to a large extent, was contributed by the larger Stokes shift of DCM.

In our works, we studied the tunability and spectral characteristics of DFB lasers made from R6G doped ethanol and DCM doped methanol solutions, respectively. The refractive indices of ethanol and methanol are 1.359 and 1.326, respectively. The concentrations of R6G doped ethanol and DCM doped methanol were 0.5×10^{-3} M and 2×10^{-3} M, respectively.

3.1.2 R6G doped PMMA films

3.1.2.1 Introduction to polymer

A polymer is a substance composed of molecules with large molecular mass composed of repeating units, or monomers, connected by covalent chemical bonds. Well-known examples of polymers include plastics, DNA and proteins; while the term polymer in popular suggests “plastic”. Polymers comprise a large class of nature and synthetic materials with a variety of properties and purposes.

The structural properties of a polymer relate to the physical arrangement of the monomers along the backbone of the chain. Structure has a strong influence on the other properties of a polymer. For example, a linear chain polymer may be soluble or insoluble in water depending on whether it is

composed of polar monomers (such as ethylene oxide) or nonpolar monomers (styrene). The simplest form of polymer molecule is a straight chain or linear polymer, composed of a single main chain. A branched molecule is composed of a main chain with one or more substituent side chains or branches. Special types of branched polymers include star polymers, comb polymers, and brush polymers.

In our work, we used the simplest polymer polymethyl methacrylate (PMMA) as the host matrix of laser dye to perform DFB laser experiments. PMMA is a vinyl polymer, made by free radical vinyl polymerization from the monomer methyl methacrylate (MMA). The polymerization process from the monomer MMA to PMMA is presented in Fig. 3.6. Unlike glass, PMMA transmits ultraviolet (UV) light down to 300 nm, and also PMMA allows infrared light of up to 2800 nm wavelength to pass. It transmits up to 93% of visible light (per meter). The refractive index of PMMA compounds usually ranges from 1.4893 to 1.4899.

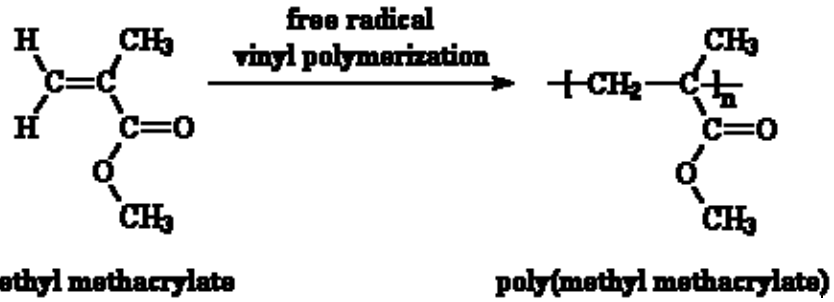

Fig. 3.6 The polymerization process from MMA to PMMA

3.1.2.2 Sample preparation

R6G-doped PMMA thick films on glass substrates were fabricated by cast-coating method. The refractive index of the glass substrates is 1.51. The synthesis procedure is sketched in block diagram in Fig. 3.7. The starting solutions consisted of PMMA and 1, 2-Dichloroethane (DCE). The PMMA was purchased from ALDRICH and was used without further purification. DCE was served as the solvent. The concentration of PMMA was of as high as 300g/L with the objective to increase the viscosity of the solutions, resulting in the films with large thickness. After the solutions were magnetically stirred for an hour, laser dyes were added into the solutions until the desired concentration of 2mM was reached. The dye doped solutions were ready for making films after keeping being stirred for around 12 hours so that PMMA and R6G could be dissolved completely. R6G doped PMMA thick films were obtained by casting the solutions onto the glass substrates drop by drop and subsequently being kept in an oven for around 2 hours with the temperature set as 83 ^{o}C to remove the residual DCE, which is the evaporation point of DCE. By adjusting the viscosity of the solutions and the quantity of the solutions dropped onto the substrates, films of various thicknesses can be obtained. The refractive index for the films was 1.49~1.498.

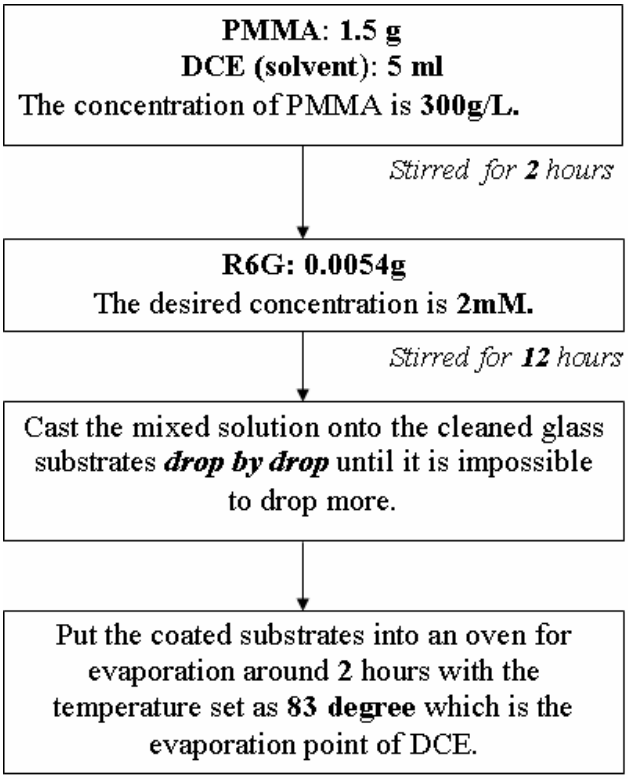

Fig. 3.7 Schematic block diagram of the preparation procedure for R6G doped PMMA films.

3.2 Experimental setup

3.2.1 Setup

In our DFB laser experiments, distributed feedback and gain were obtained by optically pumping the samples with the fringes formed by the interference of two coherent laser beams. A nanosecond pulsed frequency-doubled Nd:YAG laser (6ns) at 532nm was chosen as the pump source, considering the absorption of R6G and DCM (Fig. 3.4(a) and Fig. 3.5(a)). A beam-splitter was employed to get the two coherent pump beams from the same laser source. The Nd:YAG laser was an *s*-polarized laser source. When the two coherent beams overlap in the samples, interference patterns are generated dynamically [8]. Thus, a periodical gain and/or a periodical index modulation are induced, which contribute to the DFB modulation. DFB laser

oscillation arises from the coherent Bragg scattering in the periodic modulation of the gain medium. The grating-like interference patterns are expected to have high visibility to reduce the pump threshold energy, to lead to narrow linewidth of DFB laser output and to improve the output energy and the stability.

The optical arrangement of the reflection DFB lasers is illustrated in Fig. 3.8. A polarizer and a filter were placed in the exit path of the Nd:YAG laser to set the polarization direction of the pump beam to be *s*-polarized, and to filter out the unwanted 1.06 um component, respectively. Then the pump beam was divided into two coherent parts of approximately equal intensities. These two coherent beams were redirected by two identical rotatable plane mirrors to combine in the samples at an intersection angle of 2Θ. A convex lens with the focal length, f =500 mm, was used to focus the pump beams. The lens was expected to give a smaller spot pumped region in the samples with increased pump energy density.

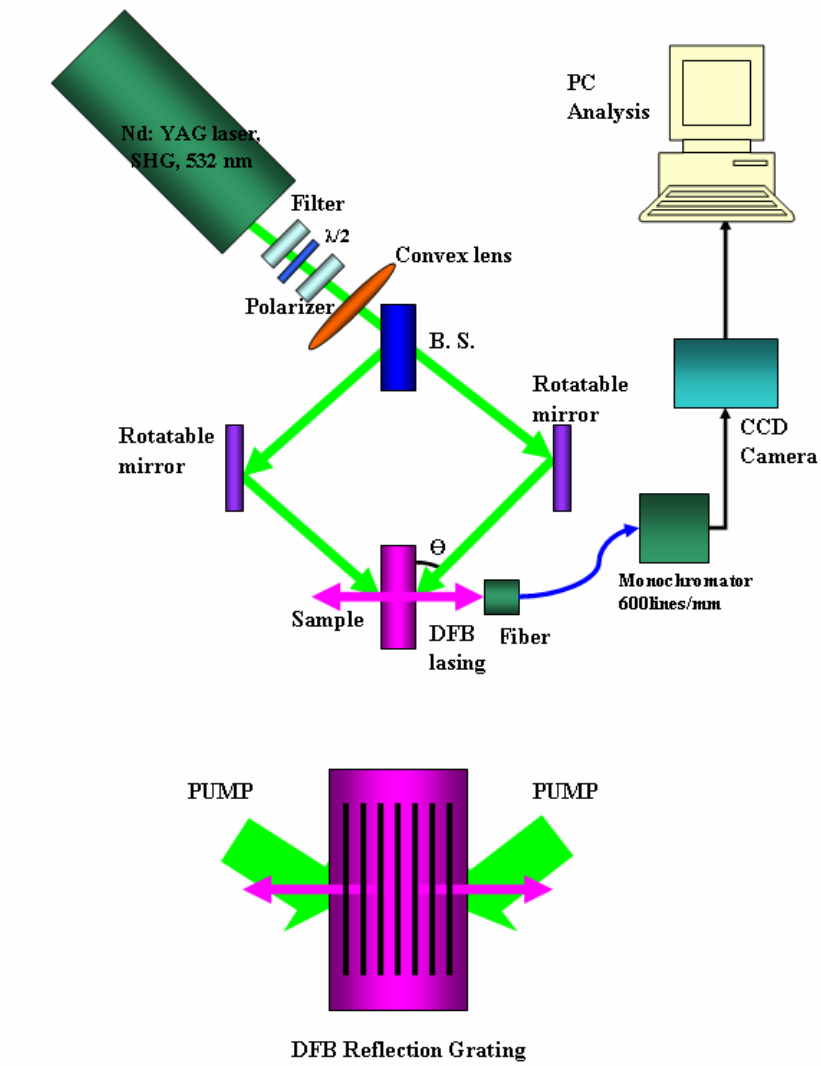

(a)

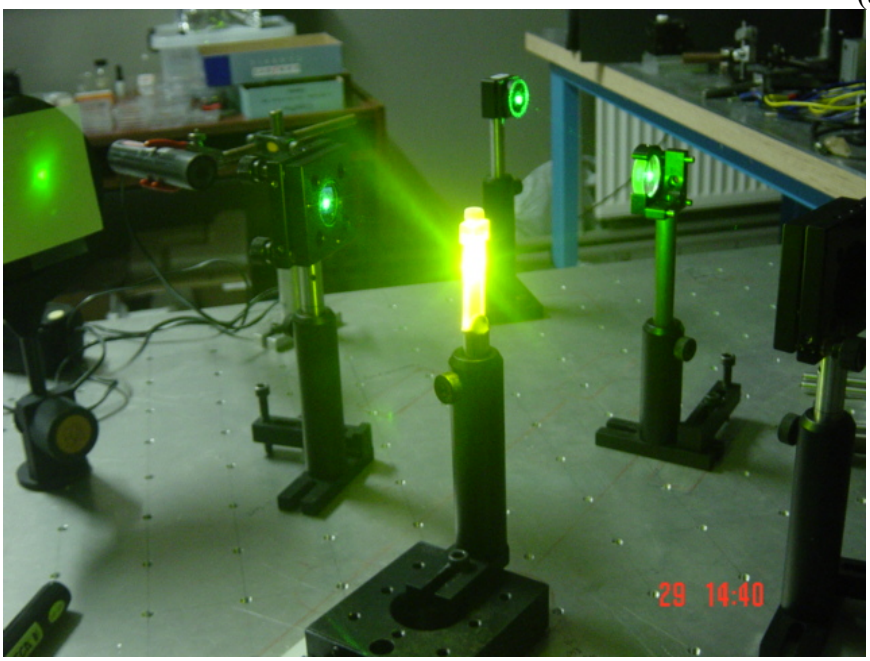

(b)

Fig. 3.8 Experimental setup of our DFB lasers in reflection pumping geometry.

As described in the section 2.2.2 in Chapter II, in reflection pumping geometry, the periodical spatial interference pattern of the two pump beams was generated in the combined region inside the samples after their refraction at the interfaces between the sample surface and air. The grating planes are parallel to the sample surface, and the DFB lasing emission is normal to the sample surface. The period of the gain/index modulation is given as

$$\Lambda = \lambda_p / 2n_2 \sin\theta_{in}, \tag{3.1}$$

where λ_p is the wavelength of the pump laser source, θ_{in} is the intersection angle of the pump beams inside the gain medium, and n_2 is the refractive index of the gain medium at the lasing wavelength. The samples, which were mounted on a translation stage, can be finely translated along the Y direction. Hence the intersection angle of the two crossing beams can be varied continuously by finely rotating those two plane mirrors and by moving the samples, resulting in continuous variation of the period of the interference patterns. Distributed feedback occurs near the Bragg condition [9], that is, when the wavelength in the medium is equal to 2Λ. Denoting λ_L as the DFB oscillation wavelength in air, the Bragg condition can be written as

$$2n\Lambda = M\lambda_L, \tag{3.2}$$

where n is the refractive index at λ_L and M is the Bragg reflection order. Combining (3.1) and (3.2), the spectral selection equation can be obtained for our reflection DFB lasers:

$$\lambda_L = \frac{\lambda_p}{M \sin\theta_{in}}. \tag{3.3}$$

The DFB wavelength is independent on the refractive indices of the laser media. This equation is the theoretical base of the wavelength tuning of our DFB lasers.

The desired pump energy density can be adjusted by translational movement of the convex lens back and forth. Increasing the pump energy above the threshold at an appropriate intersection angle (an appropriate period of modulation), the DFB lasing would emit along the same direction of the grating vector of the reflection DFB grating. The DFB laser signal was collected with an optical fiber probe. It was dispersed and analyzed with a 600 lines/mm grating coupled to a spectrometer (Huet M25), coupled to a cooled CCD camera (Hamamatsu C4742-95) for spectral measurements. The CCD camera was controlled by the software Hipic. The polarization property of the DFB laser output can be determined by a polarizer inserted in front of the fiber probe. The output beam profiles can be captured by using a digital camera. The pump energy was measured by a powermeter.

3.2.2 Calibration of the detection system

A Neon lamp was used to calibrate the detection system. The standard emission spectrum of Neon lamp is shown in Fig. 3.9 (a). By hand-adjusting the position of the grating of the monochromator, a 2-dimensional (2-D) light intensity image (Fig. 3.9 (b)) of the Neon spectrum with a suitable wavelength range, of which we concerned, was captured. Since our CCD camera has a 1024×1024 pixels detection matrix, one can get that, the wavelength interval between any two pixels is 0.02 nm, and the wavelength-band of the CCD

camera is only around 22 nm. This narrow wavelength-band of CCD camera determines that the whole fluorescence emission spectrum of the dye doped solvents and dye doped polymer samples would not be obtained in our setup. With the software Matlab in combination with Origin, the light intensity picture of the spectrum can be converted and plotted in one-dimensional (1-D) form (Fig. 3.9 (c)).

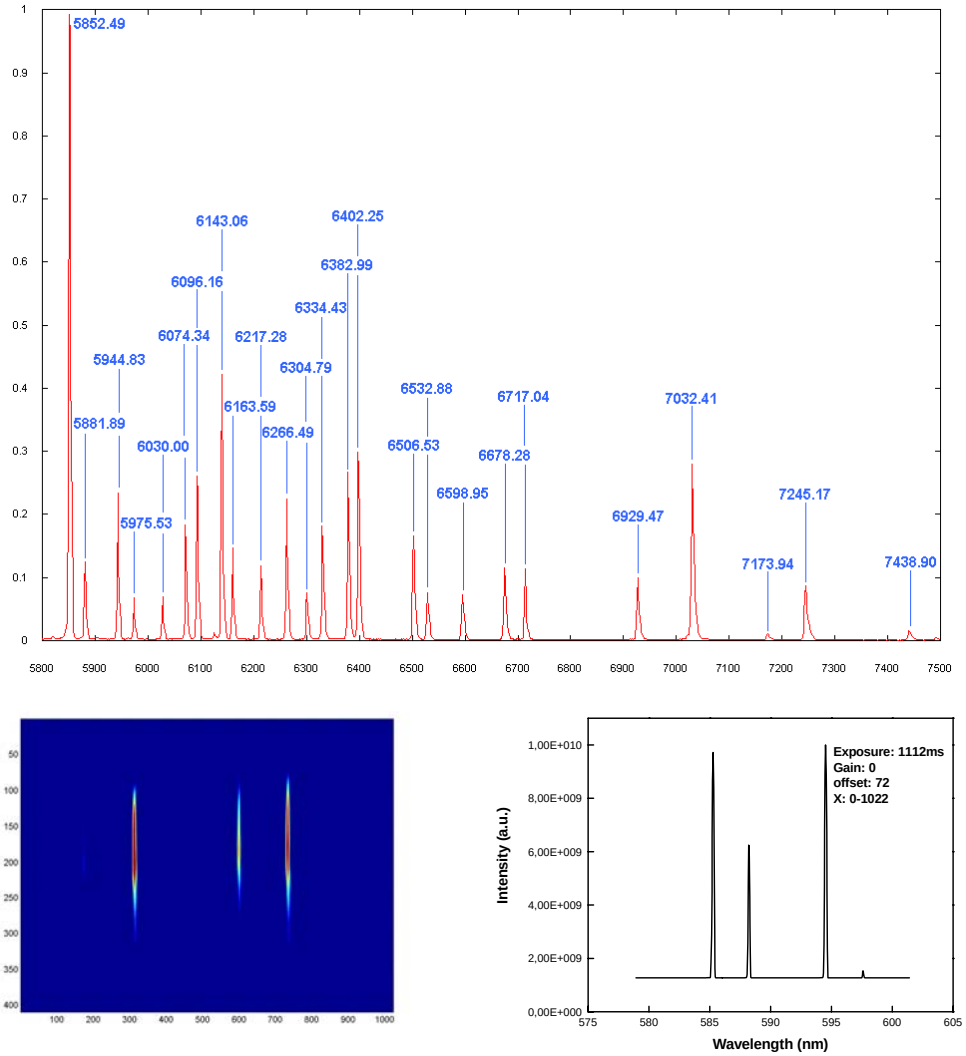

Fig. 3.9 (a) The standard emission spectrum of Neon lamp; (b) Image obtained by CCD camera (A part of the emission spectrum of Neon Lamp); (c) A part of the emission spectrum of Neon Lamp.

The resolution limit of our detection system is 0.1 nm. The experimental errors come from mainly three sources: the reading of the intersection angle of the two coherent pumping beams; the reading of the position of the diffraction grating in the monochromator; the determination of the lasing peaks during the lasing intensity image processing.

3.3 Summary

In this Chapter, laser gain media adopted in our reflection DFB laser experiments were introduced. R6G doped ethanol and DCM doped methanol were prepared as liquid solution gain media, the dye concentrations were 0.5×10^{-3} M and 2×10^{-3} M, respectively. R6G doped PMMA thick films were prepared on glass substrates, which served as solid gain media. The preparation procedure by cast-coating method was illustrated in very detail.

The experimental construction of reflection DFB lasers by two interfering beams was described. A nanosecond pulsed frequency-doubled Nd:YAG laser (6ns) at 532nm was employed as the pump source.The DFB laser signal was dispersed and analyzed with a 600 lines/mm grating coupled to a spectrometer (Huet M25), coupled to a cooled CCD camera (Hamamatsu C4742-95) for spectral measurements. The whole detection system was calibrated by a Neon lamp. The possible experimental errors were also mentioned.

References

[1] X. L. Zhu and D. Lo, “Distributed-feedback sol-gel dye laser tunable in the near ultraviolet”, *Appl. Phys. Lett.* **77**, p2647, 2000

[2] F. Chen, J. Wang, C. Ye, W. H. Ni, J. Chan, Y. Yang, and D. Lo, “Near infrared distributed feedback lasers based on LDS dye doped zirconia-organically modified silicate channel waveguides”, *Opt. Express*, **13**, p1643, 2005

[3] H. Du, R. A. Fuh, J. Li, A. Corkan, J. S. Lindsey, “Photochem CAD: A computer-aided design and research tool in photochemistry”, *Photochemistry and Photobiology*, **68**, p141, 1998

[4] R. R. Birge, *Kodak Laser dyes*, 1987

[5] R. F. Kubin and A. N. Fletcher, “Fluorescence quantum yields of some rhodamine dyes”, *J. Luminescence*, **27**, p455, 1982

[6] M. Meyer, J.-C. Mialocq and B. Perly, “Photoinduced intramolecla charge transfer and trans-cis isomerization of the DCM styrene dye. Picosecond and nanosecond laser spectroscopy, high-performance liquid chromatography and nuclear magnetic resonance studies”, *J. Phys. Chem.* **94**, p89, 1990

[7] J. M. Drake, M. L. Lesiecki and D. M. Camaioni, “Photophysics and cis-trans isomerization of DCM”, *Chem. Phys. Lett.* **113**, p530, 1985

[8] N. K. Viswanathan, S. Balasubramanian, L. Li, S. K. Tripathy and J. Kumar, “A detailed Investigation of the Polarization-Dependent

Surface-Relief-Grating Formation Process on Azo Polymer Films", *Jpn. J. Appl. Phys.* **38**, p5928, 1999

[9] H. Kogelnik and C. V. Shank, "Coupled-wave theory of distributed feedback lasers", *J. Appl. Phys.* **43**, p2327, 1972

Chapter IV

First-order DFB Laser Effect in Reflection Pumping Geometry Based on Dye Doped Solvents and Dye Doped Polymer

Due to the compact structure and wavelength tunable property [1], DFB lasers attracted much research interests. Lo's group successfully realized many kinds of tunable waveguide DFB lasers by using two crossing pump beams [2-7]. Rocha *et al*. fabricated DFB lasers based on a permanent surface relief grating (SRG) achieved by using a photoinduced patterning technique [8]. By adopting the Lloyd-mirror device, Gindre *et al.* obtained DFB laser emission in dye doped polymers [9]; Carro *et al.* realized near-infrared imprinted DFB lasers by adopting room-temperature nanoimprint lithography [10]. These mentioned DFB lasers were generally operated in a transmission grating pumping geometry whatever the periodical modulations were permanent or dynamic.

There have been reports on DFB lasing action in a permanent reflection grating too. Light amplification and DFB lasing was obtained in a permanent reflection photonic bandgap (PBG) structure composed of dye-doped polymer dispersed liquid crystal by Luchetta *et al.* and Wu *et al.*, respectively [11-12]. The DFB grating were created using two crossing pump beams in a configuration similar to the one used in the standard holography. The periodic structures were induced by a gain modulation and/or an index modulation in

the laser media [13]. The periodicity was defined by the interference angle of the two crossing beams. The structure selectively reflected light satisfying the Bragg reflection condition. The comparison between the traditional transmission DFB grating and reflection DFB grating has been described in detail in Chapter Ⅲ.

In our works, for the first time, *dynamic* DFB laser action in *transient* reflection pumping geometry was successfully realized. In this chapter, our recent results are reported: DFB lasing output based on transient reflection grating configuration in R6G doped ethanol, DCM doped methanol solutions and R6G doped PMMA films, respectively [14-15].

4.1 DFB lasing effect in R6G doped ethanol for the first Bragg order

4.1.1 Spectral properties

R6G doped ethanol was prepared for laser measurements. The concentration was 0.5×10^{-3}M. The refractive index of ethanol is 1.359. The experimental setup has been discussed in Chapter Ⅲ. R6G, also called rhodamine 590 chloride, is one of best known of all laser dyes. It is a xanthene derivative, ionic and highly polar. Its chemical structure is shown in Fig. 3.3. In ethanol solution, R6G exhibits an absorption peak at around 530 nm and a fluorescence peak at 556 nm. It has a high fluorescent quantum yield of 95%. These properties make it highly efficient dye for both pulsed and continuous-wave laser action with fairly good chemical stability.

Fig. 4.1 shows the spectra of absorption of R6G doped ethanol at different concentrations. The absorption peak was at 536 nm which allowed

efficient pumping at 532 nm by frequency-doubled Nd:YAG laser. The absorption was around up to 3.1 at 532 nm. Broad fluorescence emission spectrum, which almost liked a mirror image of the absorption spectrum, is centered at 575.7 nm with a bandwidth of about 66 nm (In Fig. 4.2).

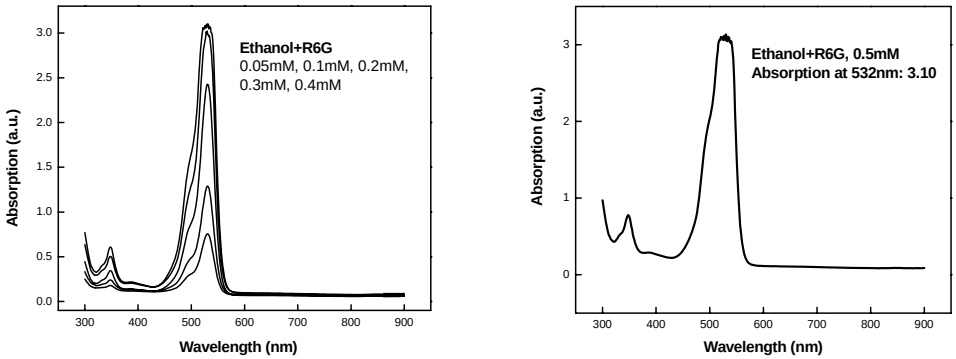

Fig. 4.1 Absorption spectra for R6G doped ethanol of different concentrations

At higher pump energy, narrowing of the spectral width that is indicative of the process of single pass stimulated radiation-amplified spontaneous emission (ASE) was achieved (Fig. 4.2). The peak of ASE had a red-shift compared with the fluorescence peak. The DFB lasing was tuned within the gain range of the ASE spectrum. We also compared the ASE spectra measured from the lateral side of the dye cell in transversely pumping geometry (Fig. 4.3 (a)) and the surface of the dye cell in reflection pumping (Fig. 4.3 (b)). The peak of ASE spectrum measured from the lateral side centered at around 567.2 nm. Compared with the central wavelength of 559.9 nm of the ASE measured from the surface of the dye cell, it has a red-shift of 7 nm, which is due to a bigger re-absorption since the ASE from the lateral side has a longer propagation length (a longer gain length) compared to that from the surface, although ASE is less easy to be influenced by other factors such as re-

absorption during light propagation through the sample. The full width at half maximum (FWHM) was 5.3 nm and 5.7 nm for the two cases.

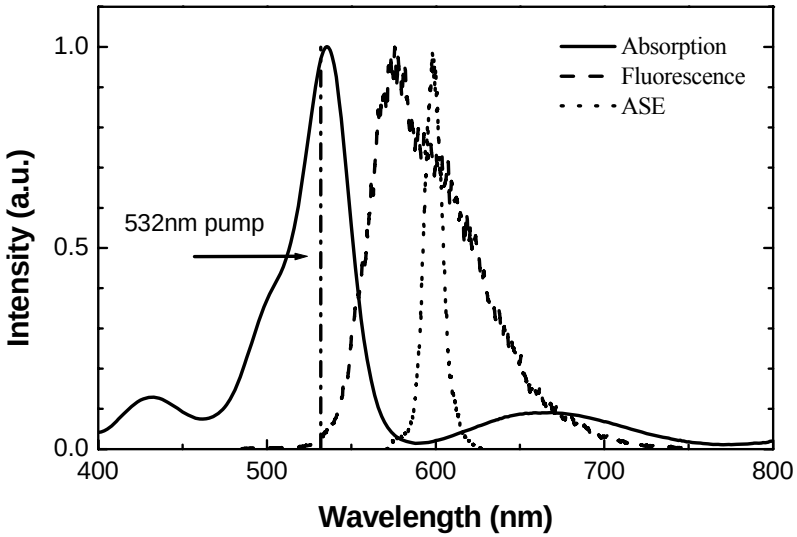

Fig. 4.2 Absorption, fluorescence and ASE spectra for R6G doped ethanol.

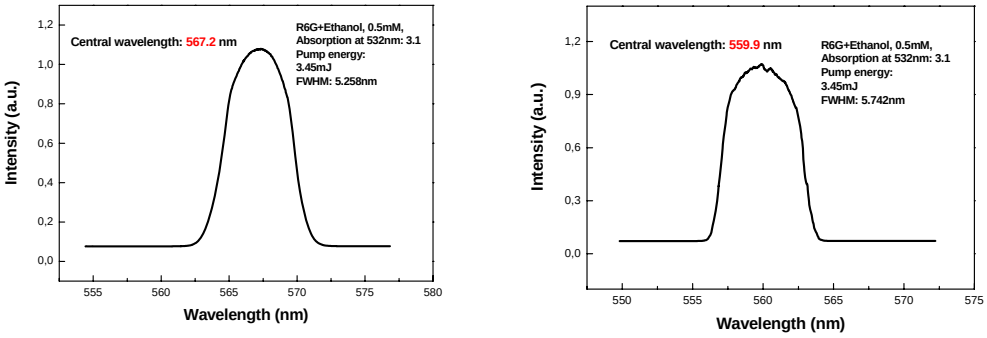

(a) (b)

Fig. 4.3 ASE spectra from R6G doped ethanol solution measured from the lateral side (a) and the surface of the dye cell (b), respectively. The concentration was 0.5 mM.

4.1.2 Tuning behavior

DFB laser action was firstly observed in R6G doped ethanol. Tunable narrow linewidth DFB laser output was obtained when the pump energy was

up to 0.84 mJ per pulse, after counting for the reflection, scattering and transmission losses of the pump beam. With our 6 mm diameter of the pump laser, this corresponds to a laser threshold of 3.0 mJ/cm^2. Continuous tuning of the output wavelength was achieved by varying the intersection angle ɵ of the two crossing beams, hence the period of the modulation. Single peak lasing emission was observed throughout the tuning range from 557.5 nm to 562.9 nm. Fig. 4.4 shows the spectral variation as the intersection angle. The laser spectrum exhibits a single prominent peak near the center of the gain profile (565.6 nm). When the laser was tuned away from the gain centre, significant ASE appeared in the background.

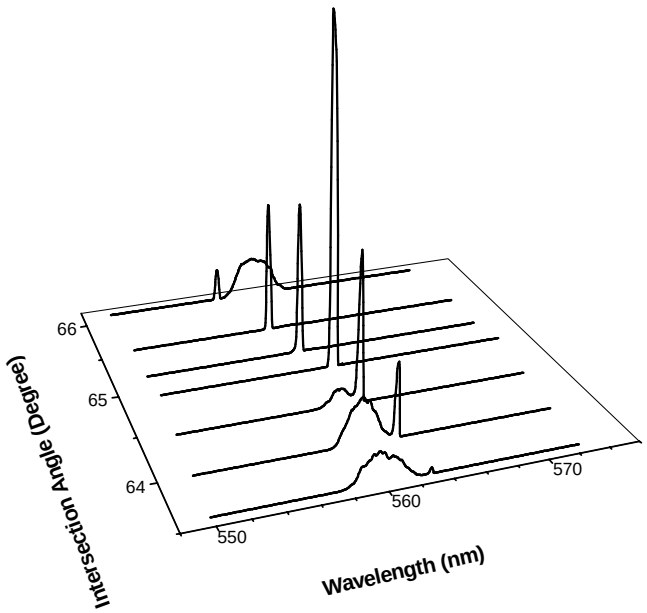

Fig. 4.4 Lasing spectra for the reflection DFB R6G doped ethanol lasers

Fig. 4.5 shows the experimental data of the angle tuning versus the theoretical fit (solid line) of the index-independent tuning equation in reflection

pumping geometry (Eq. 3.3). The first Bragg order (M=1) was satisfied in our experiments. Very good agreement between the experimental data and the theory was seen. The linewidth of the DFB laser output was as narrow as 0.5 nm, which was in fact the resolution limit of our detection system.

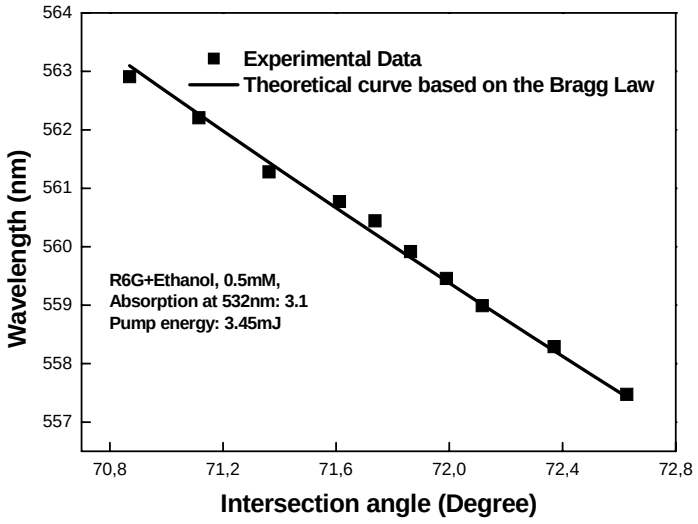

Fig. 4.5 The tuning data of the lasing emission vs. the theoretical curve based on the Bragg Law $\lambda_{theory}=2n\Lambda$ at the first Bragg order.

It should be noted that, in the case of the R6G doped ethanol reflection DFB lasers, we get lasing oscillations exactly at the Bragg frequencies, so the periodical modulation generated in R6G doped ethanol are gain modulation, and the reflection DFB gratings are relevant of a gain-type DFB grating (2.1.3.B) [13].

4.1.3 Output-Input Characteristic of DFB lasing

We also measured the slope efficiency property of the lasing output. Fig. 4.6 displays the lasing output intensity variation as the function of the pump energy at 560.5 nm, which was around the centre of the ASE of R6G doped

ethanol of 0.5 mM. The pump energy was obtained considering of the reflection and transmission losses of the pump beams. As the pump energy was increased from 1.9 mJ to 3.5 mJ, the output energy increased essentially linearly. The straight line represents the linear fit curve. The threshold pump energy was about 0.84 mJ, which was measured at a state that DFB lasing just appeared incidentally with a very weak intensity when the pump energy was decreased gradually.

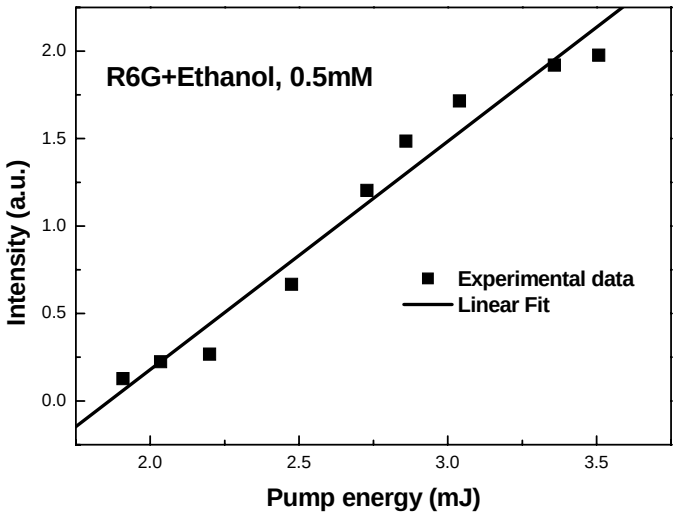

Fig. 4.6 The output intensity variation as the function of the pump energy at **560.5nm.**

4.1.4 Cavity lasing

In our DFB laser experiments, significant cavity lasing was observed as well when the DFB lasing emission was collected with the optical fiber probe, since the dye-solution cuvette was set roughly vertical to the optical table during the operation of the DFB lasers. Once the pump intensity was higher than a certain threshold for a given gain length and dye concentration, highly

directional superradiant lasing (ASE) can be obtained in both the forward and the backward directions. The cavity lasing, generated by the Fresnel reflection feedback from the two parallel optical windows of the cuvette, should be in the spectral range of the ASE. When the cuvette was inclined by few degree from the normal position, one can distinct the ASE and cavity lasing. But if the tilt angle was larger than 3^o to 4^o, cavity lasing was no longer observed owing to a big deviation of the cavity axis; however, strong forward and backward superradiant simulated emission still existed. This point will be discussed in detail in the experiments of DCM doped methanol reflection DFB lasers.

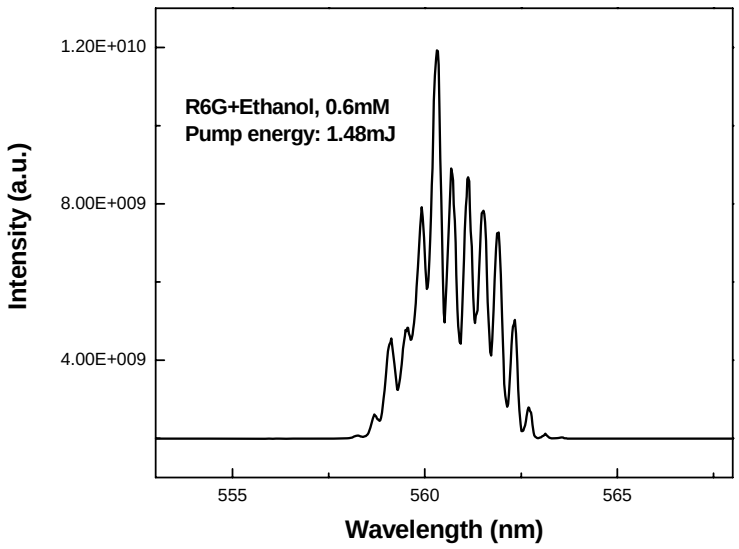

Fig. 4.7 Measured spectral curve for cavity lasing from a R6G doped ethanol filled cuvette.

Fig. 4.7 displays the cavity lasing spectrum from R6G doped ethanol cuvette on a small wavelength scale. The spectral width was around from 2 nm to 3 nm. One finds that the cavity lasing shows a periodic modulation structure. Because the cavityless lasing (ASE) shows no modulation structure, the

modulation is not related to the gain medium itself. Also the cavity lasing generated from the Fresnel reflection feedback between the two parallel optical windows of the cuvette would not give the discrete spectral structure. In order to interpret the observed spectral modulation, one has to somehow assume that there should be either an equivalent Fabry-Perot etalon structure or an equivalent distributed feedback structure with the same small spatial period. In the following discussion, we show that this spectral modulation is due to the multicavity structure formed by the two windows of the dye-solution cuvette [16-17].

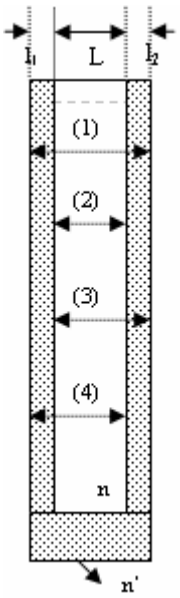

Fig. 4.8 Detailed structure of subcavities provided by a quartz cuvette filled with a dye solution.

Fig. 4.8 shows the detailed structures of the dye solution-filled cuvette in the normal cavity lasing position. In this case, four subcavities are involved for cavity lasing; the discrete modulation structures of the cavity lasing should possibly fulfill the following resonant conditions:

$$\begin{aligned} 2[nL + n'(l_1 + l_2)] &= K_1\lambda, \\ 2nL &= K_2\lambda, \\ 2(nL + n'l_2) &= K_3\lambda, \\ 2(nL + n'l_1) &= K_4\lambda, \end{aligned} \tag{4.1}$$

where L is the thickness of the dye solution, l_1 and l_2 are the thicknesses of the two windows of the cuvette, n is the refractive index of the dye solution, n' is the refractive index of the fused-quartz windows, and K_1, K_2, K_3 and K_4 are arbitrary integers. Subtracting the fourth equation from the third in Eqs. (4.1) leads to

$$2n'(l_2 - l_1) = (K_3 - K_4)\lambda = K'\lambda. \tag{4.2}$$

Here K' still is an arbitrary integer. One can see that the resonant conditions imposed by these five equations are identical to the maximum transmission condition of five Fabry-Perot etalons with corresponding optical thicknesses. This implies that the cavity lasing spectra will be modulated by these five Fabry-Perot etalons.

During the operation of our reflection DFB lasers, the dye cell was slightly tilted in order for the DFB lasing to be spatially separated from the cavity lasing.

4.2 DFB lasing effect in DCM doped methanol for the first Bragg order---- 1-D *dynamic* PC DFB dye laser

4.2.1 ASE and Cavity lasing

DCM doped methanol was prepared for our laser experiments. The concentration was 2×10^{-3}M. The refractive index of methanol is 1.326. The experimental setup was the same to the one used for R6G doped ethanol DFB

lasers. An additional 0.5 m focal lens was inserted into the optical path to focus the pump beam into a small spot with increased energy density. DCM has good chemical stability, high fluorescence efficiency and broad tunable range. It has a big absorption at 532 nm and a maximum of fluorescence of 627 nm, which suggests that frequency-doubled Nd:YAG laser is quite fitting for pumping the DCM dye laser.

When the pump intensity of the focused pump beam was higher than a certain threshold, ASE can be obtained in both the forward and the backward directions from the surfaces of the dye solution filled cuvette. Fig.4.9 (a) shows the ASE spectrum observed from the surface of DCM doped methanol cuvette, with the concentration of 2 mM. The central wavelength was around 638 nm. The FWHM was around 9 nm. By titling the dye cell for few degrees (less than 3^o to 4^o), one can see ASE spectrum and cavity lasing spatially separately (Fig. 4.8 (b)). As ASE is a one single-pass gain process which propagates along the direction of the pump beam, while cavity lasing comes from the multiple Fresnel reflection feedback from the two parallel optical windows of the cuvette, which propagates along the direction normal to the surfaces of the cuvette, as a result, the cavity lasing (right band of the spectrum), which experienced multiple self-absorption processes, has a red-shift relative to ASE (left band of the spectrum).

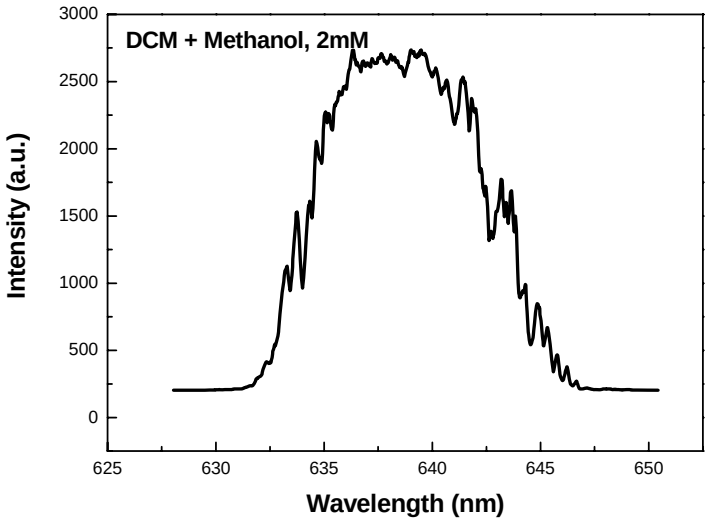

(a)

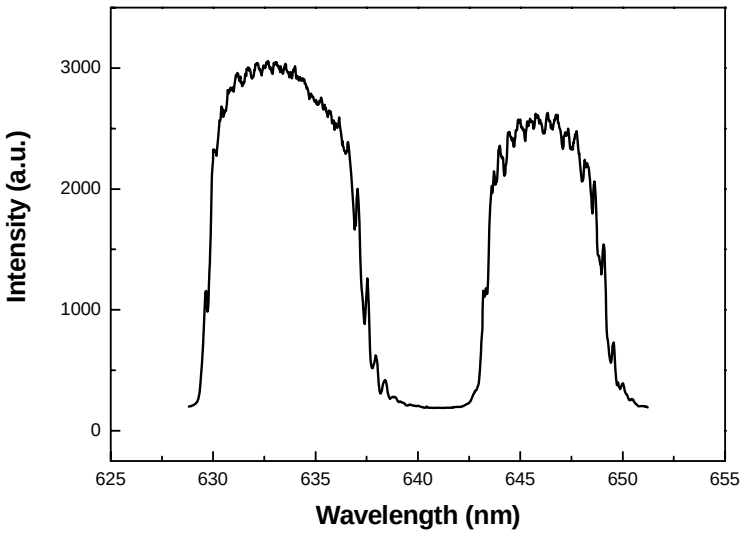

(b)

Fig. 4.9 (a) The ASE spectrum measured from the surface of DCM doped methanol filled cuvette; (b) The spectrum of separated ASE and cavity lasing. The concentration was 2 mM.

By hand-adjusting the dye cuvette slightly, the discrete spectral structure of cavity lasing observed from R6G doped ethanol can also be obtained from DCM doped methanol (Fig.4.10). The same to R6G doped ethanol, the five Fabry-Perot etalons dominated the modulation of the discrete structures.

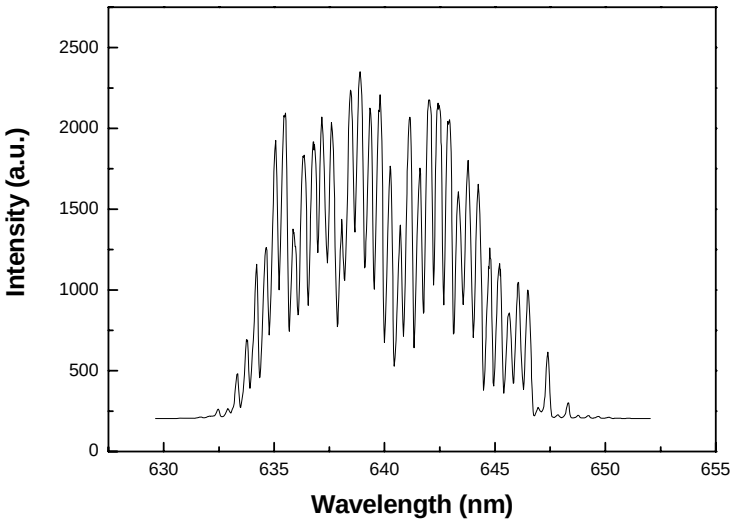

Fig. 4.10 Measured discrete spectral structure for cavity lasing from DCM doped methanol filled cuvette.

4.2.2 Tuning behavior

DFB lasing action was observed when the pump energy was above 0.19 mJ. With our 6 mm pump diameter of the focused pump beam, this corresponds to a laser threshold of 6.1 mJ cm^{-2}. Continuous angle tuning of DFB laser output was achieved by varying the intersection angle of the two crossing beams. In contrast with lasing in R6G doped ethanol, dual-peak lasing emission was obtained in DCM doped methanol. Each emission peak was doubled with an average interval of 0.29 nm or a shoulder. The tuning spectra as the intersection angle are shown in Fig. 4.11 (a). The tuning range was from 629 nm to 644 nm. Fig. 4.11 (b) shows the angle tuning data as the function of the intersection angle. The solid curve is the theoretical fit based on the Bragg condition for the first Bragg order. We see very good agreement.

In the case of DCM doped methanol, the dual-peak lasing structure indicates the existence of a light induced index-type DFB reflection grating in

addition to the regular gain grating [13]. For the first time, a *dynamic* 1-D PC with tunable PBG was thus generated in our reflection DFB lasers from DCM doped methanol [18-20] (In 2.3 in chapter II).

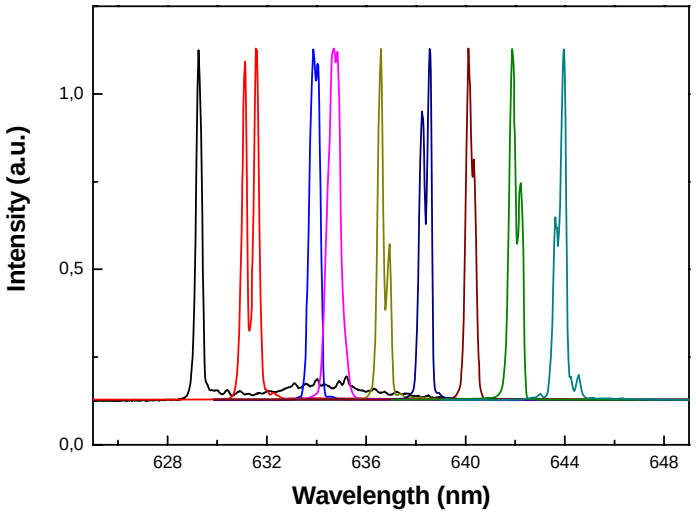

(a)

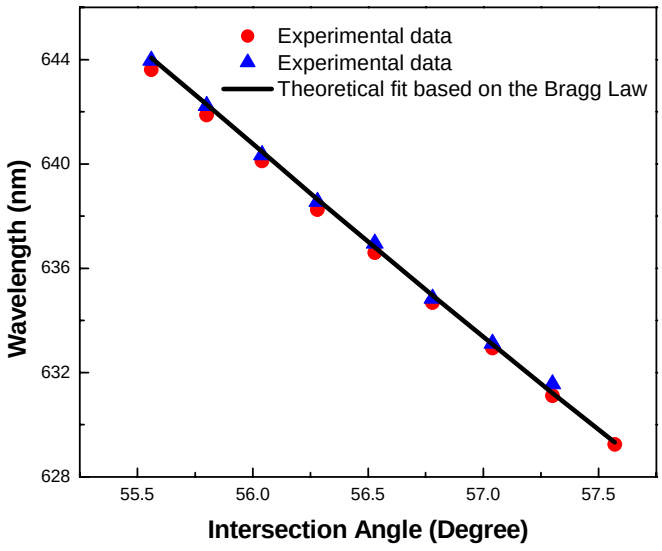

(b)

Fig. 4.11 The tuning spectra at different intersection angles (a); Angle tuning data vs. theoretical fit based on the Bragg condition (b). Circles and triangles represent the lasing wavelengths of the double peaks at every intersection angles.

4.2.3 1-D tunable PC (tunable PBG) in DCM reflection DFB lasers

Considering the index-type DFB grating in DCM doped methanol DFB lasers, the index-coupling dominated the feedback for the lasing oscillation [13]. When the two crossing beams overlapped inside the dye cuvette, a weak index-modulation was induced in the laser medium. Then a periodical dielectric structure was generated. So it can be referred as a 1-D PC [18-19]. As a result, a tunable PBG was obtained during the tuning process of the DFB lasers. In the following, an explanation is given for the dual-peak lasing action, according to the coupled-wave theory of Kogelnik and Shank [13] (In 2.1 in chapter Ⅱ).

In the coupled-wave model, the complex propagation constant of the DFB lasing waves γ is determined by the dispersion relation

$$\gamma^2 = \kappa^2 + (\alpha - j\delta)^2 \tag{4.3}$$

where κ is the coupling constant, α is the gain constant, and δ is the normalized frequency. Assuming that the periodic grating in our experiments with DCM is purely gain-free, we have $\alpha = 0$ and κ real, there will thus be a stop band centered at the Bragg frequency ω_0 in the dispersion curves. The width of the stop band is 2κ [13]. Consequently, the DFB lasing will oscillate at frequencies located symmetrically on both sides of the Bragg frequency. The coupling constant is expressed as

$$\kappa = \pi n_1 / \lambda_0 + \tfrac{1}{2} j\alpha_1 \tag{4.4}$$

where n_1 represents the amplitude of the spatial index modulation. So, κ increases as the index modulation.

As known from nonlinear optics, a variation of the refractive index can be produced in a medium by an intense laser light. This is so-called optical Kerr effect. In the optical Kerr effect, an intense beam in a medium can itself provide the modulating electric field, without the need for an external field to be applied. The electric field is given by:

$$E = E_\omega \cos(\omega t) \tag{4.5}$$

where E_ω is the amplitude of the wave. For a nonlinear material, the electric polarization field P will depend on the electric field E:

$$P = \varepsilon_0 \chi^{(1)} : E + \varepsilon_0 \chi^{(2)} : EE + \varepsilon_0 \chi^{(3)} : EEE + ... \tag{4.6}$$

where ε_0 is the vacuum permittivity and $\chi^{(n)}$ is the n-th order component of the electric susceptibility of the medium. Combining these two equations produces a complex expression for P. Taking only linear terms and those in $\chi^{(3)} |E_\omega|^3$:

$$P \simeq \varepsilon_0 (\chi^{(1)} + \frac{3}{4} \chi^{(3)} |E_\omega|^2) E_\omega \cos(\omega t). \tag{4.7}$$

It is a linear susceptibility with an additional non-linear form:

$$\chi = \chi_{LIN} + \chi_{NL} = \chi^{(1)} + \frac{3\chi^{(3)}}{4} |E_\omega|^2, \tag{4.8}$$

and since:

$$n = (1+\chi)^{1/2} = (1 + \chi_{LIN} + \chi_{NL})^{1/2} \simeq n_0 (1 + \frac{1}{2n_0^2} \chi_{NL}) \tag{4.9}$$

where $n_0 = (1+\chi_{LIN})^{1/2}$ is the linear refractive index. Using a Taylor expansion as $\chi_{NL} \ll n_0^2$, this gives an *intensity dependent refractive index* (IDRI) of:

$$n = n_0 + \frac{3\chi^{(3)}}{8n_0}\left|E_\omega\right|^2 = n_0 + n_2 I \tag{4.10}$$

where n_2 is the second-order nonlinear refractive index, and I is the intensity of the wave. The refractive index change is thus proportional to the intensity of the light traveling through the medium: $\Delta n = n - n_0 = n_2 I$.

In the coupled-wave theory, this Δn is identified with n_1 in the coupling constant (Eq. 4.4). It means that the coupling constant κ is proportional to the pump beam intensity. Since the width of the stop band is 2κ, experimentally, the spectral interval of the double lasing peaks should increase as the pump energy.

We studied the spectral variation as the function of the pump energy. Fig. 4.12 shows the laser spectra at different pump energies and at a constant intersection angle of 56.04^o between the two crossing beams, corresponding to a Bragg wavelength of 639 nm. The variation of the spectral interval between the two peaks with pump energy is illustrated in Fig. 4.13. The solid curve is simply a linear fit. We see that the spectral interval is proportional to the pump energy. The experimental results are consistent with our theoretical prediction. The pump energy in Fig. 4.13 was determined with consideration of the reflection and transmission losses.

In Fig. 4.11 (a), we note that the DFB lasing tuning spectra have a variation of the dual-peak interval against the lasing output wavelength; this dispersion of the interval was due to that the nonlinear index of the gain medium was strongly frequency dependent at the Bragg resonances, also the

pump energy variation can not be excluded on changing the intersection angle of the two crossing pump beams.

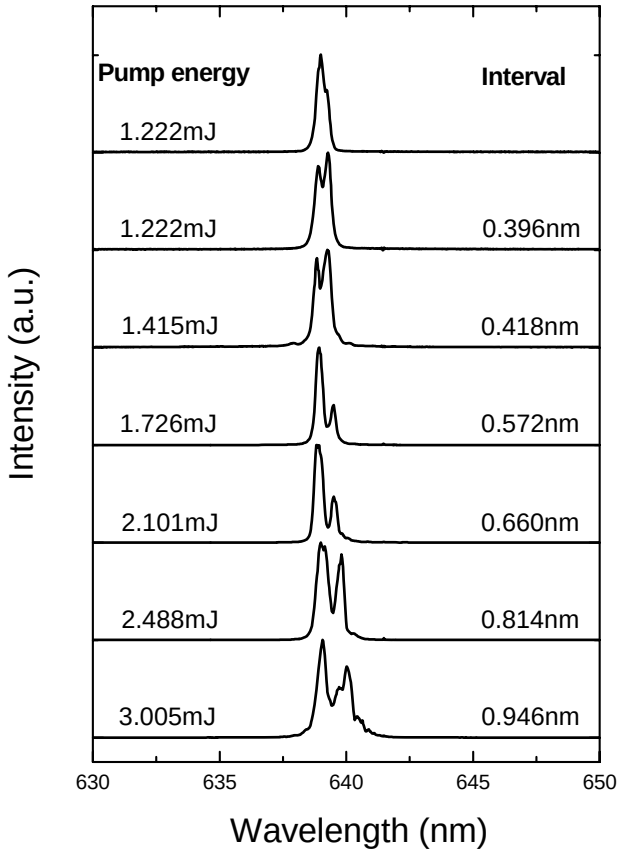

Fig. 4.12 Dual-peak structure of DFB lasing from DCM-doped methanol at different pump energies and at a constant intersection angle of 56.04°, which corresponds to a Bragg wavelength of 639 nm.

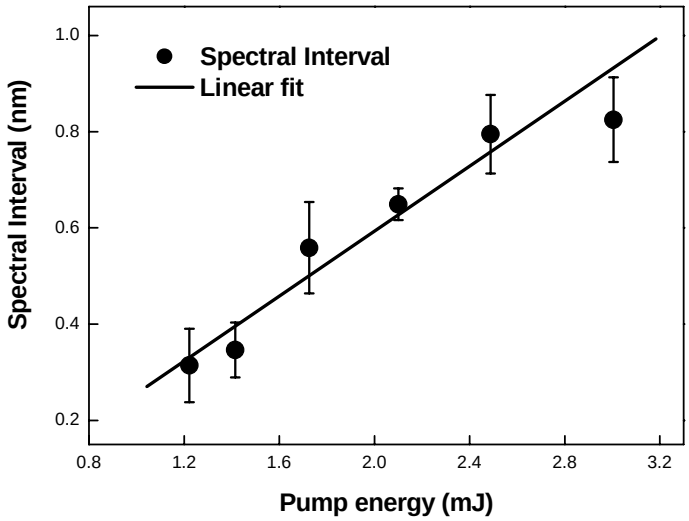

Fig.4.13 Variation of the dual-peak spectral interval as a function of the pump energy. The solid curve is a linear fit with a slope of 0.3 nm/mJ.

From the linear fit with the slope of 0.3 nm/mJ in Fig. 4.13, we get $n_2 = 6.2 \times 10^{-4}\,mJ^{-1}$. Using our experimental pump parameters, this corresponds to a resonant nonlinear refractive index $n_2 = 1.1 \times 10^{-12}\,cm^2/W$. At the lowest pump energy, DFB lasing sometimes occurred with only one single peak with or without a shoulder, as shown by the uppermost spectrum in Fig. 4.11. This may be indicative of a "threshold" to generate the index modulation DFB grating, thus the stop band. We interpret this threshold as the level at which index-coupling dominates gain-coupling. Observation of the PBG may be more possible in our experiments of DCM doped methanol DFB lasers. Because DCM presents a rather large Stokes shifted emission, also DFB coupling at the first order can be stronger than at higher orders.

The PBG observed in the DFB lasing emission spectra gives a measure of the nonlinear refractive index of the gain medium. So we propose this

reflection DFB laser configuration for the estimation of the nonlinear refractive index coefficient of luminescent materials.

From the PC appoint of view, the 1-D tunable DFB laser demonstrated in reflection pumping geometry from DCM doped methanol can be referred as a 1-D dynamic PC DFB laser (In 2.3 in chapter II). Index-coupling dominated the optical feedback. The periodical dielectric layers of the 1-D PC was induced due to the optical Kerr-nonlinearity effect caused by the interference of the two coherent pumping beams. The width of the PBG was proportional to the amplitude of the dielectric constant difference of the DFB grating.

4.2.4 Tuning summary

We summarized the tuning behavior of the two kinds of DFB lasers. Fig. 4.14 shows all of the tuning data obtained from R6G doped ethanol and DCM doped methanol.

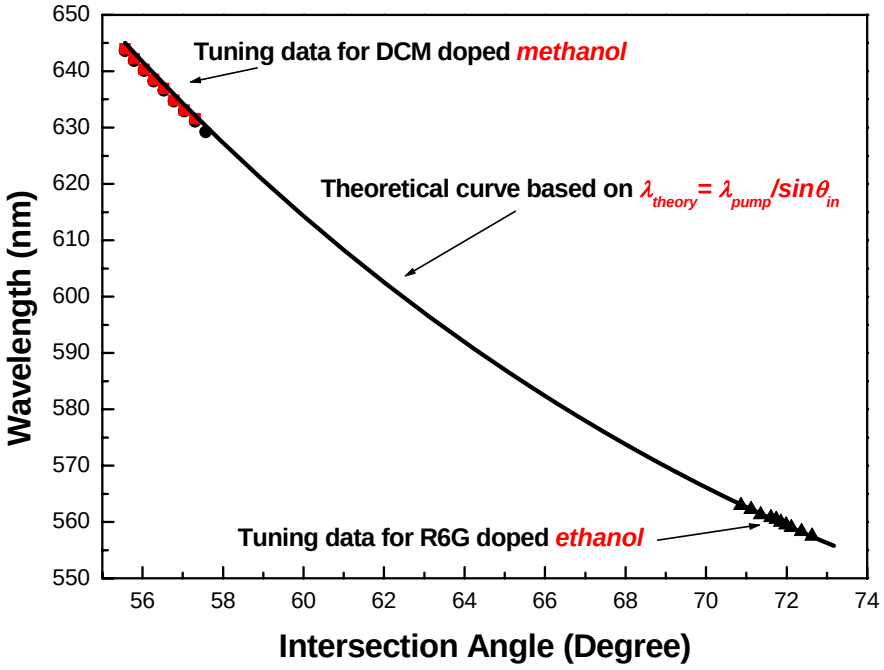

Fig. 4.14 The tuning summary of the DFB lasers from R6G doped ethanol and DCM doped methanol in reflection pumping geometry.

In Fig. 4.14, circles represent the DFB tuning data of DCM doped methanol (n=1.326) and triangles represent the DFB tuning data of R6G doped ethanol (n=1.359). Tuning for the two cases has different output wavelength ranges owing to different simulated emission ranges of the dyes. The solid curve, which passes through all the tuning data, is the theoretical prediction based on the DFB tuning equation for reflection geometry: $\lambda_L = \lambda_{pump} / \sin(\theta_{in} / 2)$. As seen in Fig. 4.13, the theoretical curve fits perfectly with both sets of the experimental tuning data. The DFB lasing wavelength is independent on the refractive indices of the dye doped solutions, which is an essential difference between reflection and the more traditional transmission DFB grating geometry.

4.3 DFB lasing effect in R6G doped PMMA films for the first Bragg order

R6G doped PMMA films were prepared on glass substrates by cast-coating method for DFB lasing experiments. The preparation procedure has been illustrated in Chapter Ⅲ. The concentration of R6G was 2×10^{-3}M. The refractive index of PMMA is around 1.49~1.498. The refractive index of the glass substrates is 1.51. The experimental arrangement of DFB lasers in reflection geometry was the same to the one used in our previous works. Tunable DFB lasing action was realized from R6G doped PMMA thick films. Gain modulation and an additional index modulation were created in the films by two crossing beams. Under low pump energy, permanent gain modulation caused by dye bleaching was generated while index modulation of the medium caused by photodamage was induced at high pump energy. Dual-peak DFB lasing emission indicative of an index grating was observed from the dye doped films under high pump energy. The first Bragg order was satisfied in our experiments. Tuning of the DFB output wavelength was achieved by varying the intersection angle, hence the period of the modulation. The DFB lasing tuning equation was also the same to the one in dye doped solution reflection DFB lasers, which is an index-independent form.

4.3.1 ASE spectrum

Narrow bandwidth ASE spectrum of R6G doped PMMA was measured along the normal direction from the surface of the film, when the pump intensity was above a certain threshold. Fig. 4.15 shows the typical spectrum.

The central wavelength was around 559.3 nm and the FWHM was 5.4 nm. Since the films were not uniform due to the cast-coating preparation method, resulting in various thicknesses at different positions of the film, we got different ASE spectra with shifted central wavelengths caused by various re-absorptions from different positions of a same sample. DFB lasing was tuned within the range of the ASE spectrum.

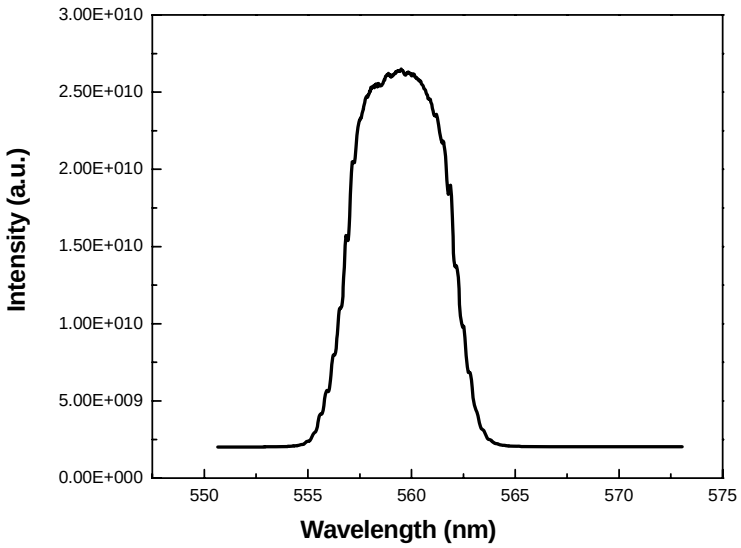

Fig. 4.15 ASE spectrum measured from R6G doped PMMA films.

4.3.2 DFB lasing characteristics

Narrow linewidth DFB lasing was observed in R6G doped PMMA films. The output lasing direction was perpendicular to the sample surfaces. Tuning of the output wavelength was obtained by varying the intersection angle. Fig. 4.16 illustrates the angle tuning spectra. The pump energy used was 2.9 mJ after considering the reflection and transmission losses. The laser spectrum exhibits a single prominent peak emission throughout the tuning range. ASE appeared in the background when the lasing was tuned away from the centre of

gain profile. Fig. 4.17 shows the experimental data of the angle tuning. The solid line is the theoretical prediction based on the DFB tuning equation for reflection geometry: $\lambda_L = \lambda_{pump} / M \cdot \sin(\theta_{in} / 2)$, in which the refractive index of PMMA was set to 1.49. The tuning data generally followed the theoretical fit. Reasonable agreement is seen. We note that the experimental data laid below the fit curve at long-wavelength-range and above the fit curve at short-wavelength–range. It is because we used a fixed value for the refractive index to fit the experimental data and ignored the dispersion effect of R6G doped PMMA films. In general, the refractive index of R6G doped PMMA films decreased slightly as the propagation wavelength increased in the tuning region. Since the single peak DFB lasing was tuned, the reflection DFB grating was relative to a gain-type grating. Gain modulation dominated the optical feedback for laser oscillation.

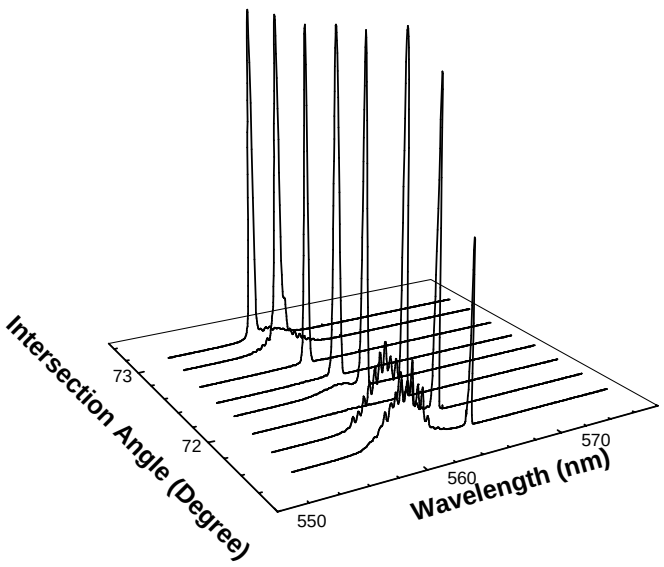

Fig. 4.16 Single peak DFB lasing emission spectra from R6G-doped PMMA films.

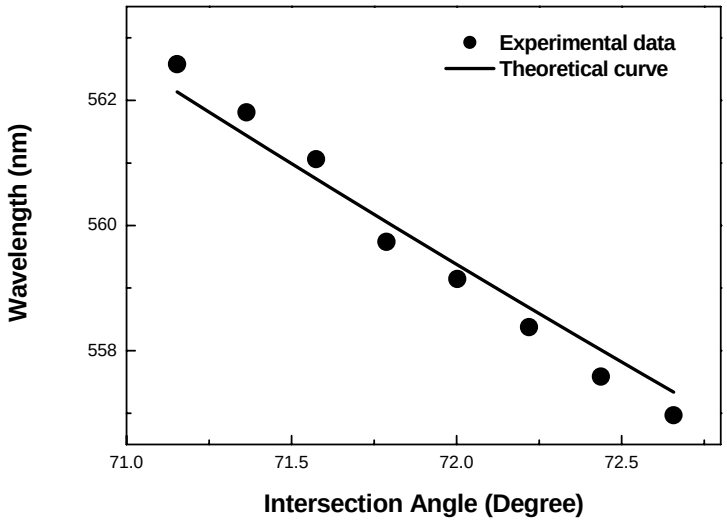

Fig. 4.17 Angle tuning as a function of the intersection angle. Solid line is the theoretical fit based on reflection grating geometry at the first Bragg order.

By increasing the pump energy, a 1-D PC with tunable PBG was achieved from R6G doped PMMA DFB lasers. Tunable dual-peak DFB lasing emission was obtained. The angle tuning of lasing spectra are illustrated in Fig. 4.18. The widening of the linewidth of the DFB lasing was due to the enhanced ASE background, resulting from the higher pump energy. Although the strong ASE background influenced the quality of the DFB lasing, the dual-peak structure of DFB lasing could still be distinguished. The origin of the tunable dual-peak lasing was attributed to the dynamic stop bandgap effect, coming from the generation of an additional index modulation grating in dye doped PMMA films under the higher energy pumping [13, 21]. The explanation has been presented in great detail in the above. Fig. 4.19 shows the tuning data and the theoretical fit based on the Bragg condition at the first order.

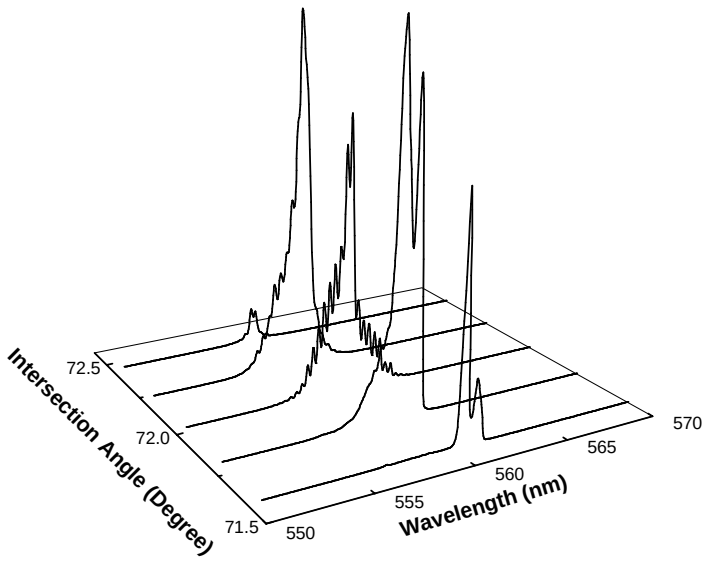

Fig. 4.18 Dual-peak lasing spectra from R6G doped PMMA films.

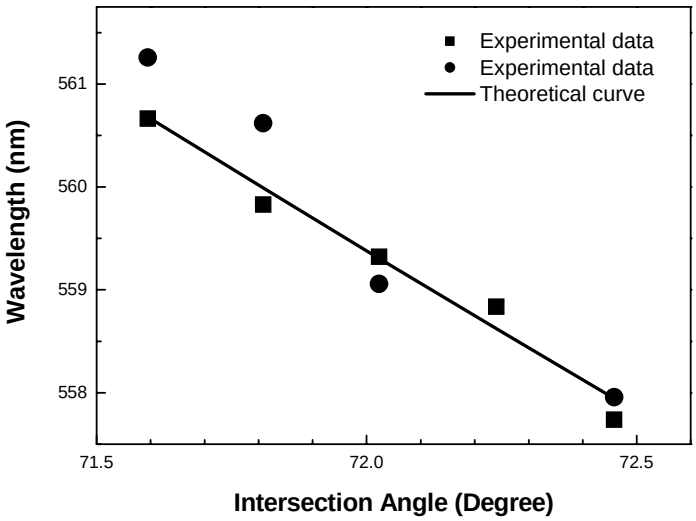

Fig. 4.19 Angle tuning data versus the theoretical fit for the first Bragg reflection order. Circles and rectangles represent the lasing wavelengths of the double peaks at every intersection angles.

In our experiments, we noticed that the DFB lasing could not be observed instantly when the two crossing pump beams overlapped, interfered

and created the light intensity periodical patterns inside the R6G doped PMMA films. Only after pumping a same sample position around two minutes with a pump frequency of 5 Hz, the DFB lasing could be generated from the sample surfaces. Considering of this point, the feedback for the lasing oscillation was supposed not being given by transient gain/index grating modulation but by permanent periodic modulation caused by photobleaching or photodamage of the organic dyes in the films. From the dramatic variation of the DFB lasing spectra as the pump energy increased from low to high, we claim that under a lower pump energy, permanent gain modulation caused by dye bleaching dominated the generation of DFB lasing; in contrast, under a higher pump energy, the additional index modulation of the medium caused by photodamage provided the feedback for the lasing, correspondingly, resulting in the tunable stop band effect, hence the tunable dual-peak DFB lasing emission.

The large dispersion of the spectral interval of the dual-peak lasing emissions was caused by the large dispersion of the nonlinear refractive index of R6G doped PMMA films at the Bragg resonances. Also the big variation of the pump energy made a contribution of changing the intersection angles, thus the periods of the modulations.

Referring to the above mentioned experimental results, we can also propose the method of reflection DFB laser configuration to evaluate the index changes in photodamage dye doped polymer materials.

We also studied the influence of the gain length to the generation of the DFB lasing oscillation in R6G doped PMMA films, that is to say, the influence of the film thickness to the DFB lasing emission. Various thicknesses of the films can be controlled by adjusting the viscosity of the mixed solution of PMMA and the solvent DCE, and the quantity of the solution dropped onto the glass substrates. Under a same pump energy of around 2.9 mJ, with samples of a same dye concentration of 1mM, at a same DFB lasing output wavelength of 558.7 nm, which was the central wavelength of the ASE gain range, DFB lasing action was achieved in a R6G doped PMMA film sample at a thickness as small as 150 um, which indicated the shortest gain length required for lasing oscillation, corresponding to a Bragg grating of about 800 repetition units created in the film. Fig. 4.20 shows the DFB lasing spectrum observed from the R6G doped PMMA film of a thickness of 150 um.

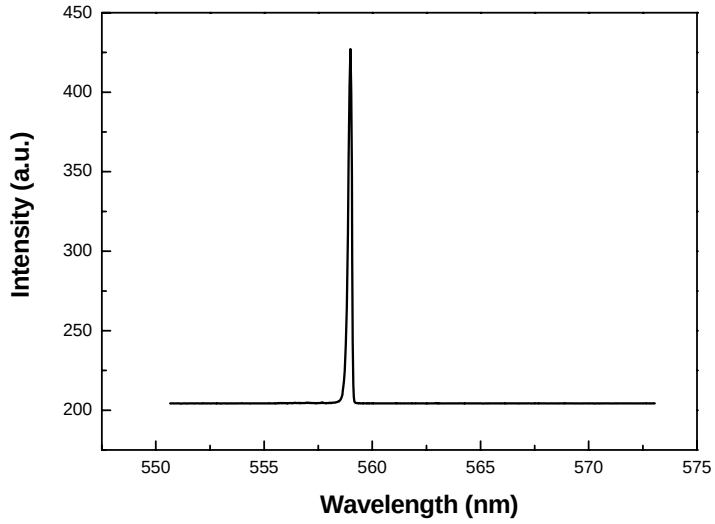

Fig. 4.20 DFB lasing spectrum observed from the R6G doped PMMA film of a thickness of 150 um.

4.3.3 Cavity lasing

Cavity lasing coming from some subcavities of R6G doped PMMA films on glass substrates could also be observed in our DFB laser experiments. Some tuning spectra in Fig.4.16 and Fig. 4.18 are the coexistence of the DFB lasing and the discrete multiple longitudinal modes structure. Fig. 4.21 shows a typical spectrum of the coexistence phenomenon. The mechanism which induced cavity lasing oscillations has been described in great detail in 4.1.4. Here we omit the explanation.

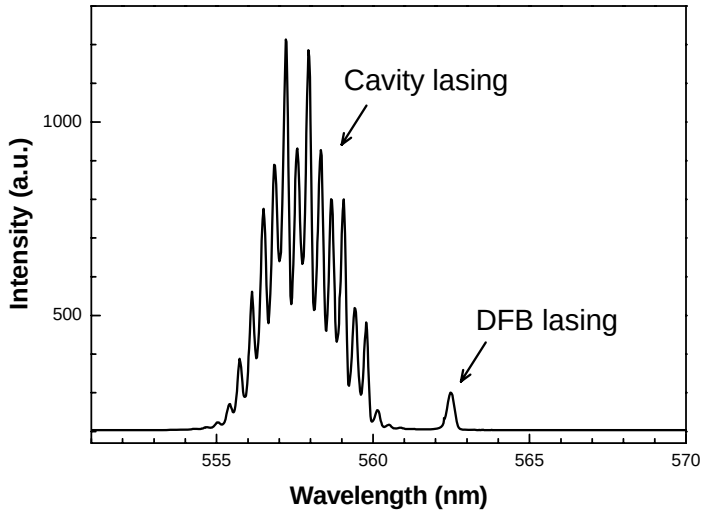

Fig. 4.21 A typical spectrum of the coexistence of DFB lasing and the cavity lasing

The threshold of DFB lasing could not be measured accurately due to the competition between the DFB lasing and cavity lasing. The DFB laser output dropped to half of its initial intensity after pumping a same sample position for hundreds of pulses. The short operation lifetime of the R6G doped PMMA

films was probably a result of photobleaching or photodamage of the gain medium.

4.4 Summary

Tunable DFB lasing output based on reflection grating configuration instead of the traditional transmission one was realized from R6G doped ethanol and DCM doped methanol, respectively. Pure gain-coupling and additional index-coupling were created for the feedback of lasing oscillation. In contrast with the transmission geometry, the tuning for the reflection grating geometry was found to be independent on the refractive index of the gain media. Dual-peak lasing emission indicative of the existence of an index grating was observed in DCM doped methanol, which was caused by the large Stokes shift of the laser dye DCM and the strong coupling achieved at the first Bragg order. The interval between the dual-peaks increased with the pump energy. This gives a measure of the nonlinear refractive index of the gain medium. Considering the index-coupling case in DCM doped methanol, our tunable 1-D DFB lasers can be referred as a 1-D dynamic PC, and tunable PBG was achieved in the operation of the lasing measurements.

R6G doped PMMA thick films were fabricated by cast-coating method. The thickness can be varied by controlling the quantity of the dye doped solutions dropped onto the glass substrates. Wavelength tunable lasing with single peak or dual-peak structure was demonstrated in the films based on reflection DFB gratings for the first Bragg order. A permanent grating of pure

gain modulation and/or an additional index modulation induced by photobleaching or photodamage of dye molecules in polymer host was proposed providing feedback for the single peak and dual-peak DFB lasing generation, respectively. The laser action could be achieved in a R6G doped PMMA film of a thickness as small as 150 um. The lifetime of the films was around hundreds of pulses.

References

[1] H. Kogelnik and C. V. Shank, “Stimulated emission in a periodic structure”, *Appl. Phys. Lett.* **18**, p152, 1971

[2] D. Lo, L. Shi, J. Wang, G.-X. Zhang and X.-L. Zhu, “Zirconia and zirconia-organically modified silicate distributed feedback waveguide lasers tunable in the visible”, *Appl. Phys. Lett.* **81**, p2707, 2002

[3] J. Wang, G.-X. Zhang, L. Shi, D. Lo and X.-L. Zhu, “Tunable multiwavelength distributed feedback zirconia waveguide lasers”, *Opt. Lett.* **28**, p90, 2003

[4] L. Shi, G.-X. Zhang, J. Wang and D. Lo, “Distributed feedback laser action in sol-gel glass symmetric waveguides”, *J. Opt. A: Pure Appl. Opt.* **5**, pL1, 2003

[5] F. Chen, J. Wang, C. Ye, D. Lo and X.-L. Zhu, “Distributed feedback sol-gel zirconia channel waveguide lasers”, *Appl. Phys. Lett.* **85**, p4284, 2004

[6] C. Ye, L. Shi, J. Wang, D. Lo, X.-L. Zhu, “Simultaneous generation of multiple pairs of transverse electric and transverse magnetic output modes from titania zirconia-organically modified silicate distributed feedback waveguide lasers”, *Appl. Phys. Lett.* **83**, p4101, 2006

[7] C. Ye, J. Wang, D. Lo, “Two-photon-pumped distributed feedback zirconia waveguide lasers”, *Appl. Phys. B* **78**, p539, 2004

[8] L. Rocha, V. Dumarcher, C. Denis, P. Raimond, C. Fiorini, J.-M. Nunzi, “Laser emission in periodically modified polymer films”, J. *Appl. Phys.* **89**, p3067, 2001

[9] D. Gindre, A. Vesperini, J.-M. Nunzi, H. Leblond and K. D. Dorkenoo, “Refractive-index saturation-mediated multiple line emission in polymer thin-film distributed feedback lasers”, *Opt. Lett.* **31**, p1657, 2006

[10] P. Del Carro, A. Camposeo, R. Stabile, E. Mele, L. Persano, R. Cingolani and D. Pisignano, “Near-infrared imprinted distributed feedback lasers”, *Appl. Phys. Lett.* **89**, p201105-1, 2006

[11] D. E. Luchetta, L. Criante, O. Francescangeli, S. Fimoni, “Laser amplification by dye-doped holographic polymer-dispersed liquid crystals”, *Appl. Phys. Lett.* **84**, p4893, 2004

[12] S.-T. Wu, A. Y.-G. Fuh, “Lasing in photonic crystals based on dye-doped holographic polymer dispersed liquid crystal reflection grating”, *Jpn. J. Phys. Lett.* **44**, p977, 2005

[13] H. Kogelnik and C. V. Shank, “Coupled-wave theory of distributed feedback lasers”, *J. Appl. Phys.* **43**, p2327, 1972

[14] F. Chen, D. Gindre and J.-M. Nunzi, “First-order distributed feedback dye laser effect in reflection pumping geometry”, *Opt. Lett.* **32**, p805, 2007

[15] F. Chen, D. Gindre and J.-M. Nunzi, “First order distributed feedback dye laser effect in reflection pumping geometry for nonlinear optical measurements”, *Proc. SPIE.* **6653**, 665303, 2007

[16] G. S. He, L. X. Yuan, Y. P Cui, M. Li and P. N. Prasad, “Studies of two-photon pumped frequency-upconverted lasing properties of a new dye material”, *J. Appl. Phys.* **81**, p2529, 1997

[17] G. S. He, R. Signorini and P. N. Prasad, “Two-photon-pumped frequency-upconverted blue lasing in Coumarin dye solution”, *Appl. Opt.* **37**, p5720, 1998

[18] E. Yablonovitch, “Inhibited Spontaneous emission in Solid-state Physics and Electronics”, *Phys. Rev. Lett.* **58**, p2059, 1987

[19] S. John, “Strong Localization of Photons in Certain Disordered Dielectric Superlattices”, *Phys. Rev. Lett.* **58**, p2487, 1987

[20] J. M. Bendickson, J. P. Dowling, M. Scalora, “Analytic expressions for the electromagnetic mode density in finite, one-dimensional, photonic band-gap structures”, *Phys. Rev. E* **53**, p4107, 1987

[21] V. Dumarcher, L. Rocha, C. Denis, C. Fiorini, J.-M. Nunzi, F. Sobel, B. Sahraoui and D. Gindre, *Pure. Appl. Opt.* **2**, p279, 2000

Chapter V

DFB Laser Action by Polarization Modulation Based on Reflection Pumping Geometry

5.1 Introduction

As described in Chapter II, DFB laser action is made possible by the presence of periodic perturbations in the gain medium that provide feedback by backward Bragg scattering [1,2]. The periodic perturbations can be affected by the spatial modulation of the refractive index [2] or gain or a combination of both [2]. In a waveguide structure, a periodic change of the guiding film thickness was also proven effective in inducing DFB laser action [3]. The periodic perturbations can be permanent or transient, with the transient effect often produced by crossing two beams from the output of the same laser to generate a concentration grating [2,4].

Light wave is a vector field. It can be characterized by its intensity and its state of polarization, which can be further specified by its ellipticity, orientation of the major axis, and rotation direction. When two coherent beams intersect, they will vectorially add to produce a total vectorial field in the intersection region. The new total light field may have different intensity and polarization state from either of the two coherent beams but it is always a planar polarization ellipse. Since the phase difference between the two beams is spatially varying, the polarization ellipse of the total field usually varies spatially in both its intensity and the state of the polarization. In certain cases,

the vectorial interference can be arranged so that the intensity or the state of the polarization is modulated separately. For example, in conventional scalar holography [5], the two writing beams are linearly polarized perpendicular to the plane of incidence (*s*-polarized), and the polarization state of the total field remains the same as the writing beams. The spatially varying phase difference in this case causes only an intensity modulation manifested as a familiar intensity fringe pattern. On the other hand, if the two writing beams are orthogonally linearly polarized (e. g., one *p*- and the other *s*-polarized), the variation of the phase difference induces a pure polarization modulation with no intensity modulation. The overall intensity is unity in this case. A hologram recorded by intensity modulations is called a scalar hologram as it stores only the intensities and phases of the two recording beams without involving the state of polarization. However, a hologram recorded by polarization modulation will store the polarization information of the writing beams as well. The phenomena of polarization grating on dye doped materials have been studied for application in holographic recording [7].

Significantly, the polarization modulation has been introduced in the DFB lasers for providing the optical feedback. The polarization effects of DFB lasing during optical pumping have been reported in [8, 9]. Recently, Lo's group reported a detailed experimental investigation of the polarization properties of DFB lasing output by polarization modulation based on dye doped solutions and dye doped sol-gel waveguides in the conventional *transmission* pumping geometry [10,11]. They demonstrated that a transient

polarization grating resulting from polarization modulation can be used to generate DFB laser action. The polarization grating induced by the optical anisotropy of the gain medium provides the periodic perturbations needed for DFB lasing. The degree of polarization of the laser output was observed showing an increasing trend as the Bragg scattering order (the intersection angle). In their works, the output polarization characteristics were prescribed by the concepts with the same vein of polarization volume hologram [12, 13]. The change of degree of polarization of the DFB laser output as the Bragg order was understood in terms of the projection of the spatially varying polarization ellipse on the plane perpendicular to the direction of propagation of the DFB laser beam. The periodical and spatially varying field generated by the crossing beams resulted in the periodically varying polarization ellipse, the ellipticity of the projected polarization ellipse determined the degree of polarization of the laser output beam.

The schematic of the crossing beams DFB laser experiment based on transmission pumping geometry is illustrated in Fig. 5.1. The two beams are shown to have their polarization directions at an angle Φ. The crossing beams must have an *s*-polarized ($\Phi = 0^o$) component for the formation of an intensity interference pattern (intensity modulation).

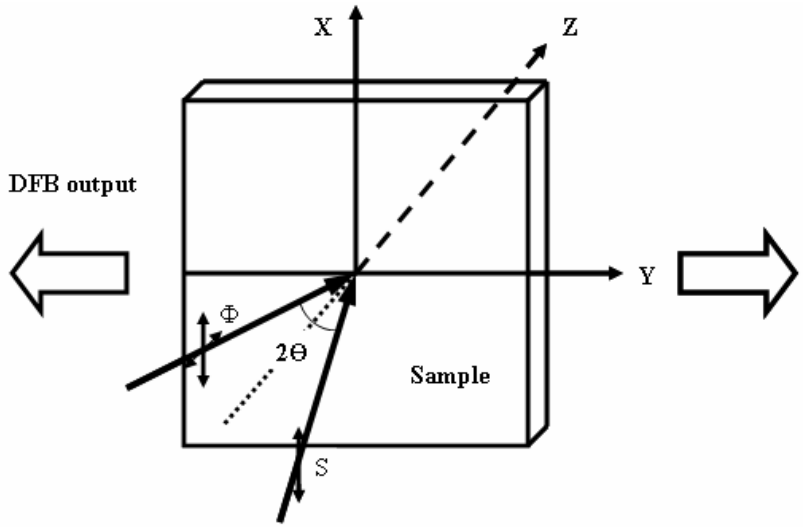

Fig. 5.1 Schematic of the crossing beams DFB laser experiments. The polarization of one of the beams is at an angle Φ with respect to the *s*-polarization. The other beam is *s*-polarized.

The intensity interference pattern in the gain medium produces a concentration grating of excited-state atoms/molecules, which is to provide the periodic change in gain and refractive index necessary for DFB laser action. The crossing of an *s*-polarized beam with a *p*-polarized beam ($\Phi = 90^o$) does not produce an intensity interference pattern. No spatial modulation of atoms/molecules concentration could result in the gain medium. Instead a periodic change of the polarization of the resultant field, which changes from the linear polarization to elliptical polarization to circular polarization and then back to elliptical polarization after one period, is created [6]. The excited-state atoms/molecules align themselves along the preferred direction of the polarization across the gain medium. The grating resulted is a polarization grating. The similar case is the crossing of a left-handed circular polarized beam with a right-handed circular polarized beam. The induced interfering grating includes an additional polarization grating. The type of gratings (modulations) is relative to the interference geometries (transmission or

reflection) and the interference angles of the two pumping beam (bigger or smaller). One can see this point in the following text. In our works, we will show that in our DFB lasers based on reflection grating geometry, both intensity modulation and additional polarization modulation dominate the optical feedback for the DFB lasing oscillation at the same time, and the additional polarization grating effectively controls the polarization properties of the DFB lasing output.

Since polarization modulation produces no change in the scalar amplitude of either the gain or the refractive index in the gain medium, the mechanism by polarization modulation can not be described by coupled-wave theories based on the scalar equation.

In this chapter, we present our recent results of DFB lasers from dye doped solvents by a combination of intensity modulation and additional *polarization modulation* based on *reflection* pumping geometry. DFB lasing action was generated in dye doped liquid solutions by crossing two pump beams from a frequency-doubled Nd:YAG laser. The angle between the polarization directions of the two beams was changed properly to obtain the desired pumping schemes: left-handed circular polarized: left-handed circular polarized (LCP:LCP) pumping, right-handed circular polarized: right-handed polarized (RCP:RCP) pumping, left-handed circular polarized: right-handed circular polarized (LCP:RCP) pumping, *s*-polarized: *p*-polarized (*s*:*p*) pumping and *p*-polarized: *p*-polarized (*p*:*p*) pumping. Tunable narrow linewidth circular

polarized DFB lasing output was realized from DCM doped methanol. It was found that a chiral photonic DFB structure was induced by crossing two circular polarized pumping beams with a same rotation direction (LCP:LCP and RCP:RCP cases). Dual-peak circular polarized lasing emissions with desired rotation directions were obtained. The intensity modulation attributed to the creation of the tunable DFB PC, thus the generation of the tunable dual-peak DFB lasing emission; while the polarization modulation effectively controlled the polarization properties of the laser output.

The rotation direction of the polarization was relative to the chiral property of the DFB structures. It would be understood in considering of a generation of periodically and spatially varying polarization ellipses caused by the periodic total field of the crossing beams. This underlying physics can be prescribed by applying the DFB lasing feedback mechanism in the vein of dye doped cholesteric liquid crystals (CLCs) [14]. In the following, we will describe in detail this mechanism, since it's very necessary for a good understanding of our experimental phenomena. First of all, an introduction of polarization interference in the polarization holography will be given [12, 13].

5.2 Polarization interferences analysis

5.2.1 Introduction to the polarization holography in transmission grating geometry

Photoanisotropic materials are commonly used for recording of polarization volume hologram based on photoinduced dichroism and birefringence. Microscopically speaking, the mechanism of such photoinduced

vectorial recording is achieved by an orientationally dependent photoisomerization of the highly anisotropic dye molecules in dynamic photoanisotropic organic materials [12, 13].

The process of the photoisomerization can be achieved by exposure of a dye molecule to visible light so that it jumps to the excited triplet state by absorbing a photon, thus inducing its optical properties distinct from those in its original ground state. As a result, interferometrically produced spatially varying light pattern can be converted to a spatially varying perturbation of the optical constants to record a holographic grating. For isotropic dye molecules, they absorb a photon with equal probability for arbitrary spatial orientation of the input polarization. But for anisotropic dye molecule, the absorption cross section depends on the molecule's orientation relative to the polarization direction of the acting light in addition to its dependence on light intensity. When the principal absorption oscillator axis of a dye molecule is parallel to the incident linear polarization direction, the probability of absorbing a photon is the highest; the probability is the lowest when the oscillator axis is perpendicular to the polarization direction. As a result of this anisotropic transition probability, for a uniform orientational distribution of dye molecules, more dye molecules whose absorption axes are parallel to the polarization direction are isomerized than molecules which have other absorption axis orientations. Finally, some degree of polarization-dependent photoisomeric population redistribution of the molecules can be achieved, even without intensity variation, leading to photoinduced birefringence, dichroism, and optical activity [13].

From the above description, we know that the transition probability of the dye molecule is polarization-dependent, and so is the population distribution. Because of this polarization-dependent behavior, we can store polarization information based on spatially varying oriented population distribution of the dye molecules. The polarization holography in Ref. 13 and Ref. 14 are operated in the conventional *transmission* geometry (in Fig. 5.2). To obtain polarization-dependent transition probability and population distribution, the first thing is to solve for the polarization state of the total field. The process of building the interference vectorial fields and the analysis of polarization state of the fields in transmission grating geometry from two beams with arbitrary polarizations has been described in great detail in Ref. 13.

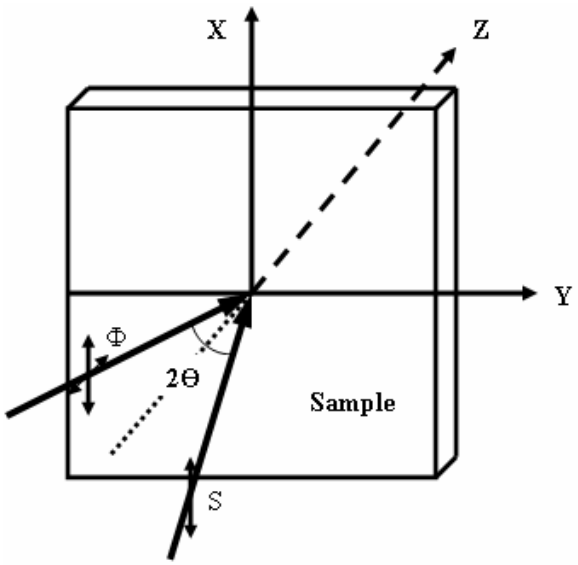

Fig. 5.2 Formation of a polarization grating, with two arbitrary polarized beams separated by an angle 2Θ in the *YZ* plane incident symmetrically onto the sample in a transmission grating geometry.

In Fig. 5.2, when two interfering beams of arbitrary polarization intersect; due to the phase variation between the two beams, the state of polarization of

the total field changes spatially in its magnitude and orientation, with the same spatial periodicity as the corresponding intensity fringe pattern. The polarization state of the total field, in general, is a planar ellipse and is different at each point. The polarization ellipse was illustrated in three-dimension for one period of the total field [12]. To better visualize three-dimensional ellipses, the projections of the ellipses on the *XY* and *YZ* planes were also analyzed. It was found that, when Θ is large, the total polarization tips and tits in three-dimension in the coordinates *XYZ* and their major and minor axes and the plane containing the polarization ellipses vary spatially. When Θ is small, the polarization ellipses lie almost completely in the *XY* plane. In this case, the polarization component in the *XY* plane is a good approximation of the actual three-dimensional optical polarization ellipse. The corresponding ellipsoids of photoinduced index changes by the polarization ellipses were also obtained with a tensor description [12].

Since the good approximation of the projection of the polarization field on *XY* plane, of much interest was involved in the spatially varying field projected on *XY* plane, which are represented by thinner curves. Referring to Ref. 14, we describe four archetypical cases of polarization interferences in transmission geometry: (a) *s*-polarized: *s*-polarized interference ($\Phi = 0^o$): the two beams are polarized perpendicular to the plane of incidence. The state of polarization of the total field is linear, and the direction remains unchanged. The phase modulation between the two interfering beams is encoded as a pure intensity modulation. (b) *s*-polarized: *p*-polarized interference ($\Phi = 90^o$): the

polarization directions of the two beams are orthogonal; there is no intensity modulation in this case. The variation of the phase difference between the two beams is thus encoded in the variation of the polarization state of the total field instead of the spatial variation of the intensity. (c) Left-handed circular polarized: left-handed circular polarized (LCP:LCP) interference: the two beams are circularly polarized and have the same rotation direction. The total field has the same polarization state as the two recording beams and is circularly polarized as well; such a situation would be identical to the *s*-polarized: *s*-polarized interference case. (d) Left-handed circular polarized: right-handed circular polarized (LCP:RCP) interference case: this case is an orthogonal circular polarization case. In this case, the spatial rotation of the polarization direction caused by a spatially linearly varying phase difference between the two equal-amplitude orthogonally circularly polarized beams encodes the interference field; the polarization state is everywhere linear but rotates in space with a constant angular frequency along the grating period. We note that there is also a nonzero contribution from the intensity modulation [13]. Fig. 5.3 illustrates the periodic spatial variations through one period of the total interference patterns projected onto the *XY* plane in the above four types of holographic recording geometries. The thinner curves of the projections of the periodical ellipses of all kinds of patterns were obtained with Jones Matrix (In appendix). A similar discussion on interferences of beams with different polarizations is also presented in an investigation of the polarization-dependent surface-relief-grating (SRG) formation process in AZO polymer films [15].

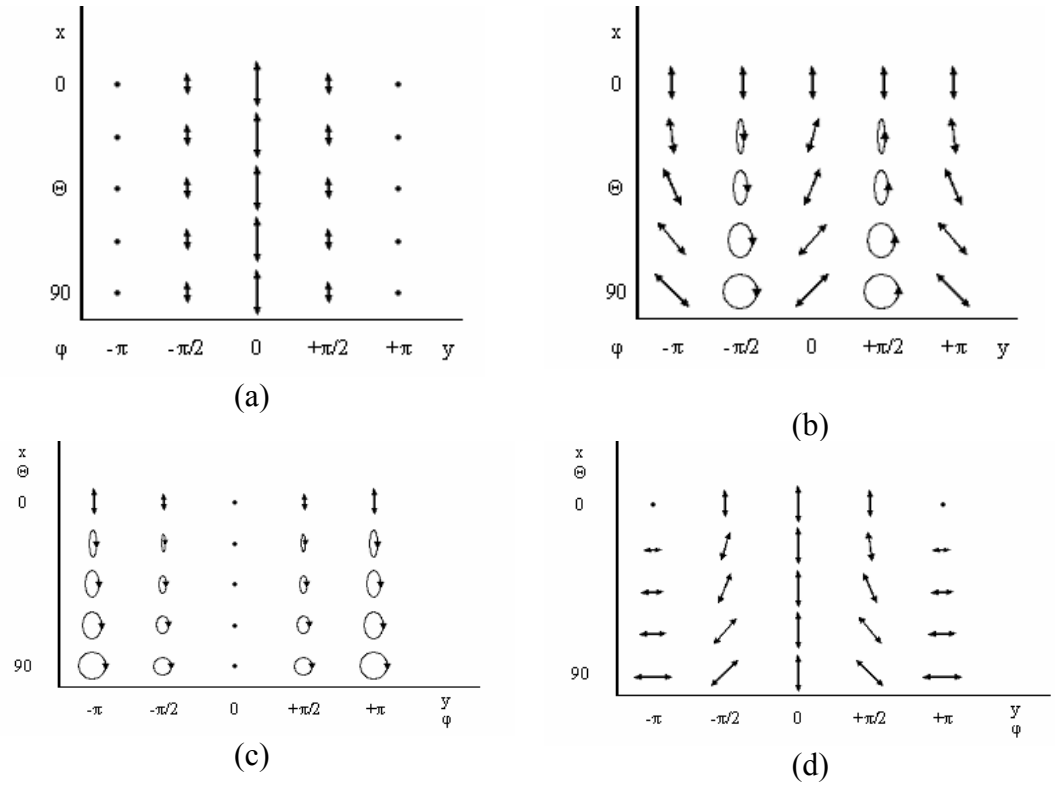

Fig. 5.3 One period of the interference patterns projected onto the *XY* plane at different intersection angles for four types of interference schemes (not completely to scale): (a*) s:s*; (b) *s*:*p*; (c) LCP:LCP; (d) LCP:RCP.

5.2.2 Interferences of beams with different polarizations in reflection grating geometry

In 5.2.1, we have learned the methodology of analysis of polarization modulation induced by two interfering writing beams in polarization holography based on the transmission geometry. The Jones Matrix provides an effective means for the polarization state analysis and expression of the interference field.

As mentioned in Introduction (5.1), Lo's group has demonstrated DFB lasing output by polarization modulation in the conventional *transmission* pumping geometry [10, 11]. They found that a transient polarization grating resulted from polarization modulation can be used to generate DFB laser action.

The polarization grating induced by the optical anisotropy of the gain medium provides the periodic perturbations needed for DFB lasing. It was verified that the degree of polarization of the output beam followed the ellipticity of the projected polarization ellipse on the plane perpendicular to the direction of propagation of the DFB laser beam, which was resulted from the total periodically and spatially varying interference polarization field.

In our work, we will realize and investigate the DFB lasing emission by polarization modulation based on a reflection grating geometry. Fig. 5.4 shows a simplified scheme of our DFB laser configuration. The DFB grating is formed by the interference of two pumping beams from the opposite sides of the sample. The grating planes are parallel to the sample surface, and the DFB lasing emits along the direction normal to the sample surface, that is to say, vertical to the reflection grating planes or same to the grating vector.

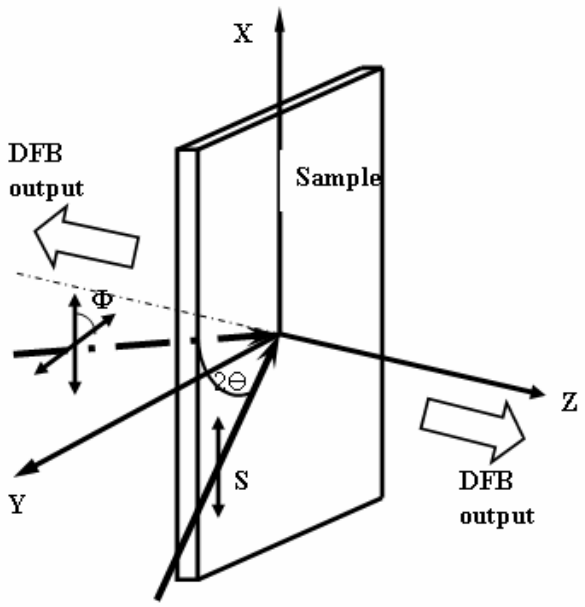

Fig. 5.4 A simplified scheme of the DFB laser by polarization modulation in reflection grating geometry.

Since the DFB lasing in reflection geometry emits vertical to the grating planes; also, we have known that, in transmission geometry, the state of polarization of DFB lasing emission was mainly determined by the ellipticity of the projected polarization ellipse of the interference field, on the plane perpendicular to the direction of propagation of the DFB laser beam [10, 11]; therefore we would expect that, in the reflection grating geometry, the polarization of DFB laser output should also follow the ellipticity of the projection of the polarization ellipse on the reflection grating planes.

Subsequently, we will focus our attention on the analysis of projected polarization ellipse of the total polarization field by the interference of two pumping beams with different polarizations, on the plane perpendicular to the direction of the DFB laser beam (*XY* plane in Fig.5.4), in reflection grating geometry. Six kinds of pumping schemes are considered, viz., *s*:*s* crossing; *s*:*p* crossing; *p*:*p* crossing; left-handed circular polarized: left-handed circular polarized (LCP:LCP) crossing; right-handed circular polarized: right-handed circular polarized (RCP:RCP) crossing; left-handed circular polarized: right-handed circular polarized (LCP:RCP) crossing. The analysis will be deduced in the right-handed Cartesian coordinates shown in Fig. 5.4.

(1) *s*:*s* crossing

For *s*:*s* crossing, $\mathbf{E_1}$ and $\mathbf{E_2}$ can be expressed by their complex amplitudes

$$\mathbf{E_1} = \hat{x}E_1 e^{-ik_1 \cdot r},$$

$$\mathbf{E_2} = \hat{x}E_2 e^{-ik_2 \cdot r}, \qquad (5.1)$$

where $\hat{x}$ denotes the unit vector along the direction of electric field vector. When the two beams intersect at an angle Θ, the interference field $\mathbf{E_{s:s}}$ is the superposition of two waves

$$\mathbf{E_{s:s}} = \mathbf{E_1}+\mathbf{E_2} = \hat{x}(e^{-i\varphi}+1)Ee^{-ik_2\cdot r}, \tag{5.2}$$

where φ is the phase difference between the two pumping beams, $\varphi = k_1 \cdot r - k_2 \cdot r$ and $|\mathbf{E_1}| = |\mathbf{E_2}| =$ E. With Jones matrix, we can write the interference field in the form of Jones vector at an arbitrary intersection angle:

$$\mathbf{E_{s:s}} = \mathbf{E_1}+\mathbf{E_2} = \begin{vmatrix} E_x \\ E_y \\ E_z \end{vmatrix} = E \begin{vmatrix} e^{-i\varphi}+1 \\ 0 \\ 0 \end{vmatrix}. \tag{5.3}$$

From Equation (5.3), the pictorial representation of the interference pattern can be deduced. By normalizing the Jones vector and neglecting common phase factors for the interference field, the expression can be simplified. Fig. 5.5 illustrates one period of the interference pattern, projected onto the *XY* plane, for *s*:*s* pumping scheme. Obviously, from Eq. (5.4), we see that the interference pattern doesn't change as the intersection angle Θ (0^o~90^o) of the two crossing beams. According to the field distribution, we can refer the reflection grating as an intensity grating, and a concentration grating will thus be resulted to supply feedback for DFB lasing. The state of polarization of DFB lasing output will be a linear polarization along the *s*-polarized direction.

$-\pi$	$-\pi/2$	0	$+\pi/2$	$+\pi$
•	↕	↕	↕	•

Fig. 5.5 One period of the polarized interference patterns projected onto the *XY* plane for *s*:*s* pumping scheme (not completely to scale)

(2) *s*:*p* crossing

For *s*:*p* crossing, the expressions of $\mathbf{E_1}$ and $\mathbf{E_2}$ become as

$\mathbf{E_1} = \hat{x}E_1 e^{-ik_1 \cdot r}$,

$\mathbf{E_2} = (-\hat{y}E_2 \sin\Theta + \hat{z}E_2 \cos\Theta)e^{-ik_2 \cdot r}$. (5.4)

with Jones Matrix, their interference field can be written as

$$\mathbf{E_{s:p}} = \begin{vmatrix} E_x \\ E_y \\ E_z \end{vmatrix} = E \begin{vmatrix} e^{-i\varphi} \\ -\sin\Theta \\ \cos\Theta \end{vmatrix}. \quad (5.5)$$

According to Eq. (5.5), one can see that, the interference pattern is relative to the intersection angle Θ, in other words, the reflection grating will change as a function of the intersection angle. The projection of the interference field by thinner curves on the *XY* plane at an intersection angle of around 60° is plotted in one grating period (Fig. 5.6). From Eq. (5.6), we can also deduce that there is no spatial variation of the intensity; the electric fields of the two interfering beams are orthogonal to each other for all intersection angles. The modulation in this situation is thus a pure polarization modulation. We predict that the DFB lasing emission will be depolarized.

$-\pi$	$-\pi/2$	0	$+\pi/2$	$+\pi$
				

Fig. 5.6 One period of the interference pattern projected onto the *XY* plane for *s*: *p* pumping scheme (not completely to scale).

(3) *p*:*p* crossing

The two crossing beams can be expressed as

$\mathbf{E_1} = (\hat{y}E_1 \sin\Theta + \hat{z}E_1 \cos\Theta)e^{-ik_1 \cdot r}$,

$$\mathbf{E_2} = (-\hat{y}E_2 \sin\Theta + \hat{z}E_2 \cos\Theta)e^{-ik_2 \cdot r}, \tag{5.6}$$

The interference field $\mathbf{E}_{p:p}$ has the form

$$\mathbf{E}_{p:p} = \begin{vmatrix} E_x \\ E_y \\ E_z \end{vmatrix} = E \begin{vmatrix} 0 \\ (e^{-i\phi} - 1)\sin\Theta \\ (e^{-i\phi} + 1)\cos\Theta \end{vmatrix}. \tag{5.7}$$

Again, the interference pattern on the *XY* plane at an arbitrary intersection angle is plotted in one grating period (Fig. 5.7). We can get that the induced reflection grating is an intensity grating, resulting in an intensity modulation in this case. And the amplitude of the interference pattern is relative to the intersection angle Θ. The state of polarization of DFB laser output should follow the polarization of the interference field. So a *p*-polarized DFB lasing emission would be expected in this situation.

$-\pi$	$-\pi/2$	0	$+\pi/2$	$+\pi$
⟷	↔	•	↔	⟷

Fig. 5.7 One period of the interference pattern projected onto the *XY* plane for *p*:*p* pumping scheme (not completely to scale).

(4) LCP:LCP crossing

The two exciting circular polarized beams are parallel, with left-handed rotation direction. They can be written as

$$\mathbf{E_1} = \frac{1}{\sqrt{2}}(\hat{x}iE_1 + \hat{y}E_1 \sin\Theta + \hat{z}E_1 \cos\Theta)e^{-ik_1 \cdot r},$$

$$\mathbf{E_2} = \frac{1}{\sqrt{2}}(\hat{x}iE_2 - \hat{y}E_2 \sin\Theta + \hat{z}E_2 \cos\Theta)e^{-ik_2 \cdot r}, \tag{5.8}$$

The interference field $\mathbf{E}_{\mathrm{LCP:LCP}}$ is

$$\mathbf{E}_{\mathrm{LCP:LCP}} = \begin{vmatrix} E_x \\ E_y \\ E_z \end{vmatrix} = \frac{1}{\sqrt{2}} E \begin{vmatrix} i(e^{-i\varphi}+1) \\ (e^{-i\phi}-1)\sin\Theta \\ (e^{-i\phi}+1)\cos\Theta \end{vmatrix}. \tag{5.9}$$

The projection of the interference pattern on the *XY* plane at an intersection angle of around 60^{o} is illustrated in one grating period (Fig. 5.8). In this situation, the intensity of the total incident field is spatially varying due to the varying electric field amplitude according to Eq. (5.9). The polarization state is everywhere linear but rotates in space with a constant angular frequency along the grating period. Thus the grating is not only an intensity grating but also a polarization grating. So we get that the modulation in LCP:LCP pumping scheme is a combination of both intensity modulation and polarization modulation. Since the excited dipole moment of dye molecules will have a distribution along all of the linear polarization directions on the *XY* plane in one grating period, we predict that the DFB lasing will be a roughly circular polarized beam.

$-\pi$	$-\pi/2$	0	$+\pi/2$	$+\pi$
				

Fig. 5.8 One period of the interference pattern projected onto the *XY* plane for LCP:LCP pumping scheme (not completely to scale)

(5) RCP:RCP crossing

The two exciting circular polarized beams are parallel, with right-handed rotation direction. They can be written as

$$\mathbf{E_1} = \frac{1}{\sqrt{2}}(-\hat{x}iE_1 + \hat{y}E_1\sin\Theta + \hat{z}E_1\cos\Theta)e^{-ik_1\cdot r},$$

$$\mathbf{E_2} = \frac{1}{\sqrt{2}}(-\hat{x}iE_2 - \hat{y}E_2\sin\Theta + \hat{z}E_2\cos\Theta)e^{-ik_2\cdot r}, \tag{5.10}$$

The interference field $\mathbf{E}_{\mathrm{RCP:RCP}}$ is

$$\mathbf{E}_{\mathrm{RCP:RCP}} = \begin{vmatrix} E_x \\ E_y \\ E_z \end{vmatrix} = \frac{1}{\sqrt{2}}E\begin{vmatrix} -i(e^{-i\varphi}+1) \\ (e^{-i\phi}-1)\sin\Theta \\ (e^{-i\phi}+1)\cos\Theta \end{vmatrix}. \tag{5.11}$$

The interference pattern on the *XY* plane at an intersection angle of around 60^o is illustrated for one grating period in Fig. 5.9. The similar to the LCP:LCP crossing case, the periodic modulation is a combination of both intensity modulation and polarization modulation. The difference is that the polarization state of the interference field rotates in space in an opposite direction comparing to the LCP:LCP crossing case. The DFB lasing will also be a roughly circular polarized beam.

$-\pi$	$-\pi/2$	0	$+\pi/2$	$+\pi$
↔	⤡	↕	⤢	↔

Fig. 5.9 One period of the interference pattern projected onto the *XY* plane for RCP:RCP pumping scheme (not completely to scale)

In addition, in the LCP:LCP and RCP:RCP pumping schemes, we mentioned in the above that, the total field polarization state is everywhere linear but rotates in space with a constant angular frequency along opposite rotation directions respectively. This will determine the rotation direction of

the circular polarized DFB lasing emissions. This point will be verified in our DFB laser experiments. Since the modulation is contributed by both of the intensity modulation and polarization modulation, the feedback of DFB lasing oscillation is provided by both. The intensity modulation mainly dominates the generation of tunable PC in the DFB structure; while the polarization modulation effectively controls the polarization properties of the laser output.

By analyzing the rotation direction of the interference field along the grating period, we can also obtain that, in the LCP:LCP crossing case, the interference pattern presents a left-handed helix structure, while a right-handed helix structure of the interference field is obtained in the RCP:RCP crossing case. Consequently, left-handed and right-handed chiral photonic structures are created in LCP:LCP pumping and RCP:RCP pumping, respectively, which is similar to the chiral photonic structures formed by cholesteric liquid crystals (CLCs) [14]. In this case, we see that, we can get a *dynamic* chiral photonic structure in reflection DFB lasers easily by manipulating the polarization state of the two pumping beams. The polarization state of DFB lasing emission in this chiral photonic structure can also be predicted.

(6) LCP:RCP crossing

The two exciting circular polarized beams are orthogonal, we have

$$\mathbf{E_1} = \frac{1}{\sqrt{2}}(\hat{x}iE_1 + \hat{y}E_1\sin\Theta + \hat{z}E_1\cos\Theta)e^{-ik_1\cdot r},$$

$$\mathbf{E_2} = \frac{1}{\sqrt{2}}(-\hat{x}iE_2 - \hat{y}E_2\sin\Theta + \hat{z}E_2\cos\Theta)e^{-ik_2\cdot r}, \qquad (5.12)$$

Their interference field becomes

$$\mathbf{E}_{\mathrm{LCP:RCP}} = \begin{vmatrix} E_x \\ E_y \\ E_z \end{vmatrix} = \frac{1}{\sqrt{2}} E \begin{vmatrix} i(e^{-i\varphi} - 1) \\ (e^{-i\phi} - 1)\sin\Theta \\ (e^{-i\phi} + 1)\cos\Theta \end{vmatrix}. \tag{5.13}$$

The projected interference pattern on the *XY* plane at an intersection angle of around 60^{o} is shown in Fig. 5.10. From the interference pattern, we see that, the projected field on the *XY* plane is roughly elliptically polarized with a right-handed rotation direction around the direction vertical to the *XY* plane for the whole grating period. The electric field amplitude varies along the grating period. Such a situation is similar to the *s*:*s* crossing case, an elliptical intensity grating is induced; intensity modulation will dominate the DFB lasing oscillation. The polarization state of the lasing output should be roughly elliptically polarized.

$-\pi$	$-\pi/2$	0	$+\pi/2$	$+\pi$
				

Fig. 5.10 One period of the interference pattern projected onto the *XY* plane for LCP:RCP pumping scheme (not completely to scale).

5.3 Lasing in chiral photonic structures constructed by self-organized cholesteric liquid crystals (CLCs) ---- A 1-D periodic anisotropic structure with the symmetry of a double helix

In the last section**,** based on reflection pumping geometry, we obtained left-handed and right-handed chiral photonic structures in the LCP:LCP

pumping and RCP:RCP pumping, respectively, by theoretical prediction. The DFB lasing feedback mechanism performed in this chiral photonic structure is similar to the one formed by cholesteric liquid crystals (CLCs) [14]. The polarization property of the DFB lasing output shows an identical behavior same to the lasing oscillation in dye doped CLCs [14]. In the below, a brief introduction of the DFB lasing dynamics in dye doped CLCs will be given.

Liquid crystals (LCs) containing chiral molecules such as CLCs can self-organize into anisotropic 1-D PC due to their self-assembly property. The LC directors are self-organized into a helical structure with a pitch that can be right or left-handed [14]. The director means the average direction of the long molecule axis in the molecule layers. The lowest energy configuration for the photonic structures in CLCs is achieved with a rotation by a small fixed angle between consecutive CLC molecule layers, as seen in Fig. 5.11 [14]. The structures have double helix symmetry. The pitch of the structure, in which the director rotates by 360^{o}, is twice the period of the cholesteric structure. Different from other LCs, the photonic bandgap (PBG) of the CLCs is polarization-dependent. The circular polarized light with the same sense of rotation as the CLC helix structure is reflected within a band, while the circular polarized light in the opposite rotation to the helix structure transmits through the CLCs. For the reflected circular polarized light, the photon density of state (DOS) vanishes in the PBG and is enhanced at the edge of PBG [16]. The band is centered at a wavelength within the medium equal to the pitch of the helix structure. The PBG can be determined by relationship as $\lambda_0 = \langle n \rangle p$, where λ_0

represents the central wavelength of the reflection band, $\langle n \rangle$ is the average refractive index and p is the intrinsic helical pitch length. The bandwidth of the bandgap is expressed by $\Delta\lambda = \Delta n \cdot p$, where Δn is the birefringence of the CLCs. Due to the chiral photonic DFB structures, circular polarized lasing emission can be obtained from dye doped CLCs.

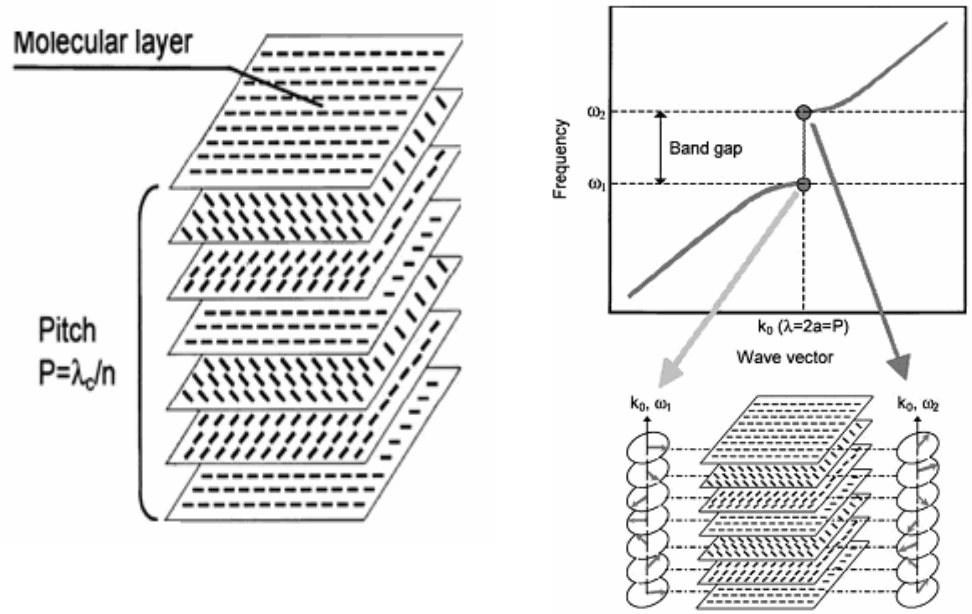

Fig. 5.11 (a) Molecular structure of CLCs. The dashes indicate the orientation of the director; (b) Photonic band structure of a CLC with period a and pitch P=2a, arrows indicate the electric field direction being aligned along or perpendicular to the director [14].

Based on the above mentioned properties, CLCs have been widely used for photonic applications, especially for DFB lasers, where CLC provides a permanent DFB structure. Many DFB lasers with circular polarized lasing output have been realized by employing CLCs. Low-threshold lasing was observed at the edge of the bandgap in a dye doped CLC film by V. I. Kopp *et al* [17]. Wu's group demonstrated a high efficient laser upon bandedge

excitation based on dye doped CLCs [18]. Also they obtained an enhanced laser action of a CLC in a dielectric multilayer cavity [19].

In the following, we will report the study of the DFB lasers in dye doped solution based on reflection grating geometry by polarization modulation. Tunable circular polarized laser emission is generated in the chiral DFB structures in LCP:LCP and RCP:RCP pumping schemes. Comparisons between the experiments and the theoretical analysis in 5.2 will be given. Also the coincidence of the rotation of DFB lasing polarization state with the one in dye doped CLCs will be discussed. The tunability, spectral characteristics and threshold of the DFB lasers will be studied in detail.

5.4 Experimental arrangement

The optical arrangement has been described in Chapter III. A frequency-doubled Nd: YAG laser of 6 ns was served as the pump source. A calcite Glan-Taylor Prism was placed into the exit path of the Nd: YAG laser to define the pump beam as *s*-polarized. The change is to employ half wave plates and quarter wave plates to manipulate the state of polarization of the two pump beams. The wave plates were inserted into the optical path, just in front of the dye cell, with the surfaces perpendicular to the propagation direction of the pump beams. Various polarization pumping geometries can be constructed as desired. The two beams intersected inside the cell at an angle Θ to create the polarization reflection grating. A periodic modulation of intensity and/or polarization was thus induced in the gain medium. The DFB tuning equation follows $\lambda_L = \lambda_{pump} / M \bullet \sin(\theta_{in} / 2)$. The first Bragg order was satisfied in the

experiments. Tuning of the modulation was achieved by varying the intersection angle. The state of polarization and the rotation direction of the polarization state of the DFB laser output were determined by a polarizer in combination with a quarter wave plate at 632.8nm. Fig. 5.12 shows a simplified illustration of the polarization crossing experiments.

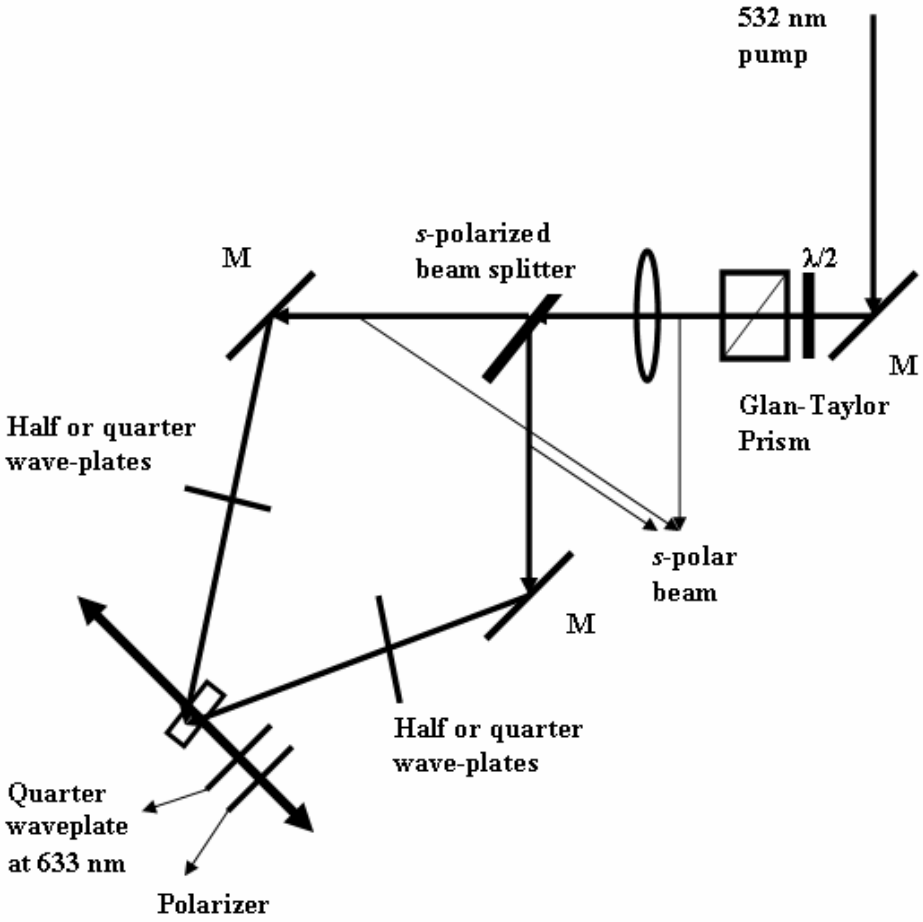

Fig. 5.12 Schematic of the polarization crossing experiments.

5.5 DFB laser operation in DCM doped methanol by polarization modulation

The first trial system was DCM doped methanol. The dye concentration was 2×10^{-3}M, which was close to the saturated concentration.

(1) LCP:LCP pumping geometry

The DFB laser experiments by polarization modulation were firstly operated in the LCP:LCP pumping geometry. Two quarter wave plates at 532 nm were inserted into the optical path in Fig. 5.10. Thus the polarization of the two pumping beams was converted to be left-handed circular polarized by properly rotating the two wave plates. A polarizer was used to examine and confirm the state of polarization of the pump beams. Fig. 5.13 presents the results, which show that the two pumping beams had a quite good circular polarization state.

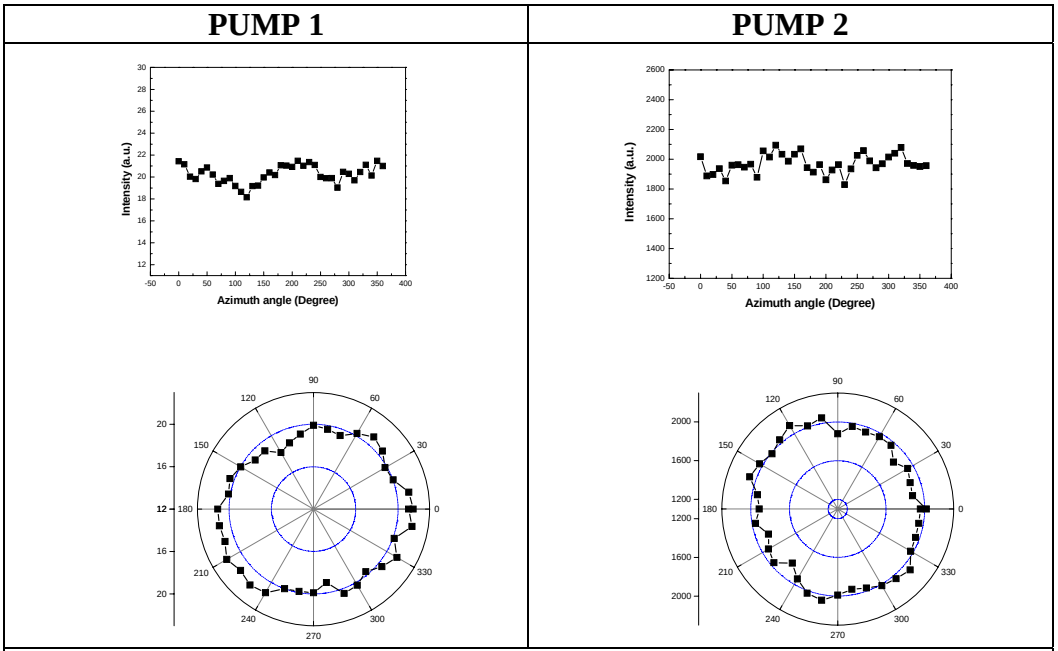

Fig. 5.13 The polarization state of the two pumping beams

By using a focal lens to increase the pump energy density, DFB lasing was observed when the pump energy was above 0.3 mJ after counting for the energy losses. Tuning of the output wavelength was obtained by varying the intersection angle. Dual-peak laser emission was achieved throughout the

tuning range. Each emission peak was doubled with an interval or a shoulder (In Fig. 5.14).

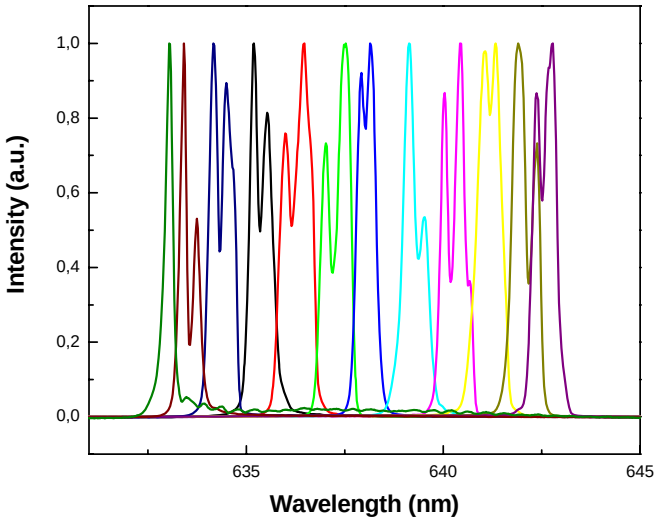

(a)

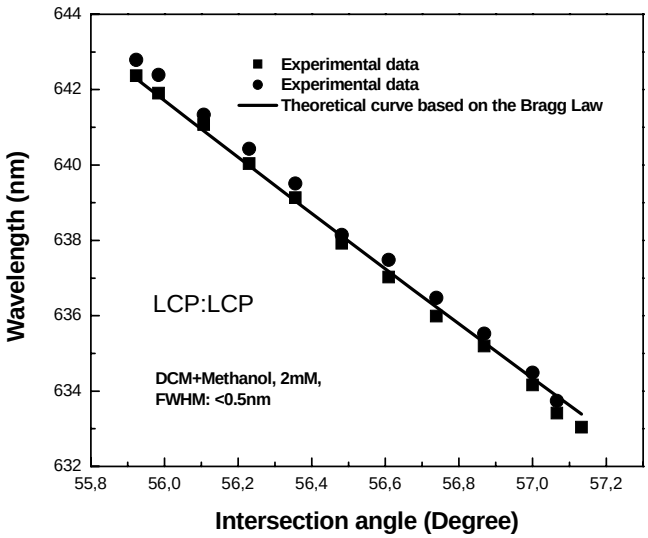

(b)

Fig. 5.14 (a) Angle tuning spectra in the LCP:LCP pumping geometry. (b) The tuning data of the DFB lasing vs. the theoretical fit based on the Bragg Law. Circles and rectangles represent the lasing wavelengths of the double peaks at every intersection angles.

As prediction in section 5.2, the induced DFB grating in LCP:LCP pumping geometry is a combination of intensity grating and polarization grating. So the modulation generated by the DFB structure included both the

intensity modulation and polarization modulation. The intensity modulation contributed to generate the periodic gain and index perturbations needed for feedback of the lasing oscillation. Surely, the polarization modulation provided a feedback as well for lasing generation. The dual-peak lasing structure is relevant of the existence of an index-type DFB grating in the gain medium, which dominated a tunable PBG, according to the coupled-wave theory of Kogelnik and Shank [2]. The interpretation of this phenomenon has been described in detail in our previous work [20].

The tuning behavior of the DFB laser is summarized in Fig. 5.14 (b). The tuning data follow the solid line very well, which is the prediction by the Bragg resonance condition for reflection configuration. The input-output characteristic was also examined. Fig. 5.15 shows the output intensity as a function of the pump energy at the gain centre, which indicates that the threshold pump energy was 0.3mJ. The last three points predicted the saturation of the output intensity occurred. The inset is the threshold spectrum.

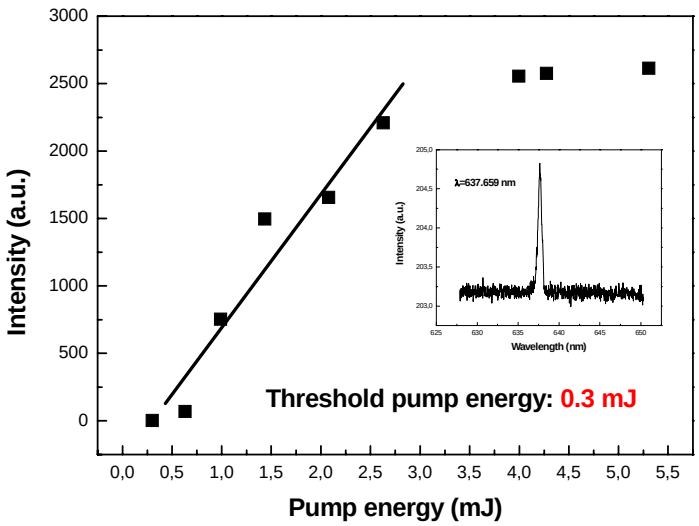

Fig. 5.15 The output intensity variation as the function of the pump energy

Since a quarter waveplate at 633 nm will have to be adopted to examine the polarization property of the DFB lasing output, the DFB lasing emission was tuned to the wavelength of around 633 nm, corresponding to an intersection angle Θ of 57.21°. Combining the quarter wave plate with a polarizer, the polarization state and the rotation direction of the polarization of the DFB lasing output were determined from both sides of the dye cell, respectively.

Firstly, the polarization state was examined only with a polarizer. The DFB lasing intensity as a function of the azimuth angle of the polarizer was obtained, as shown in Fig. 5.16. It exhibits a roughly circular distribution in polar plot. Then by inserting the quarter wave plate at 633 nm between the dye cell and the polarizer, the rotation of the polarization was further examined from both the left and the right sides of the sample. The fast axis of the quarter wave plate was perpendicular to the optical table. After passing through the quarter wave plate and the polarizer, the DFB lasing intensity distribution as the azimuth angle of the polarizer was obtained correspondingly (in Fig. 5.17). It exhibits linearly polarized characteristic for both sides.

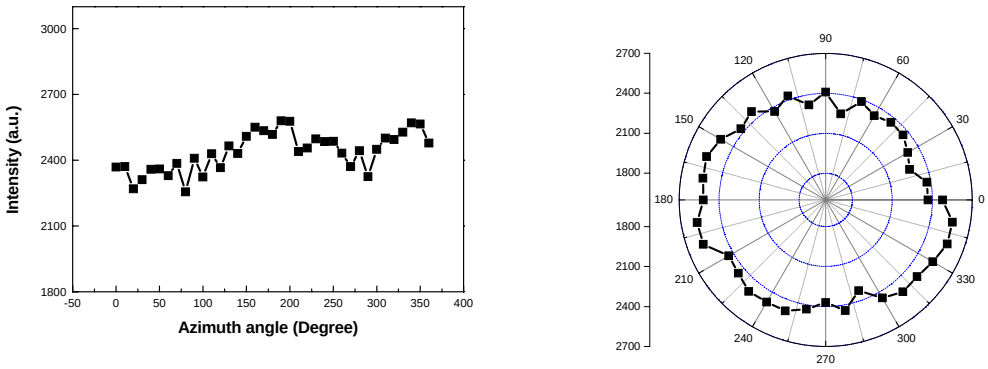

Fig. 5.16 The DFB lasing intensity as a function of the azimuth angle of the polarizer in the LCP:LCP pumping.

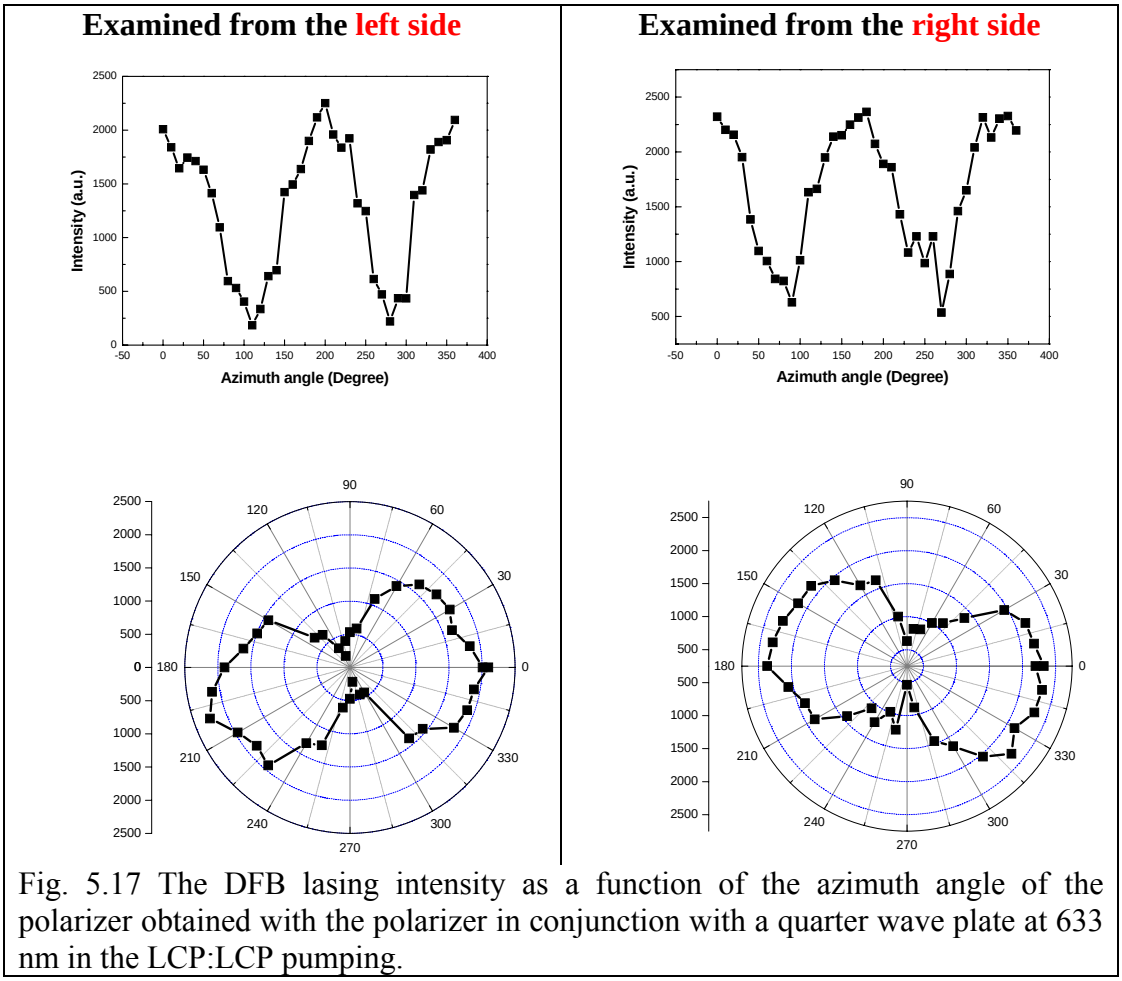

Fig. 5.17 The DFB lasing intensity as a function of the azimuth angle of the polarizer obtained with the polarizer in conjunction with a quarter wave plate at 633 nm in the LCP:LCP pumping.

From the measurements, obviously, the DFB laser emission in the LCP:LCP pumping geometry should be circular polarized since the polarization of the DFB lasing was successfully converted to linear polarization after transmitting through a quarter wave plate at the corresponding wavelength. In addition, due to that the fast axis of the quarter wave plate was vertical to the optical table, according to the rotation direction of the linear polarization of the converted DFB lasing relative to the fast axis (Fig. 5.17), the left side DFB lasing output should be identified as a left-handed circular polarized light, in contrast, the right side one should be a right-handed circular polarized light.

As discussed in 5.2, in LCP:LCP pumping geometry, at the intersection angle of 60°, the DFB grating is not only an intensity grating but also a polarization grating. The modulation is a combination of intensity modulation and polarization modulation. The total field polarization state is everywhere linear but rotates in space with a constant angular frequency, so that the excited dipole moment of dye molecules have a distribution along all of the linear polarization directions on the *XY* plane in one grating period, the DFB lasing will be roughly circular polarized. The rotation direction of the total field should determine the rotation of the circular polarized DFB lasing. From Fig. 5.7, we see that, in LCP:LCP crossing, the interference pattern presents a left-handed helix structure, resulting in a left-handed chiral photonic structure, similar to the chiral photonic structure formed by CLCs [14]. Theoretically speaking, we should get reflected left-handed circular polarized lasing output and transmitted right-handed circular polarized lasing output from the both sides. We see very good agreement between the theoretical prediction and the experiments.

In conclusion, a *dynamic* chiral photonic structure in reflection DFB lasers was completed easily by manipulating the polarization state of the two pumping beams. The polarization state of DFB lasing emission in this chiral photonic structure can also be predicted. In addition, we have to note that, the examination of the polarization of DFB lasing was only performed at an intersection angle of around 60°. As we said in the above content, the interference field on the *XY* plane also changes as the intersection angle. As a

result, the polarization properties of DFB lasing should change as the intersection angle. So our method can only give a rough picture of the polarization behavior of DFB lasing emission based on reflection pumping geometry. However, a compensator would be suggested to further study the polarization at other intersection angles. In our work, due to the experimental condition limit, we did not do it.

(2) RCP:RCP pumping geometry

Subsequently, the DFB lasers were realized in the RCP:RCP pumping geometry. In this situation, the two interfering pump beams were converted to be right-handed circular polarized by rotating the quarter wave plates at 532 nm. DFB lasing was observed by increasing the pump energy above 0.308 mJ with consideration of the energy losses. Fig. 5.18 (a) shows the tunable dual-peak lasing spectra at different intersection angles. Fig. 5.18 (b) presents the angle tuning versus the theoretical fit based on the first-order Bragg condition. Good agreement was seen. The slope of the DFB lasing output was also measured at the gain centre of DCM doped methanol, as shown in Fig. 5.19. The inset is the threshold spectrum.

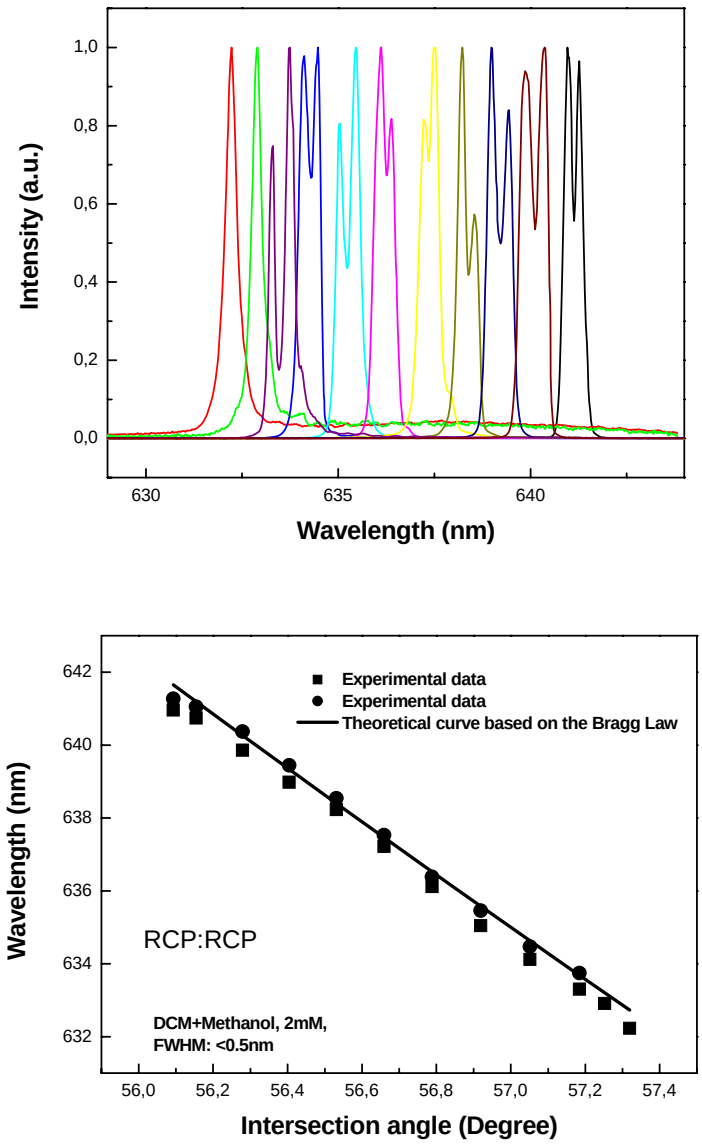

Fig. 5.18 (a) Angle tuning spectra in the RCP:RCP pumping geometry. (b) The tuning data of the lasing emission vs. the theoretical fit based on the Bragg Law for the first order. Circles and rectangles represent the lasing wavelengths of the double peaks at every intersection angles.

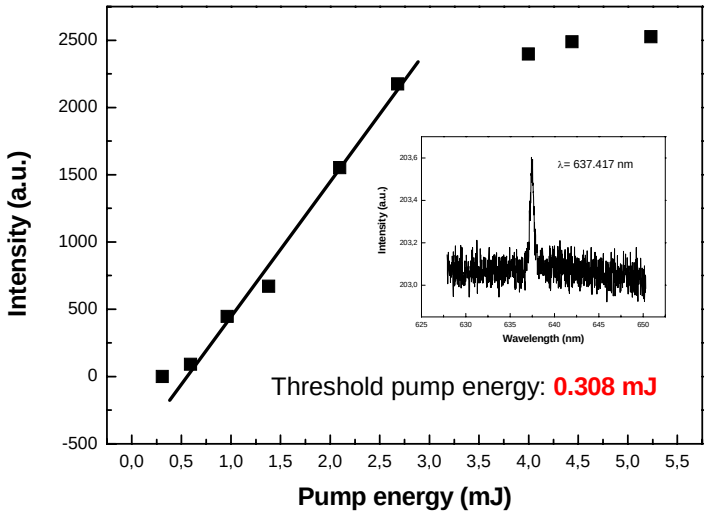

Fig. 5.19 The output intensity variation as the function of the pump energy in the RCP:RCP pumping. The inset is the threshold spectrum.

As prediction, the induced DFB grating in RCP:RCP pumping geometry was still a combination of intensity grating and polarization grating. The modulation included both the intensity modulation and polarization modulation. The intensity modulation, which dominated the tunable PBG, contributed to generate the dual-peak lasing emission.

Then the DFB lasing output wavelength was tuned to the wavelength of around 633 nm. Firstly, the polarization state of DFB lasing was examined only with a polarizer. The result is shown in Fig. 5.20. The distribution exhibits a roughly circular distribution in polar plot. Afterwards, the rotation of the polarization was further examined from both the left and right sides of the sample by employing the quarter wave plate at 633 nm. The fast axis of the quarter wave plate was perpendicular to the optical table. After passing through

the quarter wave plate and the polarizer, the lasing beam exhibits linearly polarized characteristic for both sides, as seen in Fig. 5.21.

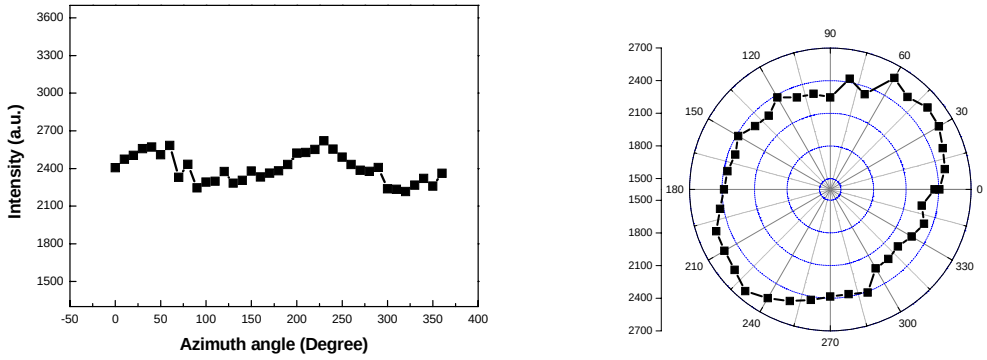

Fig. 5.20 The DFB lasing intensity as a function of the azimuth angle of the polarizer obtained in the RCP:RCP pumping.

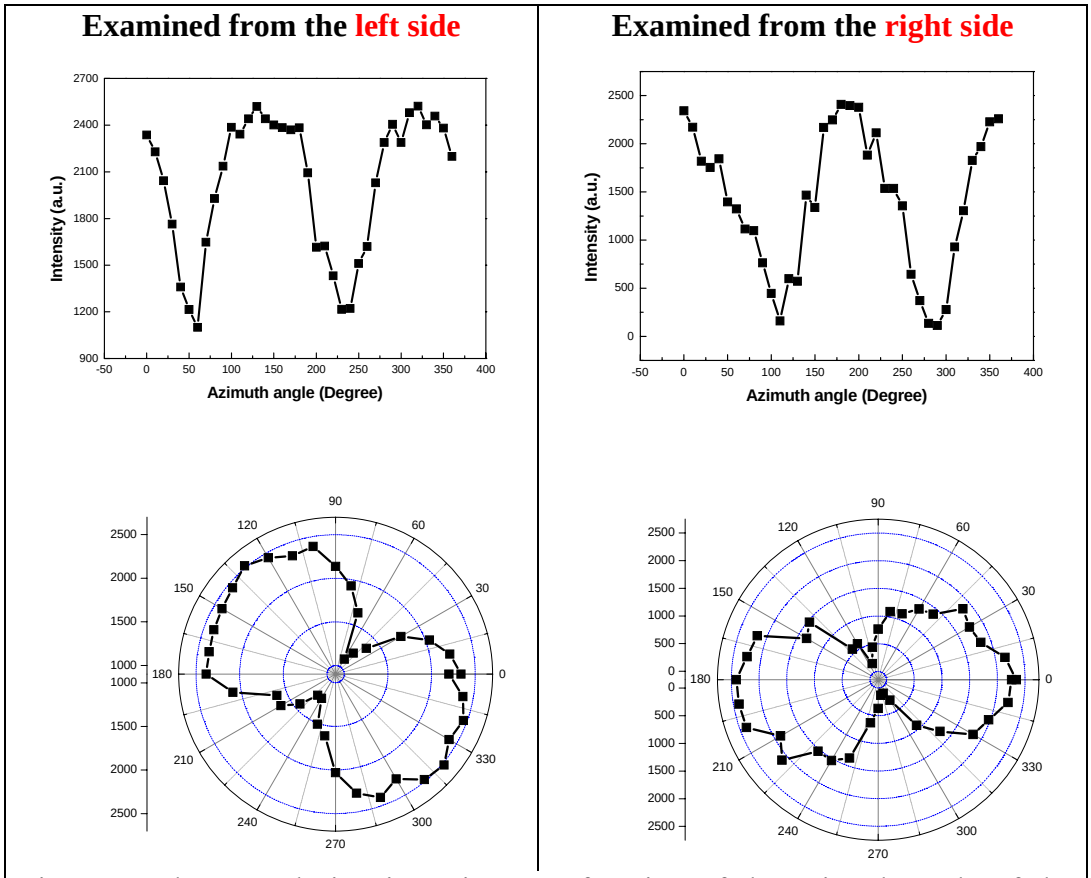

Fig. 5.21 The DFB lasing intensity as a function of the azimuth angle of the polarizer obtained with the polarizer in conjunction with the quarter wave plate at 633 nm in the RCP:RCP pumping.

From the measurements, we can get, in RCP:RCP pumping geometry, the DFB laser emission can be identified as a roughly circular polarized beam. In addition, according to the rotation direction of the linear polarization of the converted DFB lasing relative to the fast axis of the quarter wave plate (Fig. 5.21), on the contrary with LCP:LCP pumping, the left side DFB lasing output was a right-handed circular polarized light while the right side DFB lasing output was a left-handed circular polarized light. As predicted in 5.2, the DFB grating in RCP:RCP crossing is again a combination of both intensity grating and polarization grating. However, in contrast to LCP:LCP crossing, the total field polarization state rotates in space along an opposite direction around the propagation of the lasing emission. The interference pattern presents a right-handed helix structure, resulting in a right-handed chiral photonic structure. Theoretically, we should get reflected right-handed circular polarized lasing output and transmitted left-handed circular polarized lasing output meanwhile. We can see the good coincidence between the prediction and experiments. In conclusion, a *dynamic* right-handed chiral photonic structure in reflection DFB lasers was completed.

Additionally, comparing the wavelength tuning equation for our DFB lasers $2n\Lambda = M \bullet \lambda_L (M = 1)$ with the central wavelength of the PBG by the reflection band in CLCs $\lambda_0 = \langle n \rangle p$, the intrinsic helical pitch length p of the helix structure in CLCs corresponds to 2Λ in our DFB lasers. Since Λ is the period of the reflection grating in DFB lasers, while p is twice of the period of the cholesteric structure in CLCs, a reasonable correspondence is seen.

(3) LCP:RCP pumping geometry

DFB lasers were demonstrated in LCP:RCP pumping geometry by converting the two beams to be left-handed circular polarized and right-handed circular polarized, respectively. Angle tuning was achieved by varying the intersection angle. The tuning behavior is presented in Fig. 5.22. The threshold of the DFB lasers was around 0.074 mJ, as seen in Fig. 5.23, which was much lower compared with the LCP:LCP and RCP:RCP pumping geometries.

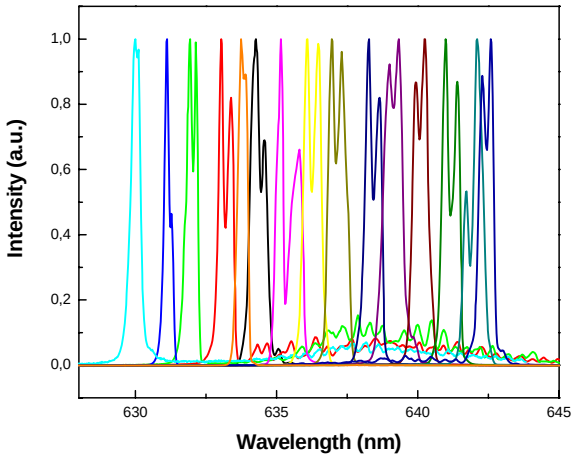

(a)

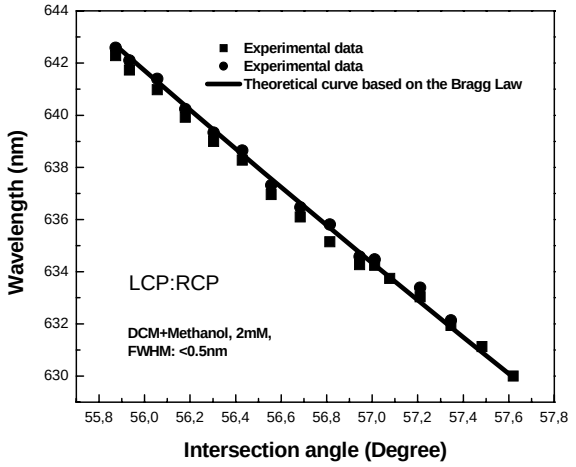

(b)

Fig. 5.22 (a) Angle tuning spectra in LCP:RCP pumping geometry. (b) The tuning data vs. the theoretical fit based on the Bragg Law for the first order. Circles and rectangles represent the lasing wavelengths of the double peaks at every intersection angles.

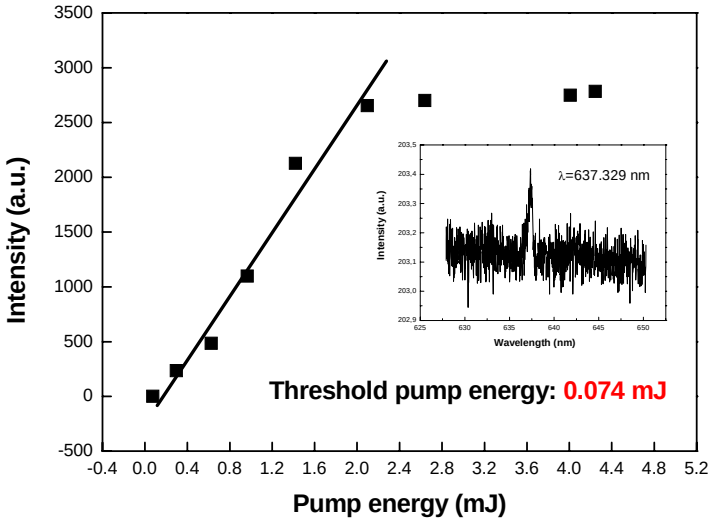

Fig. 5. 23 The output intensity variation as the function of the pump energy in the LCP:RCP pumping. The inset is the threshold spectrum.

Then the DFB lasing wavelength was tuned to the wavelength of around 633 nm for the investigation of the polarization properties. The examination result by a polarizer is shown in Fig. 5.24. It exhibits a circular distribution in polar plot. The rotation of the polarization was further examined with the quarter wave plate at 633 nm. After passing through the quarter wave plate and the polarizer, the lasing beam doesn't exhibit linear polarized, not as expected (in Fig. 5.25).

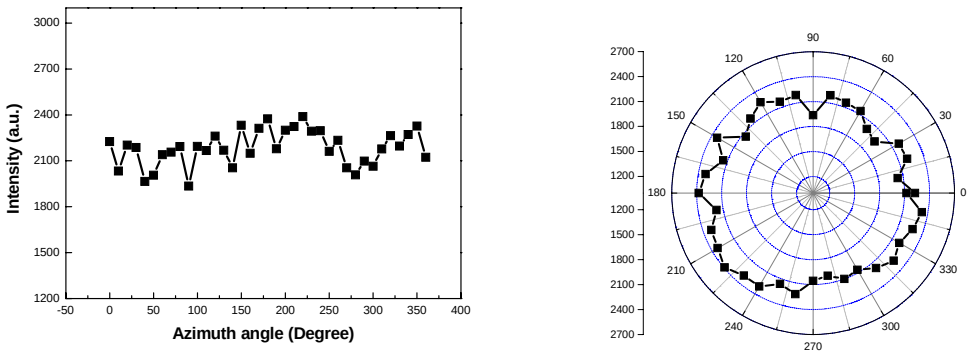

Fig. 5.24 The DFB lasing intensity as a function of the azimuth angle of the polarizer obtained in LCP:RCP pumping.

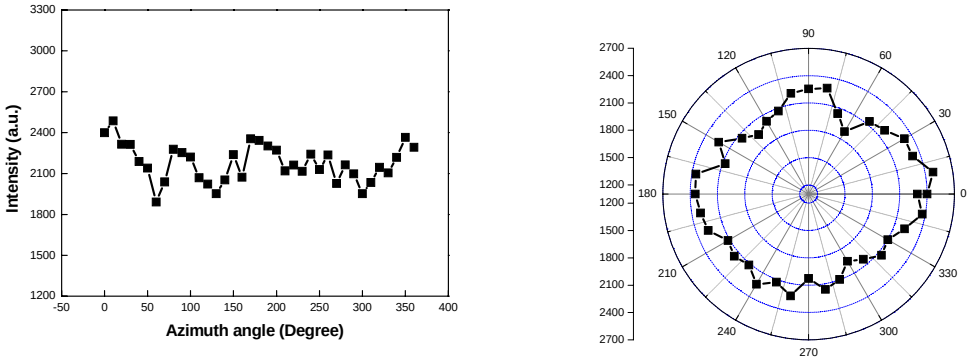

Fig. 5.25 The DFB lasing intensity distribution as a function of the azimuth angle of the polarizer obtained with the polarizer in conjunction with the quarter wave plate at 633 nm in LCP:RCP pumping.

The prediction in 5.2 for LCP:RCP crossing is that: an elliptical intensity grating is induced; the projected field on the *XY* plane is roughly elliptical polarized with a right-handed rotation direction; intensity modulation provides feedback for DFB lasing oscillation; the polarization state of the lasing output should be a roughly elliptical polarized beam.

Comparing with our experiments, the tunable dual-peak lasing peaks indicates the existence of the index-modulation, which should be induced by the intensity grating. But, in order to the experiments, we could not say that the state of polarization of the DFB lasing is circular polarized, or even elliptical polarized. Considering of this point, we suggest the following points for the interpretation: Firstly, the approximated analysis of the interference field projected onto the *XY* plane causes a big deviation of the identification of the state of polarization of the DFB lasing in this pumping scheme; secondly, the interference pattern should vary as the intersection angle; however, at the intersection angle of around 60^{o}, the interference pattern on the *XY* plane can

not fully reflect the actual interference field in three-dimension; finally, the experimental error during the measurement of the state of polarization could not be excluded, as the DFB lasing output wavelength of 633 nm was not at the centre of the gain range of DCM doped methanol, resulting in the instability of the lasing output.

(4) *s*:*p* pumping geometry and *p*:*p* pumping geometry

DFB lasers were also obtained in *s*:*p* pumping geometry and *p*:*p* pumping geometry. The *p*-polarized pump beam was achieved by replacing the quarter wave plates with half wave plates at 532 nm. Tunable dual-peak lasing output was obtained in both of the two schemes. The tuning behavior is summarized in Fig. 5.26 and Fig. 5.27, respectively.

The polarization state of the DFB lasing output in *p*:*p* pumping scheme was measured. As shown in Fig. 5. 28, the lasing output intensity reached the maximum at 90^{o} and 270^{o}, and it decreased to almost zero at 0^{o} and 180^{o}. The ratio of the maximum and the minimum was several tens, which indicated that the lasing output was *p*-polarized. According to the prediction in 5.2, the DFB reflection grating is a *p*-polarized intensity grating. The modulation is intensity modulation; a *p*-polarized DFB lasing emission is expected. We see the coincidence.

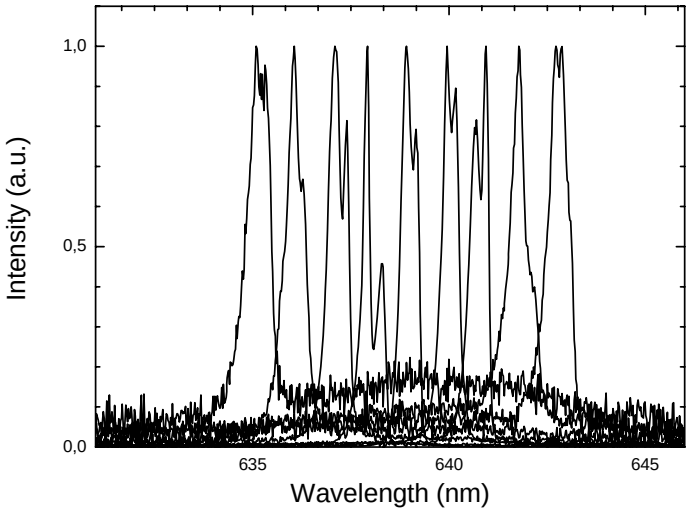

(a)

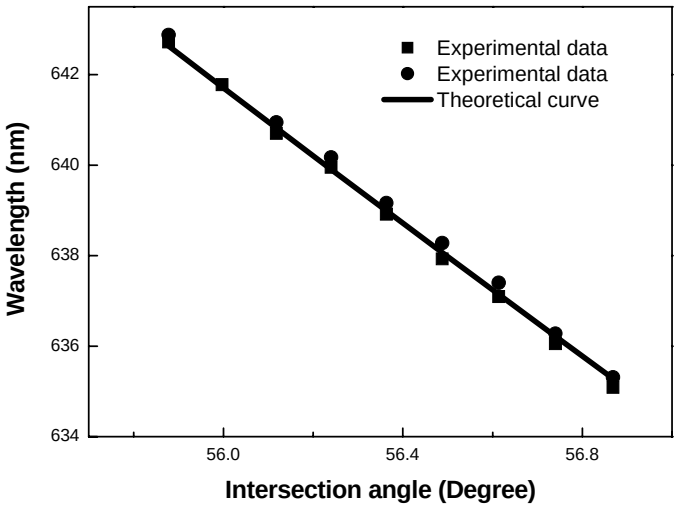

(b)

Fig. 5.26 (a) The tuning spectra at different intersection angles in *s*:*p* pumping geometry (b) The tuning curve and the theoretical fit based on the Bragg condition at the first Bragg order. Circles and rectangles represent the lasing wavelengths of the double peaks at every intersection angles.

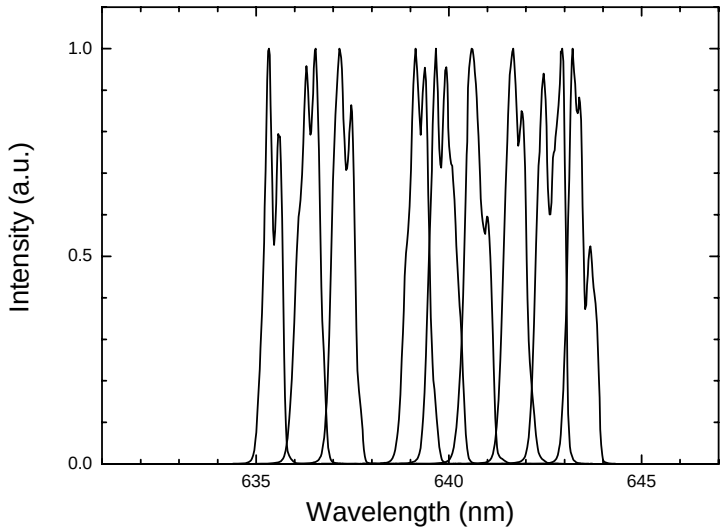

(a)

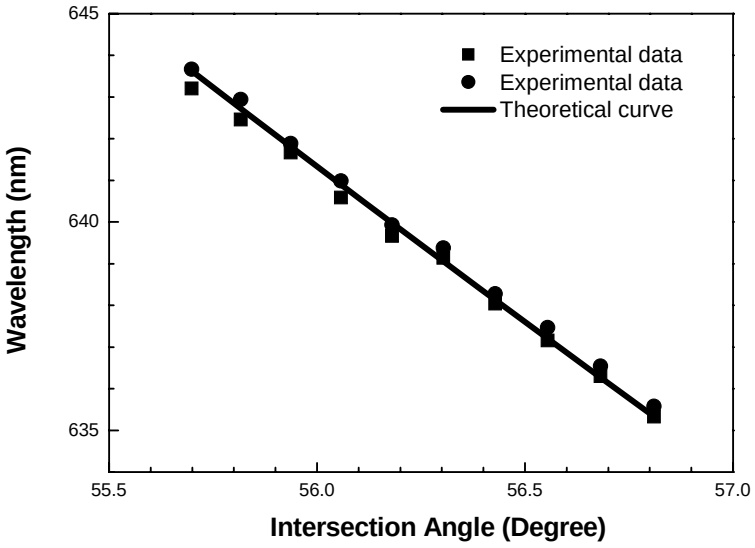

(b)

Fig. 5.27 (a) The tuning spectra at different intersection angles in *p*:*p* pumping geometry (b) The tuning curve and the theoretical fit based on the Bragg condition at the first Bragg order. Circles and rectangles represent the lasing wavelengths of the double peaks at every intersection angles.

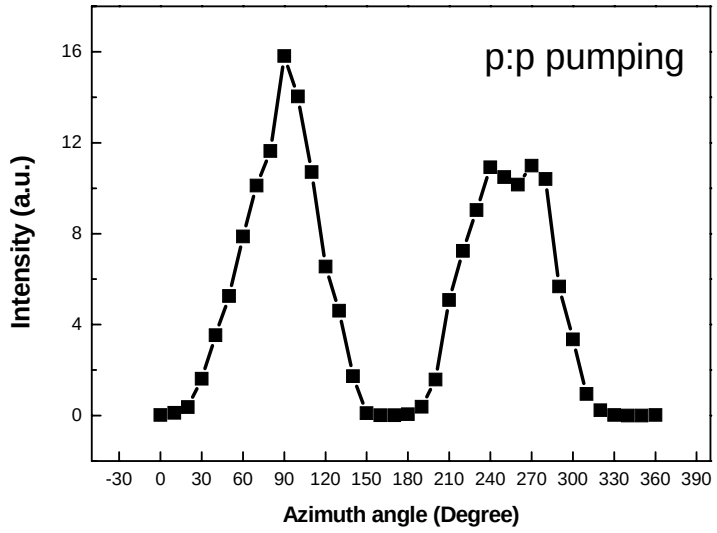

Fig. 5.28 The output beam intensity variation as the azimuth angle of the polarizer in *p*:*p* pumping scheme.

We did not measure the polarization state of the DFB lasing output in the *s*:*p* pumping, because the DFB lasing signal in this scheme was very weak even with very high pump energy. This should be reasonable, due to the nature of the generated DFB grating in *s*:*p* pumping: there is no spatial variation of the intensity; the modulation is a pure polarization modulation. In prediction, the DFB lasing emission will be depolarized.

5.6 DFB laser operation in R6G doped ethanol by polarization modulation

The series of experiments performed in DCM doped methanol were repeated in R6G doped ethanol. The dye concentration was 0.5×10^{-3}M.

(1) *s*:*p* pumping geometry

DFB lasing emission was observed when the pump energy was above 0.5mJ accounting for the energy losses. Tunable single peak lasing was

obtained throughout the gain range of R6G doped ethanol. The tuning spectra and tuning data vs. the theoretical fit are summarized in Fig. 5.29.

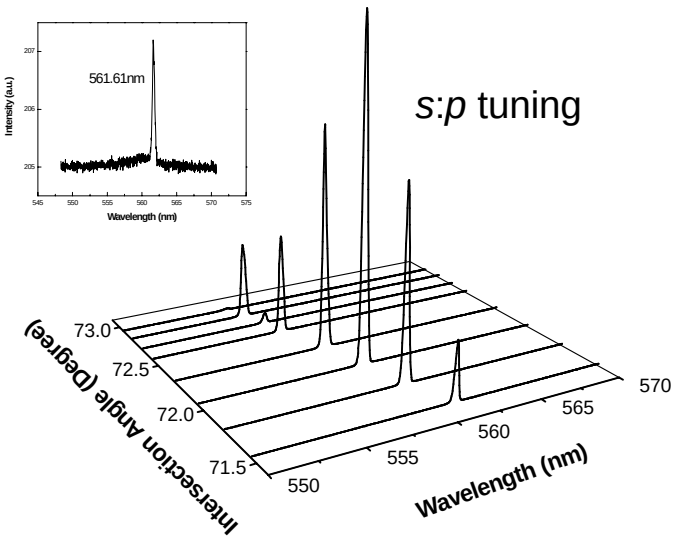

(a)

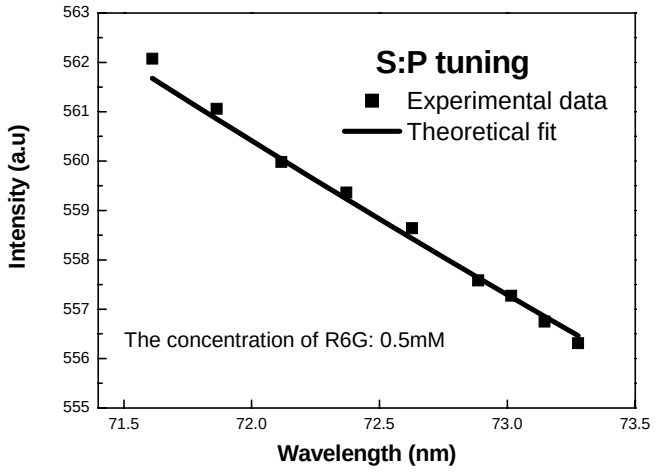

(b)

Fig. 5.29 (a) The tuning spectra at different intersection angles in R6G doped ethanol for *s*:*p* pumping, the inset shows the threshold spectrum; (b) The tuning data and the theoretical fit based on the Bragg condition.

The polarization state of the DFB lasing examined by a polarizer is shown in Fig. 5.30. Obviously, the polarization presents a depolarized characteristic, which has a good agreement with the prediction.

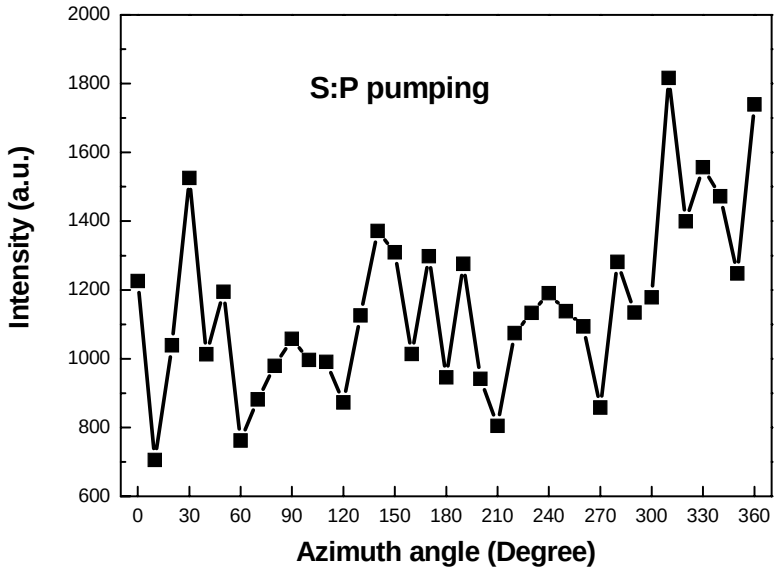

Fig. 5.30 The output beam intensity variation as the azimuth angle of the polarizer in *s*:*p* pumping scheme.

(2) *p*:*p* pumping geometry

Fig. 5.31 illustrates the tuning spectra and the tuning data vs. the theoretical fit. The inset of Fig. 5.31 (a) is the threshold spectrum. The threshold was around 0.4mJ.

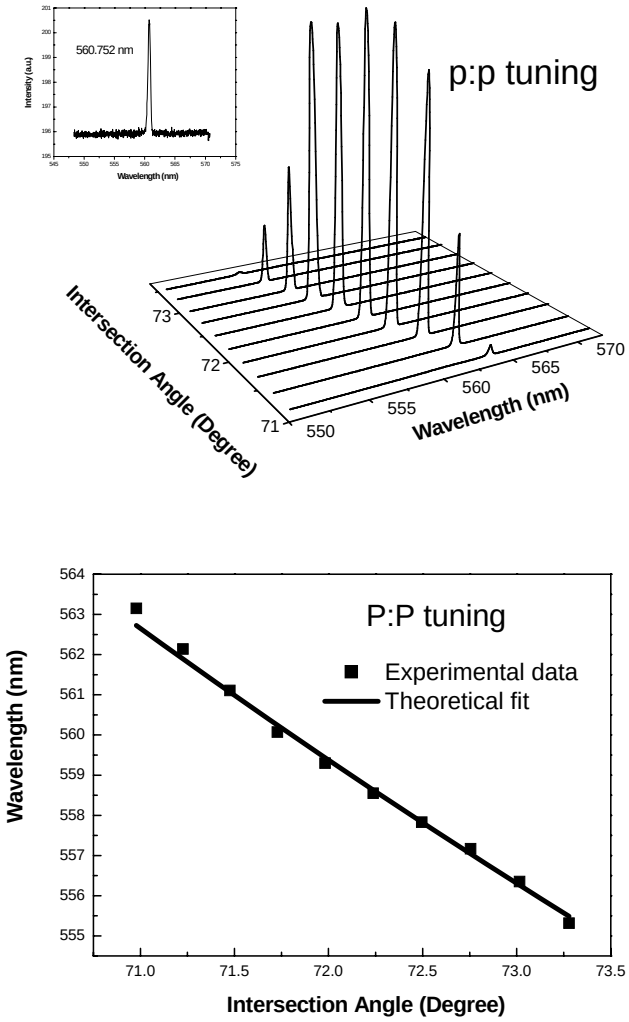

Fig. 5.31 (a) The tuning spectra at different intersection angles in R6G doped ethanol for *p*:*p* pumping, the inset shows the threshold spectrum; (b) The tuning data and the theoretical fit based on the Bragg condition.

The polarization state of the DFB lasing is shown in Fig. 5.32, which indicates a *p*-polarized DFB lasing emission as the prediction.

We note that, the DFB lasing always exhibited a single peak structure in R6G doped ethanol. It means that, in R6G doped ethanol, the DFB intensity grating in some schemes (e. g. *p*:*p* pumping case) was not strong enough to

induce an additional index modulation. Also the Stokes shift is not big enough for the dye R6G. About this point, we have discussed more detailed in Chapter IV.

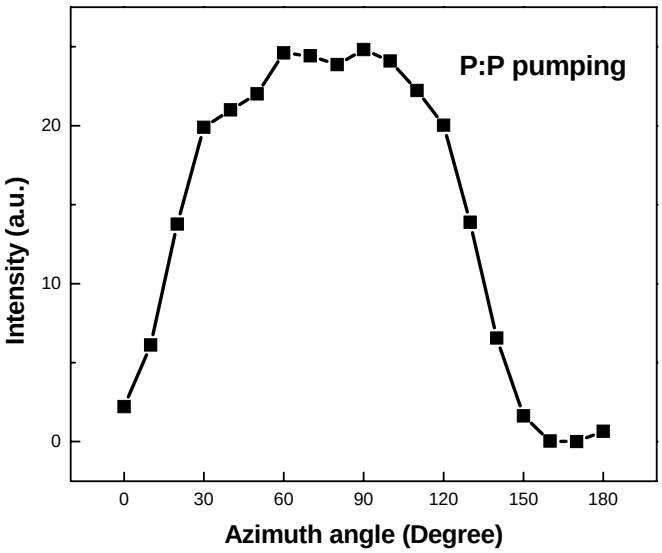

Fig. 5.32 The output beam intensity variation as the azimuth angle of the polarizer in *p*:*p* pumping scheme.

(3) The investigation of the DFB lasing polarization properties in *s*:*s* pumping, RCP:RCP pumping and LCP:RCP pumping geometries

Additionally, we studied the state of polarization of the DFB lasing output in *s*:*s* pumping, RCP:RCP pumping, and LCP:RCP pumping geometries, respectively. Fig. 5.33 presents all the results.

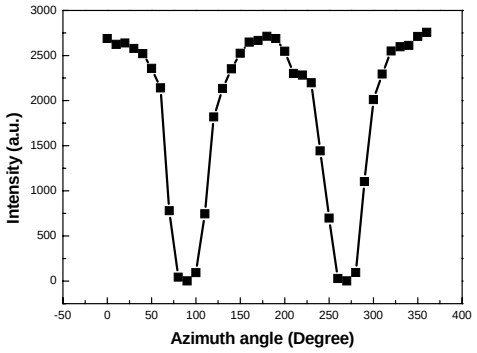

(a)

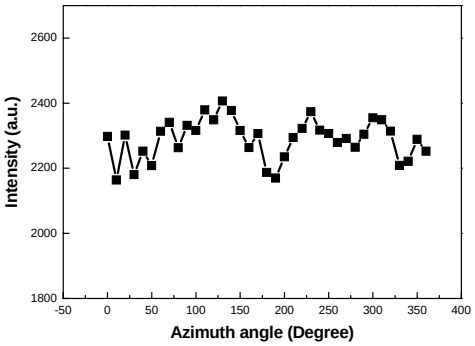

(b)

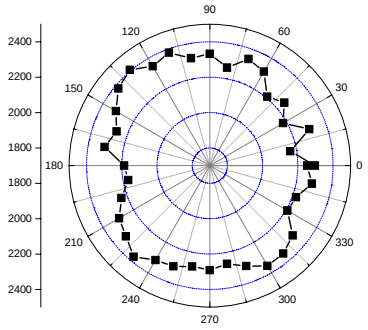

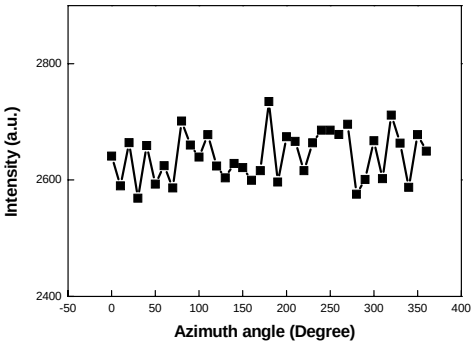

(c)

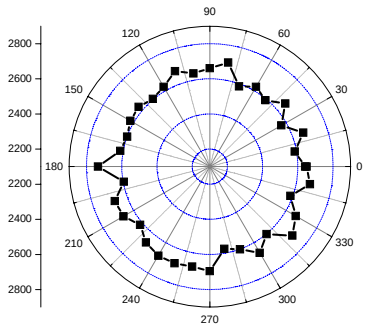

Fig. 5.33 The output beam intensity variation as the azimuth angle of the polarizer in *s*:*s* pumping scheme (a); RCP:RCP pumping scheme (b); LCP:RCP pumping scheme (c); respectively.

The DFB lasing output in *s*:*s* pumping geometry is *s*-polarized as predicted. The lasing from RCP:RCP pumping geometry should be circular polarized. The rotation of the polarization was not investigated due to the experimental condition limit. For the LCP:RCP case, from the lasing intensity distribution, it is a circularly polarized light, but we could not further examine

since we don't have a compensator. The polarization should be influenced by several factors, as described in DCM doped methanol for LCP:RCP pumping case, which we have discussed in 5.5.

During our experiments, whatever in R6G doped ethanol or DCM doped methanol, we found that, higher pump energy was needed for effective DFB grating generation, in those pumping schemes (e.g. *s*:*p* pumping), in which the polarization modulation dominated the feedback for the DFB lasing oscillation. This should be reasonable as the intensity modulation should induce a stronger coupling for lasing generation in DFB structures than polarization modulation.

5.7 Summary

Tunable DFB lasers were demonstrated based on reflection grating configuration from DCM doped methanol and R6G doped ethanol solutions. The periodic perturbations in DFB structures were generated by intensity modulation and/or polarization modulation by manipulating the state of polarization of the two interference pumping beams. The DFB lasing modulations were analyzed for different pumping geometries with Jones Matrix adopted in the same vein of polarization hologram. The tuning behavior, spectra properties, and input-output characteristics of the DFB lasers were investigated in different pumping schemes. Especially, the polarization properties of the DFB lasers were examined. All of the experimental results were compared with the theoretical predictions.

We obtained tunable circular polarized DFB lasers in DCM doped methanol based on LCP:LCP pumping and RCP:RCP pumping schemes. A modulation of a combination of intensity and polarization modulation dominated the lasing oscillation. Transient chiral photonic DFB structures were induced in the laser medium. The rotation of the circular polarized lasing output was also determined. The comparisons between the experiments and theoretical predictions were given. It was noted that the mechanism of lasing generation of the chiral DFB structures was similar to the dynamics of lasing in the chiral photonic structures consisted of dye doped CLCs. The correspondence between our DFB lasers and the dye doped CLCs DFB lasers were discussed. The comparison of the polarization properties of the lasing output between them was also analyzed.

References

[1] H. Kogelnik and C. V. Shank, “Stimulated emission in a periodic structure”, *Appl. Phys. Lett.* **18**, p152, 1971

[2] H. Kogelnik and C. V. Shank, “Coupled-wave theory of distributed feedback lasers”, *J. Appl. Phys.* **43**, p2327, 1972

[3] D. P. Schinke, R. G. Smith, E. G. Spencer, M. F. Galvin, “Thin-film distributed-feedback laser fabricated by ion milling”, *Appl. Phys. Lett.* **21**, p494, 1972

[4] J. E. Bjorkholm and C. V. Shank, “Distributed-Feedback Lasers in Thin-Film Optical Waveguides”, *IEEE J. Quantum Electron.* **8**, p833, 1972

[5] H. Kogelnik, “Coupled wave theory for thick hologram gratings”, *Bell. Syst. Tech. J.* **48**, p2909, 1969

[6] F. A. Jenkins, H. E. White, *Fundamentals of Optics*, 4th edn. (McGraw-Hill, New York 1976)

[7] S. D. Kakichashvili, “Polarization recording of holograms”, *Opt. Spectrosk.* **33**, p324, 1972

[8] S. Sivaprakasam, C. S. Babu and R. Singh, “A distributed feedback dye laser based on higher order Bragg scattering”, *Pramana J. Phys.* **46**, p299, 1996

[9] N. Khan and T. A. Hall, “Dynamic induction of gratings in DFDL produces multiple tunable laser lines”, *SPIE* **3609,** p216, 1999

[10] D. Lo, C. Ye and J. Wang, "Distributed feedback laser action by polarization modulation", *Appl. Phys. B* **76**, p649, 2003

[11] C. Ye, J. Wang, L. Shi and D. Lo, "Polarization and threshold energy variation of distributed feedback lasing of oxazine dye in zirconia waveguides and in solutions", *Appl. Phys. B* **78**, p189, 2004

[12] T. Z. Huang and K. H. Wagner, "Coupled Mode Analysis of Polarization Volume Hologram", *IEEE Journal of Quantum Electronics* **31**, p372, 1995

[13] T. Z. Huang and K. H. Wagner, "Diffraction analysis of photoanisotropic holography: an anisotropic saturation model", *J. Opt. Soc. Am. B* **13**, p282, 1996

[14] V. I. Kopp, Z.-Q. Zhang, A. Z. Genack, "Lasing in chiral photonic structures", *Progress in Quantum Electronics*, **27**, p369, 2003

[15] N. K. Viswanathan, S. Balasubramanian, L. Li, S. K. Tripaty and J. Kumar, "A detailed Investigation of the Polarization-Dependent Surface-Relief-Grating Formation Process on AZO Polymer Films", *Jpn. J. Appl. Phys.* **38**, p5928, 1999

[16] E. Yablonovitch, "Inhibited spontaneous emission in solid-state physics and electronics", *Phys. Rev. Lett.* **58**, p2059, 1987

[17] V. I. Kopp, B. Fan, H. K. M. Vithana, A. Z. Genack, "Low-threshold lasing at an edge of a photonic stop band in cholesteric liquid crystals", *Opt. Lett.* **23**, p1707, 1998

[18] Y. Matsuhisa, Y. H. Huang, Y. Zhou, S.-T. Wu, R. Ozaki, Y. Takao, A. Fujii, M. Ozaki, "Low-threshold and high efficiency lasing upon

band-edge excitation in a cholesteric liquid crystal", *Appl. Phys. Lett.* **90**, p091114, 2007

[19] Y. Matsuhisa, Y. H. Huang, Y. Zhou, S.-T. Wu, Y. Takao, A. Fujii, M. Ozaki, "Cholesteric liquid crystal laser in a dielectric mirror cavity upon band-edge excitation", *Opt. Express* **15**, p616, 2007

[20] F. Chen, D. Gindre, J.-M. Nunzi, "First-order distributed feedback dye laser effect in reflection pumping geometry", *Opt. Lett.* **32**, p805, 2007

Chapter VI

Modeling the Gain Coefficients of DFB Lasing by Polarization Pumping in Reflection Geometry

6.1 Introduction

From electromagnetic theory, the emission process from a single atom or molecule is modeled by one or more elementary radiators (oscillating electric dipoles or magnetic dipoles etc.). The polarization of the overall fluorescent emission from an ensemble of atoms or molecules depends on the orientation of the radiators in the ensemble. A random orientation produces an unpolarized emission, whereas the existence of some preferential direction favors a polarized emission. This preferential direction may be provided by the polarization of the pump source [1].

Polarization lasing output occurs when anisotropy is introduced into the laser medium. The anisotropy can be induced by an anisotropic pumping mechanism, resulting in an anisotropic excitation mechanism and a non-uniform gain. Sevchenko *et al.* first explained the polarization phenomenon in dye lasers [2]. They modeled the absorption and emission processes by electric dipole transitions, assuming that the dipoles were parallel and fixed with respect to the molecules. They found that the linearly polarized pump preferentially excited those molecules oriented in a direction close to that of the pump, which resulted a nonuniform distribution of excited molecules and hence an anisotropic gain, with a maximum along the direction of the pump

field polarization. Reyzer developed a general semiclassical formalism for the polarization characteristics of dye laser amplifiers [3-4]. It was found that, under a broad range of conditions, the polarization of the emission field tends to rotate towards the orientation of the molecules, that is to say, the polarization orientation of the pump field (or the direction of the gain maximum).

Except the polarized pump electric field, there are also some other techniques used to generate preferred molecular orientation, such as, orientation in a liquid crystal [5]. The use of liquid crystals has been an effective method for producing a strong repeated orientation of the dye molecules with a small applied field [6-7].

In the last chapter, we reported the DFB lasing emission in polarization pumping schemes. The state of polarization of the laser output followed the polarization of the interference field of the two pumping beams generally. In this chapter, we would derive the gain coefficients of reflection DFB dye lasers by polarization pumping. The deduction will be based on the formalism of Reyzer's work.

6.2 Reyzer's model

Referring to Reyzer *et al.*'s dye laser amplifier analysis [3], a four-level dye laser system is considered, as shown in Fig. 6.1. It is assumed that the pump absorption takes place only between levels one and two while stimulated emission takes place only between levels three and four. The coupling between the absorption levels and the emission levels is taken to be nonradiative

relaxation with a relaxation time τ_2 between level two and level three, and τ_4 between level four and one. Spontaneous emission is included between levels three and four with a fluorescent decay time τ_3. All four levels are assumed to be singlet states.

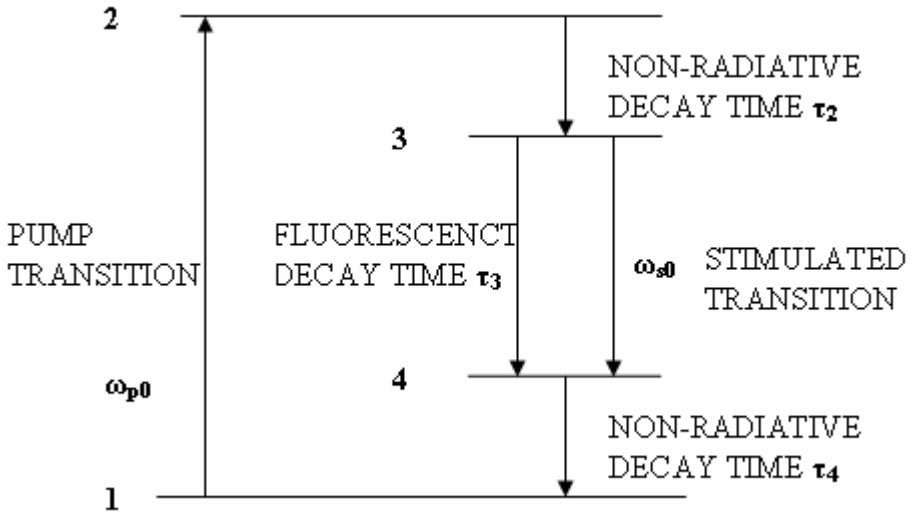

Fig. 6.1 A four energy levels model.

The orientation of the dipole moments of the dye molecules **μ** is presented by the Euler angles (θ, φ) in the right-handed Cartesian coordinate, as shown in Fig. 6.2. The absorption and emission dipoles are parallel.

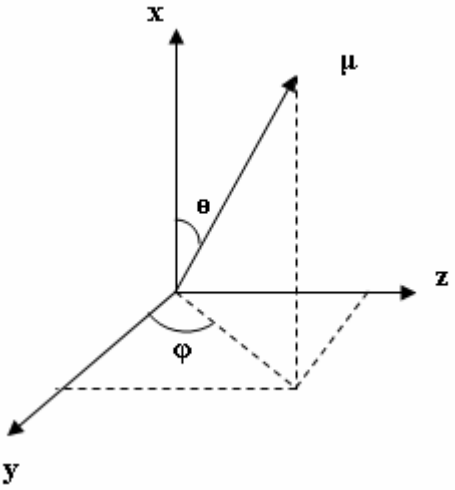

Fig. 6.2 Representation of the dye molecule dipole moment.

According to Reyzer *et al.*'s results:

$$\begin{aligned} &\left|\mu_p\right|^2 = \mu_{21}\mu_{21}^* = \mu_{21}\mu_{12}, \\ &\left|\mu_s\right|^2 = \mu_{34}\mu_{34}^* = \mu_{34}\mu_{43}, \\ &D_p = \rho_{11} - \rho_{22}, \\ &D_s = \rho_{33} - \rho_{44}, \end{aligned} \tag{6.1}$$

where ρ_{ij} are the state density functions, μ_{ij} are the matrix elements of the dipole moment operator, and D_p and D_s are population differences. We omit the algebraic manipulation and apply the formalism of Reyzer's work directly.

Under steady state approximation, the population difference between level three and level four is given by [3]

$$D_s = \frac{(\tau_3 - \tau_4)B_p}{1 + (2\tau_2 + \tau_3 + \tau_4)B_p + \tau_3 B_s + 2\tau_3(\tau_2 + \tau_4)B_p B_s} \tag{6.2}$$

B_p and B_s have the forms

$$\begin{aligned} &B_p = \left|\mu_p\right|^2 \left|E_p \bullet \mu\right|^2 \ell(\nu_p)/4\hbar^2, \\ &B_s = \left|\mu_s\right|^2 \left|E_s \bullet \mu\right|^2 \ell(\nu_s)/4\hbar^2, \end{aligned} \tag{6.3}$$

where E_p and E_s are the complex amplitudes of the pump field and the stimulating field, respectively. $\ell(\nu_p)$ and $\ell(\nu_s)$ are the normalized Lorentzian lineshape functions. For dye molecules, $\tau_3 \gg \tau_2, \tau_4$, D_s can be simplified by setting τ_2 and τ_4 equal to zero. So we get

$$D_s = \frac{\tau_3 B_p}{1 + \tau_3 B_p + \tau_3 B_s}. \tag{6.4}$$

When the laser is operated just above the threshold, the signal of the stimulated emission is so small that the $\tau_3 B_s$ can be set to zero. Thus D_s can be expanded as

$$D_s = \frac{\tau_3 B_p}{1+\tau_3 B_p} = \tau_3 B_p - \left(\tau_3 B_p\right)^2 + \left(\tau_3 B_p\right)^3 ..., \tag{6.5}$$

In the small signal gain approximation, by neglecting the higher-order terms in the right side of (6.5), combining with (6.3), we can obtain

$$D_s = \tau_3 \left|\mu_p\right|^2 \left|E_p \bullet \mu\right|^2 \ell(\nu_p)/4\hbar^2 . \tag{6.6}$$

The dipole moment μ in Fig. 6.2 is expressed as

$$\mu = \begin{pmatrix} \mu_x \\ \mu_y \\ \mu_z \end{pmatrix} = \begin{pmatrix} \cos\theta \\ \sin\theta\cos\phi \\ \sin\theta\sin\phi \end{pmatrix}. \tag{6.7}$$

For the DFB lasers, the exciting field E_p is composed of two crossing light waves E_1 and E_2.

The gain coefficients for the two orthogonal polarizations of the laser output along the propagation direction are defined by [3]

$$\begin{aligned} \alpha_x &= \sigma_s\left(\nu_s\right)\int_\Omega n\left(\theta,\phi\right) D_s \cos^2\theta d\Omega, \\ \alpha_y &= \sigma_s\left(\nu_s\right)\int_\Omega n\left(\theta,\phi\right) D_s \sin^2\theta\cos^2\phi d\Omega. \end{aligned} \tag{6.8}$$

where $\sigma_s\left(\nu_s\right)$ is the stimulated emission cross section. For an isotropic distribution of dipole moment orientation (dye molecules in a solution), $n\left(\theta,\phi\right) = N/4\pi$, N is the number density of the dye molecules. Substituting (6.6) into (6.8), we can achieve the gain coefficients in polarization pumping DFB lasers.

6.3 Gain coefficients calculation in different polarization pumping schemes

Fig. 6.3 shows the configuration of the DFB laser in reflection pumping geometry.

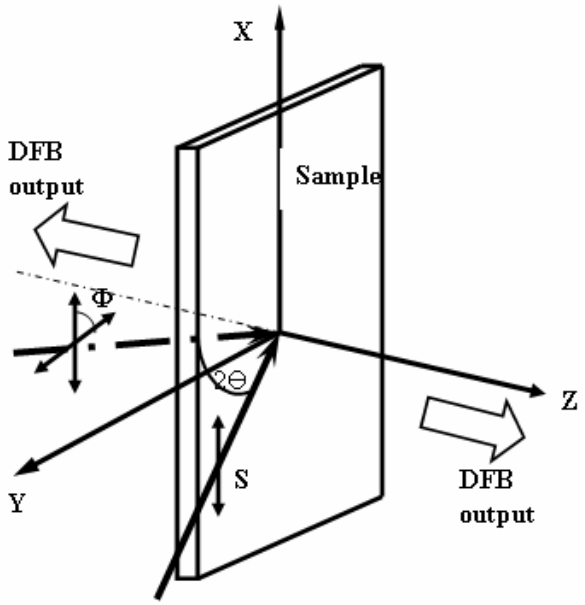

Fig. 6.3 Scheme of DFB laser setup in the right-handed Cartesian coordinates.

In Chapter V, we have obtained the interference fields of the two crossing beams for different polarization pumping schemes:

$$\mathbf{E}_{s:s} = E \begin{vmatrix} e^{-i\varphi}+1 \\ 0 \\ 0 \end{vmatrix}; \tag{6.9}$$

$$\mathbf{E}_{p:p} = E \begin{vmatrix} 0 \\ (e^{-i\phi}-1)\sin\Theta \\ (e^{-i\phi}+1)\cos\Theta \end{vmatrix}; \tag{6.10}$$

$$\mathbf{E}_{LCP:LCP} = \frac{1}{\sqrt{2}} E \begin{vmatrix} i(e^{-i\varphi}+1) \\ (e^{-i\phi}-1)\sin\Theta \\ (e^{-i\phi}+1)\cos\Theta \end{vmatrix}; \tag{6.11}$$

$$\mathbf{E}_{\mathrm{RCP:RCP}} = \frac{1}{\sqrt{2}} E \begin{vmatrix} -i(e^{-i\varphi}+1) \\ (e^{-i\phi}-1)\sin\Theta \\ (e^{-i\phi}+1)\cos\Theta \end{vmatrix}; \tag{6.12}$$

$$\mathbf{E}_{\mathrm{LCP:RCP}} = \frac{1}{\sqrt{2}} E \begin{vmatrix} i(e^{-i\varphi}-1) \\ (e^{-i\phi}-1)\sin\Theta \\ (e^{-i\phi}+1)\cos\Theta \end{vmatrix}; \tag{6.13}$$

$$\mathbf{E}_{\mathbf{s:p}} = E \begin{vmatrix} e^{-i\varphi} \\ -\sin\Theta \\ \cos\Theta \end{vmatrix}. \tag{6.14}$$

Then the gain coefficients can be calculated, respectively.

(1) *s*:*s* pumping

Combining (6.9) and (6.7), the term $\left|E_p \bullet \mu\right|^2$ in (6.6) can be calculated

$$\left|E_p \bullet \mu\right|^2_{s:s} = 2E^2\cos^2\theta + 2E^2\cos^2\theta\cos qz \tag{6.15}$$

where $q = \pm\left|k_1 - k_2\right|$, which is the grating vector along the z axis. The gain coefficients are obtained by substituting (6.15) into (6.6), and into (6.8) subsequently. We get

$$\begin{aligned} \alpha_x &= \frac{2}{5}C_1E^2 + \frac{2}{5}C_1E^2\cos qz, \\ \alpha_y &= \frac{2}{15}C_1E^2 + \frac{2}{15}C_1E^2\cos qz. \end{aligned} \tag{6.16}$$

where $C_1 = N\sigma_s(\nu_s)\tau_3\left|\mu_p\right|^2 \ell(\nu_p)/4\hbar^2$. The first terms in the right sides of (6.16) represent the average gain coefficients, and the amplitudes in the second terms represent the gain modulation amplitude.

(2) *p*:*p* pumping

With (6.10) and (6.7),

$$\begin{aligned} \left|E_p \bullet \mu\right|^2_{p:p} &= 2E^2(\sin^2\Theta\sin^2\theta\cos^2\phi + \cos^2\Theta\sin^2\theta\sin^2\phi) \\ &+2E^2(-\sin^2\Theta\sin^2\theta\cos^2\phi + \cos^2\Theta\sin^2\theta\sin^2\phi)\cos qz \end{aligned} \tag{6.17}$$

The gain coefficients are dependent on the intersection angle:

$$\alpha_x = \frac{2}{15}C_1E^2 + \frac{2}{15}(1-2\sin^2\Theta)C_1E^2\cos qz,$$
$$\alpha_y = \frac{2}{15}(1+2\sin^2\Theta)C_1E^2 + \frac{2}{15}(1-4\sin^2\Theta)C_1E^2\cos qz. \quad (6.18)$$

(3) LCP:LCP pumping

In the same way,

$$\left|E_p \bullet \mu\right|^2_{LCP:LCP} = E^2(\cos^2\theta + \sin^2\Theta\sin^2\theta\cos^2\phi + \cos^2\Theta\sin^2\theta\sin^2\phi)$$
$$+E^2(\cos^2\theta - \sin^2\Theta\sin^2\theta\cos^2\phi + \cos^2\Theta\sin^2\theta\sin^2\phi)\cos qz \quad (6.19)$$

The gain coefficients are

$$\alpha_x = \frac{4}{15}C_1E^2 + \frac{2}{15}(1+\cos^2\Theta)C_1E^2\cos qz,$$
$$\alpha_y = \frac{2}{15}(1+\sin^2\Theta)C_1E^2 + \frac{2}{15}(1-2\sin^2\Theta)C_1E^2\cos qz. \quad (6.20)$$

(4) RCP:RCP pumping

Obviously, the gain coefficients should be the same to the LCP:LCP pumping case.

(5) LCP:RCP pumping

$$\left|E_p \bullet \mu\right|^2_{LCP:RCP} = E^2(\cos^2\theta + \sin^2\Theta\sin^2\theta\cos^2\phi + \cos^2\Theta\sin^2\theta\sin^2\phi)$$
$$+E^2(-\cos^2\theta - \sin^2\Theta\sin^2\theta\cos^2\phi + \cos^2\Theta\sin^2\theta\sin^2\phi)\cos qz \quad (6.21)$$

The gain coefficients are then

$$\alpha_x = \frac{4}{15}C_1E^2 + \frac{2}{15}(\cos^2\Theta - 2)C_1E^2\cos qz,$$
$$\alpha_y = \frac{2}{15}(1+\sin^2\Theta)C_1E^2 - \frac{4}{15}\sin^2\Theta C_1E^2\cos qz. \quad (6.22)$$

(6) *s*:*p* pumping

The integral term is

$$\begin{aligned}\left|E_p \bullet \mu\right|_{s:p}^2 &= E_1^2 \cos^2\theta + E_2^2 \sin^2\Theta \sin^2\theta \cos^2\phi + E_2^2 \cos^2\Theta \sin^2\theta \sin^2\phi \\ &+2E_2^2 \sin\Theta\cos\Theta\sin\theta\cos\phi\sin\theta\sin\phi \\ &+2(E_1E_2 \sin\Theta\cos\theta\sin\theta\cos\phi + E_1E_2\cos\Theta\cos\theta\sin\theta\sin\phi)\cos\varphi\end{aligned} \tag{6.23}$$

The gain coefficients can be given by

$$\begin{aligned}\alpha_{0x} &= \frac{4}{15}C_1E^2, \\ \alpha_{0y} &= \frac{2}{15}(1+\sin^2\Theta)C_1E^2.\end{aligned} \tag{6.24}$$

Note that the expressions don't show a periodic variation, so they can not be counted on for distributed feedback mechanism. This is due to the inherent property of pure polarization modulation.

In this case, the expression of the population difference (6.6) has to be extended from the linear exciting intensity dependence to include the second order nonlinear intensity dependence contained in (6.5). So

$$D_s = (\tau_3 \left|\mu_p\right|^2 \ell(\nu_p)/4\hbar^2)\left|E_p \bullet \mu\right|^2 - (\tau_3 \left|\mu_p\right|^2 \ell(\nu_p)/4\hbar^2)^2 \left|E_p \bullet \mu\right|^4. \tag{6.25}$$

To simplify the calculation process, only the term in (6.25) that would result in a modulation is considered. We get

$$\begin{aligned}\Delta = 2(\tau_3 \left|\mu_p\right|^2 \ell(\nu_p)/4\hbar^2)^2 E_1^2 \cos^2\theta (E_2^2 \sin^2\Theta \sin^2\theta \cos^2\phi \\ +E_2^2 \cos^2\Theta \sin^2\theta \sin^2\phi)\cos 2\varphi\end{aligned} \tag{6.26}$$

The modulation amplitudes thus are

$$\alpha_{1x} = \frac{2}{35} C_2 E^4, \qquad \alpha_{1y} = \frac{2}{105}(2 - \cos 2\Theta) C_2 E^4. \tag{6.27}$$

where $C_2 = N\sigma_s(\nu_s)(\tau_3 \left|\mu_p\right|^2 \ell(\nu_p)/4\hbar^2)^2$. They depend on the fourth power of the electric field.

6.4 Summary

The gain coefficients of reflection DFB lasers were derived in different polarization pumping geometries, based on the Reyzer *et al.*'s dye laser amplifier theory. Under near threshold approximation, analytical expressions for the gain coefficients were deduced for six pumping schemes, viz. *s*:*s* pumping, *p*:*p* pumping, LCP:LCP pumping, RCP:RCP pumping, LCP:RCP pumping and *s*:*p* pumping. Particularly, the gain coefficients in the *s*:*p* pumping have a dependence of the fourth power on the electric field.

In addition, we should mention that, Dr. Jun Wang's thesis [8] was referred for the calculation of the gain coefficients in 6.3. In his thesis, a discussion of the gain coefficients of DFB lasers by polarization pumping in the transmission grating geometry was reported.

References

[1] P. P. Feofilov, *The Physics Basis for Polarized Emission*, Consultants Bureau Enterprises, New York, 1961

[2] A. N. Sevchenko, A. A. Kovalev, V. A. Pilipovich, and Y. V. Razvin, "Polarized Radiation Induced by Generation of Organic Dye Solutions", *Dokl Akad Nauk SSSR* **179**, p562, 1968

[3] K. C. Reyzer and L. W. Casperson, "Polarization characteristics of dye-laser amplifiers I. Unidirectional molecular distributions", *J. Appl. Phys.* **51**, p6075, 1980

[4] K. C. Reyzer and L. W. Casperson, "Polarization characteristics of dye-laser amplifiers II. Isotropic molecular distributions", *J. Appl. Phys.* **51**, p6083, 1980

[5] E. D. Baily and B. R. Jennings, "Simple apparatus for pulsed electric dichroism measurements", *Appl. Opt.* **11**, p527, 1972

[6] I. P. Ilchishin, E. A. Tikhonov, M. T. Shpak, and A. A. Doroshkin, "Stimulated-emission lasing by organic-dyes in a nematic liquid-crystal", *JETP Lett.* **24**, p303, 1976

[7] M. Bertolotti, G. Sansoni, and F. Scudieri, "Dye laser emission in liquid crystal hosts", *Appl. Opt.* **18**, p528, 1979

[8] J. Wang, *Experimental and Theoretical Studies of Distributed Feedback Waveguide lasers*, CUHK, Hong Kong, 2006

Chapter VII

Summary

DFB dye lasers based on reflection grating configuration instead of the traditional transmission one was realized from R6G doped ethanol and DCM doped methanol, respectively. Pure gain coupling and additional index coupling were obtained. In contrast with the transmission geometry, the tuning for the reflection grating geometry was found to be independent on the refractive index of the lasing gain media. Dual-peak lasing emission indicative of the existence of an index grating was observed in DCM doped methanol, which was caused by the large Stokes shift of the laser dye DCM and the strong coupling achieved at the first Bragg order. The interval between the dual-peaks increased with the pump energy. This gives a measure of the nonlinear refractive index of the gain medium. Considering the index-coupling case in DCM doped methanol, our tunable 1-D DFB lasers can be referred as a 1-D dynamic photonic crystal, and tunable PBG was achieved in the operation of the lasing measurements.

R6G doped PMMA thick films were fabricated by cast-coating method. The thickness can be varied by controlling the quantity of the dye doped solutions dropped onto the glass substrates. Wavelength tunable lasing with single peak or dual-peak structure was demonstrated in the films in the reflection pumping geometry for the first Bragg order. A permanent DFB

grating of pure gain modulation and/or additional index modulation induced by photobleaching or photodamage of dye molecules in polymer host was proposed providing feedback for the single peak and dual-peak DFB lasing generation, respectively. DFB laser action was observed in a R6G doped PMMA film of thickness as small as 150 um. The lifetime of the films was around hundreds of pulses.

Tunable DFB lasers were also demonstrated based on reflection grating configuration for various polarization pumping geometries. The periodic perturbations of intensity modulation and/or polarization modulation in DFB structures were created by manipulating the state of polarization of the two interference pumping beams. The periodical DFB modulations were analyzed for different pumping geometries with Jones Matrix adopted in the same vein of polarization hologram. The tuning behavior, spectral properties, and input-output characteristics of the DFB lasers were investigated in several pumping schemes. The polarization properties of the DFB lasers were examined. All of the experimental results were compared with the theoretical predictions.

We obtained tunable circular polarized DFB lasers in DCM doped methanol based on LCP:LCP pumping and RCP:RCP pumping schemes. A modulation of a combination of intensity and polarization dominated the lasing oscillation. Transient chiral photonic DFB structures were induced in the laser medium. The rotation of the circular polarized lasing output was also determined. The comparisons between the experiments and theoretical

predictions were given. It was noted that the mechanism of lasing generation of the chiral DFB structures was similar to the dynamics of lasing in the chiral photonic structures consisting of dye doped CLCs. The correspondence between our DFB lasers and the dye doped CLCs DFB lasers was discussed. The comparison of the polarization properties of the lasing output between them was also analyzed.

The gain coefficients of reflection DFB lasers were derived in different polarization pumping geometries, based on Reyzer *et al.*'s dye laser amplifier theory. Under near threshold approximation, analytical expressions for the gain coefficients were deduced for six pumping schemes, viz. *s*:*s* pumping, *p*:*p* pumping, LCP:LCP pumping, RCP:RCP pumping, LCP:RCP pumping and *s*:*p* pumping. Particularly, the gain coefficients in the *s*:*p* pumping have a dependence of the fourth power on the electric field amplitude.

Appendix

LUNA TECHNOLOGIES
Optical Component DNA

Introduction to Jones Calculus

Abstract: Jones Calculus is a mathematical technique for describing the polarization state of light and calculating the evolution of the polarization state as light passes through optical devices. Any state of polarization can be described by a two-element *Jones vector*, and the linear operation of any optical device can be fully described by a 2×2 *Jones matrix*. A system of multiple devices can be straightforwardly modeled by multiplying the component Jones matrices to yield a single system Jones matrix.

A broadly useful representation for polarized light was invented in 1941 by R. Clark Jones. Like the method of Stokes parameters and Mueller matrices, the Jones method provides a mathematical description of the polarization state of light, as well as a means to calculate the effect that an optical device will have on input light of a given polarization state. The method of Jones is unique in that it deals with the instantaneous electric field, whereas the Stokes parameters describe a time-averaged optical signal. For this reason the Stokes/Mueller method is often chosen for use with light of rapidly and randomly changing polarization state, such as natural sunlight, while the Jones method is preferred when using coherent sources such as lasers.

Since light is composed of oscillating electric and magnetic fields, Jones reasoned that the most natural way to represent light is in terms of the electric field vector. When written as a column vector, this vector is known as a *Jones vector* and has the form

$$\vec{E} = \begin{bmatrix} E_x(t) \\ E_y(t) \end{bmatrix}, \qquad \text{(EQ 1)}$$

where $E_x(t)$ and $E_y(t)$ are the instantaneous scalar components of the electric field. Note that these values can be complex numbers, so both amplitude and phase information is present. Oftentimes, however, it is not necessary to know the exact amplitudes and phases of the vector components. Therefore Jones vectors can be normalized and common phase factors can be neglected. This results in a loss of information, but can greatly simplify expressions. For example, the following vectors contain varying degrees of information, but are all Jones vector representations for the same polarization state:

$$\begin{bmatrix} E_0 e^{i\phi} \\ E_0 e^{i\psi} \end{bmatrix} \rightarrow \begin{bmatrix} e^{i\phi} \\ e^{i\psi} \end{bmatrix} \rightarrow \begin{bmatrix} 1 \\ e^{i(\psi-\phi)} \end{bmatrix}. \qquad \text{(EQ 2)}$$

Note that a complex vector is said to be normalized when the dot product of the vector with its complex conjugate yields a value of unity.

It is most often the case that the basis for the Jones vector is chosen to be the horizontal and vertical linear polarization states. In this case the representations for these two states are

$$\vec{E}_h = \begin{bmatrix} E_x(t) \\ 0 \end{bmatrix} \text{ and } \vec{E}_v = \begin{bmatrix} 0 \\ E_y(t) \end{bmatrix}, \quad \text{(EQ 3)}$$

or, in normalized form,

$$\vec{E}_h = \begin{bmatrix} 1 \\ 0 \end{bmatrix} \text{ and } \vec{E}_v = \begin{bmatrix} 0 \\ 1 \end{bmatrix}, \quad \text{(EQ 4)}$$

where $\vec{E}_h$ and $\vec{E}_v$ represent horizontally and vertically polarized light, respectively. The sum of two coherent light beams is given by the sum of their corresponding Jones vector components, so the sum of $\overrightarrow{E_h}$ and $\overrightarrow{E_v}$ when $E_y(t) = E_x(t)$ is given by

$$\vec{E}_{45^\circ} = \begin{bmatrix} E_x(t) \\ E_x(t) \end{bmatrix} \Rightarrow \frac{1}{\sqrt{2}} \begin{bmatrix} 1 \\ 1 \end{bmatrix}, \quad \text{(EQ 5)}$$

where the arrow indicates normalization. Note that this is the representation of the polarization state in which the electric field is oriented at a 45 degree angle with respect to the basis states.

Two other common polarization states are right-circular and left-circular. In both cases the two components have equal amplitude, but for right circular the phase of the y-component leads the x-component by $\pi/2$, while for left circular it is the x-component that leads. Thus the Jones vector representation for right-circular is

$$\vec{E}_R = \begin{bmatrix} E_0 e^{i\phi} \\ E_0 e^{i(\phi - \pi/2)} \end{bmatrix}. \quad \text{(EQ 6)}$$

Normalizing this expression and factoring out a constant phase factor of $e^{i\phi}$ yields

$$\vec{E}_R = \frac{1}{\sqrt{2}} \begin{bmatrix} 1 \\ e^{i\pi/2} \end{bmatrix} = \frac{1}{\sqrt{2}} \begin{bmatrix} 1 \\ -i \end{bmatrix}. \quad \text{(EQ 7)}$$

Similarly, the normalized representation for left-circular light is

$$\vec{E}_L = \frac{1}{\sqrt{2}} \begin{bmatrix} 1 \\ i \end{bmatrix}. \quad \text{(EQ 8)}$$

Next consider a beam of light represented by the Jones vector

$$\vec{E}_i = \begin{bmatrix} E_{ix} \\ E_{iy} \end{bmatrix} \quad \text{(EQ 9)}$$

incident on an optical device. The light will interact with the device, and the new polarization state of the light upon exiting the device will be

$$\vec{E}_t = \begin{bmatrix} E_{tx} \\ E_{ty} \end{bmatrix}. \quad \text{(EQ 10)}$$

The coupling between these two vectors can be fully described by a set of four coefficients according the following pair of linear equations:

$$\begin{aligned} E_{tx} &= aE_{ix} + bE_{iy} \\ E_{ty} &= cE_{ix} + dE_{iy}. \end{aligned} \quad \text{(EQ 11)}$$

These two equations can be rewritten using matrix notation as

$$\vec{E}_t = \bar{J}\vec{E}_i \quad \text{(EQ 12)}$$

where

$$\bar{J} = \begin{bmatrix} a & b \\ c & d \end{bmatrix} \quad \text{(EQ 13)}$$

is the *Jones matrix* of the optical device. A list of Jones matrices for some common optical devices appears in Table 1.

It is possible to represent the passage of a beam of light through multiple devices as the multiplication of Jones matrices. Note that the matrices do not commute, as illustrated by the following example. Let's assume a vertically polarized input signal, and look at its propagation through two devices, a linear polarizer oriented at $45°$ and a quarter-wave plate with its fast axis vertical. If the light passes through the polarizer first, followed by the wave plate, we have

$$\begin{aligned} \vec{E}_t &= \begin{bmatrix} 1 & 0 \\ 0 & -i \end{bmatrix} \begin{bmatrix} 1 & 1 \\ 1 & 1 \end{bmatrix} \begin{bmatrix} 1 \\ 0 \end{bmatrix} \\ &= \begin{bmatrix} 1 & 0 \\ 0 & -i \end{bmatrix} \begin{bmatrix} 1 \\ 1 \end{bmatrix} \\ &= \begin{bmatrix} 1 \\ -i \end{bmatrix}, \end{aligned} \quad \text{(EQ 14)}$$

where we have neglected common amplitude and phase factors for simplicity. The output is right-circularly polarized. Now if the light passes through wave plate before the polarizer, the result is

$$\begin{aligned} \vec{E}_t &= \begin{bmatrix} 1 & 1 \\ 1 & 1 \end{bmatrix} \begin{bmatrix} 1 & 0 \\ 0 & -i \end{bmatrix} \begin{bmatrix} 1 \\ 0 \end{bmatrix} \\ &= \begin{bmatrix} 1 & 1 \\ 1 & 1 \end{bmatrix} \begin{bmatrix} 1 \\ 0 \end{bmatrix} \\ &= \begin{bmatrix} 1 \\ 1 \end{bmatrix}, \end{aligned} \qquad \text{(EQ 15)}$$

which is light linearly polarized at $45°$.

While matrix multiplication is not commutative, it is associative, so a string of multiple Jones matrices representing several devices may be multiplied together yielding a single Jones matrix which describes the optical system as a whole. Therefore it is possible to condense the properties of N optical devices acting in series down to a single 2×2 matrix simply by multiplying the Jones matrices of the devices.

TABLE 1. Jones Matrices of Common Optical Devices

Vertical Linear Polarizer	$\begin{bmatrix} 0 & 0 \\ 0 & 1 \end{bmatrix}$	Right Circular Polarizer	$\frac{1}{2}\begin{bmatrix} 1 & i \\ -i & 1 \end{bmatrix}$
Horizontal Linear Polarizer	$\begin{bmatrix} 1 & 0 \\ 0 & 0 \end{bmatrix}$	Left Circular Polarizer	$\frac{1}{2}\begin{bmatrix} 1 & -i \\ i & 1 \end{bmatrix}$
Linear Polarizer at $45°$	$\frac{1}{2}\begin{bmatrix} 1 & 1 \\ 1 & 1 \end{bmatrix}$	Quarter-wave plate, fast axis vertical	$e^{i\pi/4}\begin{bmatrix} 1 & 0 \\ 0 & -i \end{bmatrix}$
Lossless fiber transmission	$\begin{bmatrix} e^{i\phi}\cos\theta & -e^{-i\psi}\sin\theta \\ e^{i\psi}\sin\theta & e^{-i\phi}\cos\theta \end{bmatrix}$	Quarter-wave plate, fast axis horizontal	$e^{i\pi/4}\begin{bmatrix} 1 & 0 \\ 0 & i \end{bmatrix}$